Solvency effects on polymer – surfactant interactions

By

Natasha C. Hirst

A thesis submitted to Cardiff University

in candidature for the degree of

Doctor of Philosophy

School of Chemistry

Cardiff University

Wales, UK

January 2008

ProQuest LLC
789 East Eisenhower Parkway
P.O. Box 1346
Ann Arbor, MI 48106-1346

DECLARATION

This work has not previously been accepted in substance for any degree and is not being concurrently submitted in candidature for any degree.

Signed..... (Candidate)

Date 2-06-05

STATEMENT 1

This thesis is the result of my own investigations, except where otherwise stated.

Other sources are acknowledged by footnotes giving explicit references. A bibliography is appended.

Signed..... (Candidate)

Date 2-06-05

STATEMENT 2

I hereby give consent for my thesis, if accepted, to be available for photocopying and for inter-library loan, and for the title and summary to be made available to outside organizations.

Signed..... (Candidate)

Date 2-06-05

Summary

Surfactants and polymers have extensive uses and applications in day to day life as detergents, cosmetics, and paints, and in industry, medicine and pharmaceuticals. Gaining a comprehensive understanding of the properties and functions of surfactant and polymer systems in a range of solvents will support the continued development of new uses for these systems.

Against this background, this study characterised the interaction of the anionic surfactant sodium dodecyl sulphate (SDS) with the nonionic polymer, poly(vinylpyrrolidone) (PVP) in ethanol/water mixtures. A wide range of techniques were used, including surface tension, fluorescence spectroscopy, Nuclear Magnetic Resonance, Electron Paramagnetic Resonance, Small-Angle Neutron Scattering, and viscometry. This enabled properties such as the, critical micelle concentration and critical aggregation concentration (or CMC1) to be determined, as well as measuring the size and shape of micelles formed and of polymer configurations and further establishing trends in these physical properties with solvent composition.

The study then went on to investigate SDS with a non-ionic triblock copolymer, Pluronic P104, in ethanol/water mixtures. This was a more challenging system and yielded some preliminary results, setting the way for further work on the interactions of ethanol with pluronics and surfactants.

To Bill Dalton

For making a scientist out of me

Acknowledgements

My thanks go to all friends, family and colleagues who have supported me on this journey that took some time more than we'd all expected!

Many thanks to my supervisor, Dr. Peter Griffiths for sticking by me and for all of the support and advice going all the way back to my undergraduate degree.

Big cheers for my labmates Dr. Alison Paul, Sarah-Jayne Waters, Dr. Claire Barrie and a whole host of others from the last few years, including Angela, Jason, Christian, Angie, Tuss, Eek, Champa… Thanks also for Department Bods and colleagues at ISIS who helped with getting the big machines working and understanding what the spectra meant.

Outside the world of chemistry, thanks to my family, especially my Dad, Auntie Kiffy, Uncle John and my big Sister; and to my friends – I'm far too popular to name you all(!) but you know who you are – thanks for helping me keep my sanity.

Contents

Chapter 2 – Experimental Theory

2.1 Context

2.2 Surface tension theory

2.2.1. Addition of solutes

2.2.2. Measurement of Surface tension

2.3 Viscometry

2.4 Fluorescence techniques

2.4.1 Theory of fluorescence spectroscopy

2.4.2 Fluorescent probes and π^*–π^* transitions

2.4.3 Pyrene probe

2.4.4 ANS – 8-anilino-1-naphththalene sulfonic acid probe

2.4.5 Fluorescence Quenching

2.5 Nuclear Magnetic Resonance (NMR)

2.5.1 Nuclear Magnetic Moments

2.5.2 Chemical Shift and proton NMR experiments

2.6 Small Angle Neutron Scattering (SANS)

2.6.1 Neutron production and instrumentation

2.6.2 Principles of neutron scattering:

2.6.3 Scattering length density, ρ, and contrast

2.6.4 Form Factor, P(Q)

2.6.5 Structure Factor, S(Q)

2.6.6 The Neutron scattering experiment

2.6.7 Data reduction

2.6.8 Data normalisation

2.6.9 Data Fitting

2.7 Electron Paramagnetic Resonance

2.7.1 Properties of EPR spectral lines

2.7.1.1 The position or g-value of the spectral lines

2.7.1.2 Intensity of spectral lines

2.7.1.3 Width of spectral lines

2.7.1.4 Multiplicity and hyperfine structure of spectral lines

2.7.2 EPR lineshape fitting and analysis

Chapter 3 – Materials and Methods

3.1 Materials

3.1.1 Surfactants

3.1.2 Polymers

3.1.3 Solvents

3.1.4 Fluorescence Probes

3.1.5 Fluorescence Quencher

3.2 Methods

3.2.1 Surface tension

3.2.2 Fluorescence

3.2.3 Fluorescence quenching

3.2.4 Small Angle Neutron Scattering, SANS

3.2.5 Viscometry

3.2.6 Nuclear Magnetic Resonance (NMR) Spectroscopy measurements

3.2.7 Electron Paramagnetic Resonance (EPR) Spectroscopy measurements

Chapter 4 - Effect of Ethanol on the Interaction between Poly(vinylpyrrolidone) and Sodium Dodecyl Sulphate

4 Context

4.1 Onset of Surfactant Micellisation.

4.1.1 SDS in ethanol/Water

4.1.2 The effect of ethanol/water on the SDS and PVP interactions

4.2.1 Structure of SDS micelles upon addition of ethanol

4.2.2 Structure of the PVP/SDS/Ethanol Complex

4.3 Discussion

4.4 Conclusions

4.5 Future Work

Chapter 5 – Pluronic and SDS

5 Context

- 5.1 Fluorescence
  - 5.1.1 Effect of Ethanol on the CMC of P104
  - 5.1.2 Effect of Temperature
  - 5.1.3 Fluorescence of P104 with SDS in water/ethanol mixtures
- 5.2 NMR
  - 5.2.1 Line shapes
  - 5.2.2 Peak assignment
  - 5.2.3 CMC determined by NMR spectral line shape change
  - 5.2.4 Chemical Shifts
  - 5.2.5 NMR comparison with fluorescence
- 5.3 Small Angle Neutron Scattering
- 5.4 Conclusions and future work

Chapter 1

1.1 Context

This study has investigated the interactions of a well characterized surfactant, sodium dodecyl sulphate (SDS), and polymers, polyvinylpyrrolidone (PVP) and the pluronic (P104) in water and ethanol mixtures. All components are widely used in chemical and pharmaceutical applications. SDS and the two polymers are reasonably well characterised in water and a number of other solvents. However, the effects of ethanol as a solvent has not been investigated in much depth, even less so for the effect of ethanol on the polymer – surfactant interactions. This chapter sets the background to the properties of surfactants and polymers and the solvency effects of ethanol and water.

1.2 Surfactants

Surface **Act**ive **Agents** (surfactants) are amphiphilic molecules consisting of a polar head group and a non-polar tail. The basic model of a surfactant consists of two components; a lyophobic group, usually hydrocarbon or fluorocarbon chain, and a lyophilic group which is usually ionic or a group with strong dipole moments. Surfactants fall into four categories depending on the type of head group – non-ionic, anionic, cationic and zwitterionic. The surfactant used in this project is the well characterized anionic surfactant, sodium dodecyl sulphate (SDS)[1]. The dual character of these molecules means that surfactants have limited solubility in either polar or non polar solvents.

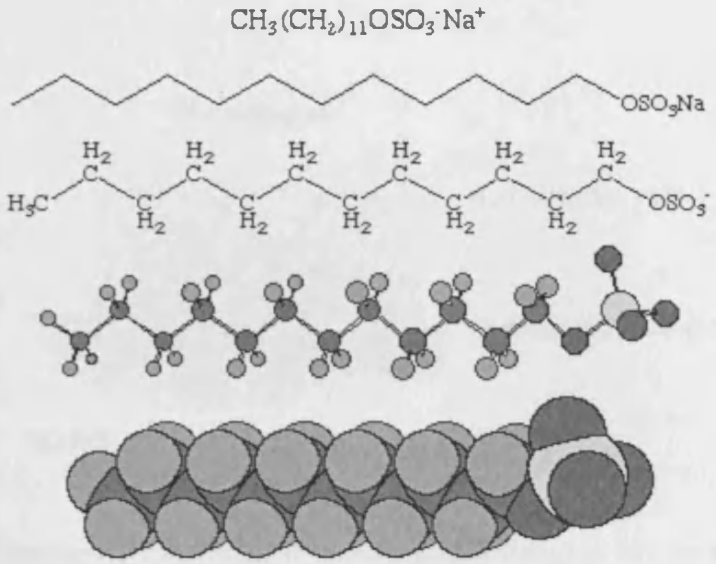

Figure 1.1 Representations of a surfactant molecule, Sodium dodecyl sulphate, showing the hydrophilic head group and the hydrophobic carbon backbone.

Considering water as a polar solvent, when surfactant molecules are in a solvent at very low concentrations, they will be solubilised as unimers. The hydrophobic group of SDS distorts the structure of water, therefore increasing the free energy of the system. To decrease the free energy, the hydrophobic tails need to be excluded from the solvent. As the surfactant concentration increases, the molecules will align at the surface since the attractive forces between the hydrocarbon tails are greater than those between the tails and water.

As a result, surfactants tend to accumulate at interfaces (of two immiscible phases), arranging themselves in such a way that both sections of the molecule are in a favourable environment, reducing the free energy of the system. The polar head can be immersed in the polar phase and the tail in the non-polar phase[1].

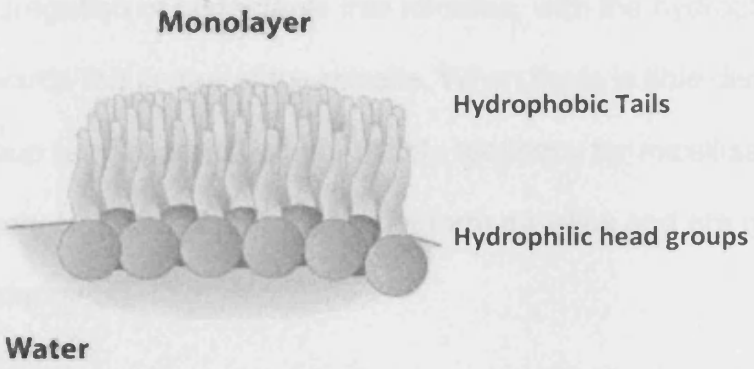

Figure 1.2 Surfactant molecules lining up on an air-water interface such that the tails point out of the water into the air and the hydrophilic head groups are immersed in water (taken from University of Montana website[2])

In systems with two or more components, the individual constituents have the option of rearranging into a separate phase or to spatially respond to an external potential[3]. Chemical potential, μ, is the thermodynamic property that determines a component's ability to redistribute. In a solvent-surfactant system phase separation is energetically unfavourable since it removes the polar head groups from the solvent. As the concentration of surfactant in water is increased, the driving force, μ, pushing the surfactant to the interface will reach a constant. At this point, surfactants self-associate to form aggregates, known as micelles, in the solvent. This is a compromise between the two extremes of phase separation and a molecular disperse solution. The formation of micelles occurs abruptly at a well-defined point known as the Critical Micelle Concentration (CMC).

The solvent distortion arising from solubilised monomers is decreased by the aggregation of surfactants into micelles, with the hydrophobic groups directed towards the centre of the micelle. When there is little distortion by the hydrophobic group (e.g. short tail), there is little tendency for micellisation to occur (hence why alcohols, such as ethanol do not form micelles and are not considered to be surfactants).

The CMC is determined by the opposing tendencies of the attractive forces between the tail groups driving the tails out of the polar phase, and the mutual repulsion of the head groups as they are brought closer together.

Very simplistically, once the CMC has been reached, any further addition of surfactant will increase the number of micelles, but not their size, i.e. at low concentration ranges, micellisation can be considered as a start-stop process, with aggregation numbers (N_{agg}) being reasonably constant (e.g. for SDS $N_{agg} \alpha$ [Surfactant]$^{0.25}$). The number of surfactant molecules in a micelle is known as the aggregation number, N_{agg}. The size and shape of the micelles and hence the aggregation number is determined by a number of factors such as head group type and size, tail group type and length, ionic strength, charge of surfactant and any impurities present[4].

If surfactant concentration is increased further, the micelle concentration may be so high that they are required to order, forming lyotropic liquid crystals. These phases may consist of bilayers, cubic arrays of spherical micelles or hexagonal arrays of rodlike micelles[11].

1.2.1 Thermodynamics of Colloids

Most colloidal dispersions (particles, 1nm → to 1μm, in solution) are inherently unstable due to thermodynamics but exist because they are kinetically stable. Thermodynamic instability[5] arises from the very large surface area that is present. If a bulk materials splits to form two new surfaces, work must be put into the system to achieve this. The greater the surface area, the more work required, thus increasing the free energy of the system and destabilising it. Thermodynamically it is more favourable for a dispersion to coalesce or phase separate to reduce the free energy.

The work required to create a new surface is proportional to the number of molecules transported to the new surface, and thus to the area of the new surface:

$$\Delta G = W = \gamma \Delta A \qquad \text{Equation 1.1}$$

Where γ is surface tension, W is work done on the system to create a new surface and ΔA the change in surface area.

At constant temperature and pressure, the work of increasing the surface area contributes to the differential Gibbs free energy:

$$dG = \gamma dA \qquad \text{Equation 1.2}$$

In a single liquid, the work $W_{AA,}$ required to pull apart a volume of unit cross-sectional area is:

$$\Delta G = W_{AA} = 2\gamma_{\alpha} \qquad \text{Equation 1.3}$$

Where γ_{α} represents a bulk phase, α, being pulled apart.

Thus, an increase in surface area, leads to a larger and positive value of ΔG, the Gibbs free energy.

Micelles are defined as colloidal systems due to their size (1→ 50nm). However, surfactants in solution are thermodynamically stable[6] despite having a large surface area. Since surfactants reduce surface tension, γ, G will only increase by a small amount even where ΔA is large and positive.

1.2.2 Theory of Surface Tension

Surface tension arises from the difference in energies of molecules in the bulk at molecules on the surface. In water, molecules in the bulk will form hydrogen bonds with other molecules in all directions, with each molecule experiencing an equal pull from all directions. Water molecules on the surface will experience a downwards pull into the bulk since there are no interactions with air to balance out the attractive forces pulling the molecules down form the surface. But since the density of water must remain the same, the surface molecules cannot be pulled into the bulk, giving rise to surface tension.

As ethanol is added to the water, the solvent becomes more hydrophobic. This alters the forces felt by molecules in the bulk and sees a reduction in surface tension, since to some extent, ethanol molecules can align at the surface to bring the hydrophobic domain into contact with the air. The determination of surface tension is described in chapter 2.

1.2.3 Thermodynamics of Micellisation

The driving force of micellisation (ΔG_{mic}°) is to obtain the lowest free energy for the system. Micellisation is a start-stop process and described by the closed association model which assumes that an equilibrium exists between surfactant monomers and micelles:

$$nS \leftrightarrow S_n \qquad \text{Equation 1.4}$$

With a corresponding equilibrium constant, K_m

$$K_m = \frac{[S_n]}{[S]^n} \qquad \text{Equation 1.5}$$

With [ ] Indicating molar concentration and n as the aggregation number. The closed association model gives;

$$\Delta G_{mic}^{\circ} = -RTlnK_m \qquad \text{Equation 1.6}$$

Going back to the concept of surface tension, at the point where the driving force or chemical potential (μ) becomes constant, there will be no further reduction in surface tension. This point also defines the formation of micelles in solution:

$$\Delta G_{mic}^{\circ} = -RTln(CMC) \qquad \text{Equation 1.7}$$

Where R is the gas constant and T the absolute temperature.

Considering the thermodynamic Gibbs equation:

$$\Delta G_{mic}^{\circ} = \Delta H_{mic}^{\circ} - T\Delta S_{mic}^{\circ} \qquad \text{Equation 1.8}$$

Where ΔH_{mic}° is the standard enthalpy change upon micellisation and ΔS_{mic}° is the standard entropy change upon micellisation. Entropy increases as the water molecules that were previously structured around the monomer tails, become free in solution and less ordered. This reduces the free energy of the system and is known as the hydrophobic effect. Although the enthalpy change is usually positive, it is smaller than the entropy term. Thus the entropy term producing a negative ΔG_{mic}^{c} is the driving force behind micellisation and largely dependent on the entropy gain as the hydrophobic tail is transferred into the micelle core.

To consider this in more detail, there are four main terms affecting the free energy of micellisation as surfactant unimers interact with each other over the micelle surface[7].

$$\Delta G_{mic}^{\circ} = \Delta G_{hydrophobe} + \Delta G_{contact} + \Delta G_{packing} + \Delta G_{head-group} + kT[\alpha] = -\mathrm{RTln}(CMC)$$

Equation 1.9

ΔG_{mic}^{c} is the Gibbs free energy for micellisation. A negative value favours micellisation by reducing the free energy of the system.

$\Delta G_{hydrophobe}$ is a large negative term for a given hydrophobic chain length (tail). Removing the hydrophobic group from solution into the oil-like core of the micelle is extremely favourable.

$\Delta G_{contact}$ is a positive term for a homologous series, reflecting the efficiency of oil-water separation upon micelle formation. The efficiency of oil-water separation upon micellisation depends on how well the micelle is packed. Water molecules can squeeze through the head group shell to penetrate the oily interior to some extent.

As head group size increases, they do not pack together so well, enabling water to penetrate into the micelle core, thus increasing the free energy.

$\Delta G_{packing}$ is a positive term for a homologous series reflecting a restriction in chain motion. When the surfactant molecule is transferred from solution to the micelle it will create an unfavourable decrease in entropy due to losing some degrees of freedom. However as the size of the head group increases for a given tail length, this term will increase, favouring micellisation.

$\Delta G_{head-group}$ is a large positive constant for equally charged solvated species and represents the electrostatic repulsion of the head groups. As the head groups approach each other they will experience steric repulsion and in the case of ionic surfactants, electrostatic repulsion also. These forces increase the free energy, disfavouring micellisation.

1.2.4 Micelle structure

The micelle formed in water from ionic surfactants such as SDS, consists of three layers; the hydrophobic core, with a radius that roughly corresponds to the length of the extended hydrophobic chain; the Stern layer, formed by the charged terminal groups; and the Gouy-Chapman layer, which consists of hydrated counterions.

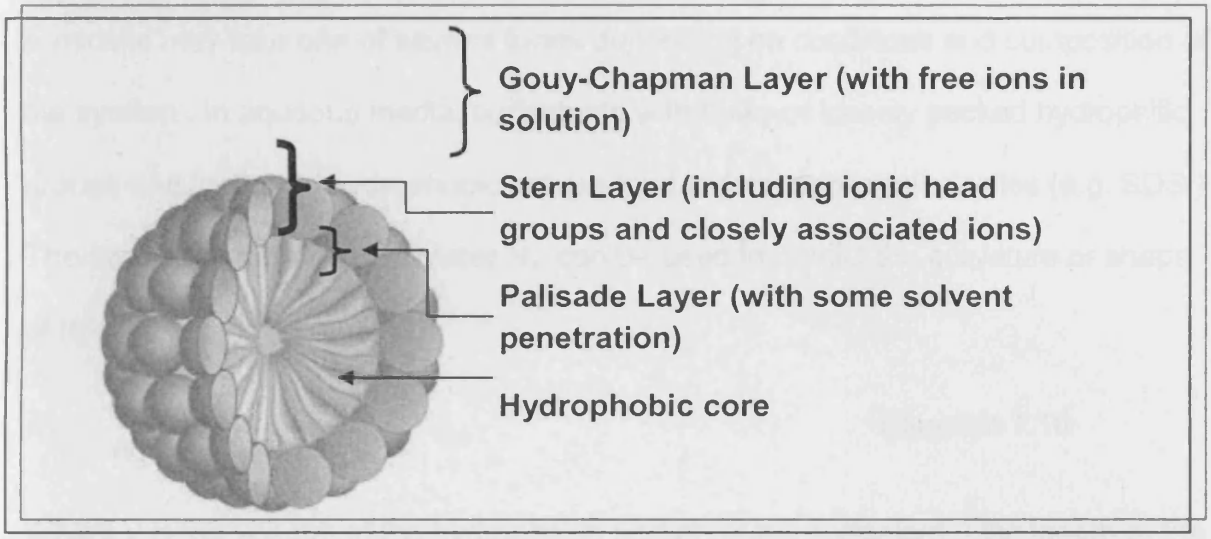

Figure 1.3 A diagrammatic representation of the layers of an ionic micelle.

In free (unbound) ionic micelles, the aqueous solution-micelle interface region consists of the ionic head groups, the Stern layer of the electrical double layer pertaining to these groups, about 50% of the counterions associated with the micelle, and water. The remaining counterions are contained in the Gouy-Chapman portion of the double layer that extends further into the solution.

The interior region of the micelle, containing the hydrophobic groups is of radius approximately equal to the length of the fully extended hydrocarbon chain. There are no gaps in the micelle core, the oily interior is equal density throughout. The aqueous phase is believed to extend beyond the hydrophilic head groups and into

the first few methylenes on the hydrophobic chain adjacent to the head group (palisade layer). The micelle interior is divided into two regions; the inner core from which water is excluded and the outer core that may be penetrated by water[1].

1.2.5 Morphology of micelles

A micelle may take one of several forms depending on conditions and composition of the system. In aqueous media, surfactants with bulky or loosely packed hydrophilic groups and long, thin hydrophobic groups tend to form spherical micelles (e.g. SDS.) The surfactant packing parameter N_s, can be used to predict the curvature or shape of micelle.

$$N_s = \frac{v}{la} \qquad \text{Equation 1.10}$$

Where v is the volume of the hydrophobic portion of the surfactant, l the length of the chain, and a, the effective area of the head group[11,8].

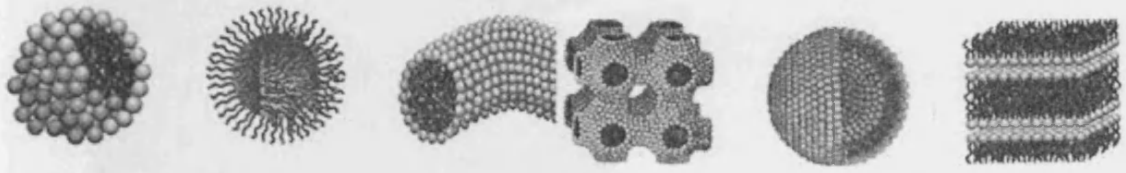

Figure 1.4 Types of aggregates depending on the packing parameter of the surfactant molecule; Left to right is spherical, inverse micelle, cylindrical, cubic, vesicle and lamellar[9].

Micellar structures	N_s
Spherical	0.33
Infinite cylinder	0.5
Planar bilayer	1
Inverted cylinder and micelles	>1

Table 1.1 Expected curvature of aggregates based on value of N_s

The shape of the micelle may change if material is solubilised within it or if environmental factors such as solvent, temperature and salt concentration change. These factors may also affect CMC's, and aggregation numbers, depending on the system being studied[10].

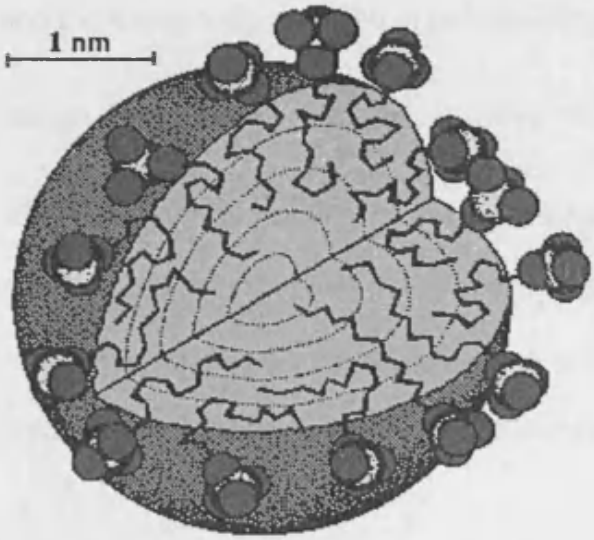

Figure 1.5: A diagrammatic representation of a spherical micelle consisting of dodecyl sulphate[11].

1.2.6 Aggregation Numbers

Aggregation numbers can be determined through a number of methods including fluorescence quenching and Small Angle Neutron Scattering (SANS), both used in this study. From geometric considerations the aggregation number would be expected to increase as the length of the hydrophobic group increases and should decrease with an increase in the volume of the hydrophobic group. For typically used surfactants the aggregation number is between 30 to 90. Aggregation number for SDS in water is 60 ± 5.

The cross sectional area of the head group for an ionic surfactant depends on the binding of the counterion to the micelle. If a counterion binds well, then it is able to reduce repulsion between the head groups, allowing more efficient packing. Binding of the counterion appears to decrease with an increase in the hydrated radius of the ion, and increases with increase in polarisability and charge.

Counterion binding to micelle: $Cs^+ > Rb^+ > Na^+ > Li^+ >$ and $I^- > Br^- > Cl^-$

If small amounts of hydrocarbons are added above the surfactant CMC in water, they will become solubilised in the micelles. Solubilisation generally causes an increase in the aggregation number. As the amount of material solubilised increases, aggregation continues to increase until the solubilisation limit is reached.

1.2.7 Factors affecting CMC

1.2.7.1 Hydrophobic Group

The hydrophobic moiety is the dominant part of the overall surfactant structure and as a result, the CMC is extremely sensitive to the structure of this component. As the alkyl chain length increases, the decrease in the free energy of micellisation becomes larger, thus making the process energetically more favourable.

In water, the CMC of ionic surfactants is generally halved by the addition of one methylene group to a straight chain hydrophobic group attached to a single hydrophilic group. At a length of 16 carbons, further addition of methylene groups has less effect and after 18 carbons, almost no effect due to the chain coiling back on itself.

The introduction of polar groups such as ethers and alcohols into the hydrophobic chain increases the CMC by making the chain more soluble.

1.2.7.2 Hydrophilic Group

In water, ionic surfactants have higher CMCs than non-ionic surfactants containing equivalent hydrophobic groups, due to greater repulsion between the head groups. The position of the hydrophilic group on the hydrocarbon chain e.g. in a more central position, and an increase in the number of hydrophilic groups, will increase the CMC due to steric constraints.

1.2.7.3 Electrolytes

In aqueous solution the presence of electrolytes has an affect on the CMC with the most pronounced effect on ionics>zwitterionics>non-ionics. If electrolytes are added to ionic surfactants, the CMC will decrease due to a decrease in electrostatic repulsion of head groups in the micelle.

1.2.7.4 Organic additives

Small amounts of organic material may produce a marked change in CMC.

Class I materials

These materials affect the CMC by being incorporated into the micelle. They are generally polar organic compounds such as alcohols and amides and reduce the CMC. The shorter chain members adsorb mainly in the outer portion of the micelle, close to the water-micelle interface. These molecules decrease the work necessary to initiate micellisation, thus lowering the CMC.

Class II materials

These materials alter the CMC by modifying solvent-micelle or solvent-surfactant interactions and include urea, formamide, ethylene glycol and short chain alcohols. These materials change the CMC at bulk phase concentrations that are much higher than for class I materials. The CMC is increased since the class II materials disrupt the water structure around the surfactant molecules causing a decrease to the entropy gain on micellisation, resulting in a higher CMC.

1.2.7.5 Temperature

The effect of temperature on the CMC of surfactants in aqueous media is complex. An initial temperature increase causes a decrease in the hydration of head groups, favouring micellisation. As the temperature increases further, thermal agitation of the water molecules surrounding the hydrophobic chain causes disorganisation of the structure, thus increasing the CMC (disfavouring micellisation). The magnitude of the two effects determines whether the CMC increases or decreases over a given temperature range.

1.2.8 Effects of alcohol on surfactant systems.

In many applications, surfactants are used with a number of additives to improve their properties, alcohols being frequently used. With increasing concentration of alcohol, the properties and structure of the aqueous solvent mixture[12] are modified in such a manner that the solubility of an ionic surfactant increases *i.e.* the solution is more hydrophobic. The dielectric constant (a relative measure of solvent polarity) of water is 80.1 at 20°C and ethanol has a dielectric constant of 24.3. On addition of ethanol, the dielectric constant of the solvent decreases, which increases the electrostatic interaction between the ionic head groups. Both these factors have the effect of increasing the critical micelle concentration (CMC), a process known as the co-solvent effect[12,13]. However, an opposing effect can occur as the non-ionic character of the alcohol leads to a diluted surface charge density in the palisade layer[1], a process that promotes a decrease in the CMC. This is known as the "co-surfactant effect".

The effects of ethanol on micellar systems have been widely studied[16] but there is still some discrepancy with respect to the precise role of ethanol within these systems. The alcohol will partition itself between the palisade region of the micellar pseudo-phase and intermicellar[14] solution, according to a partition co-efficient, K_P[10]. Ethanol is likely to be predominantly solubilised in solution. Short chain alcohols penetrate little into the micelles and instead act on the micellisation process by modifying the properties of water. As such, ethanol is thought to act as a co-solvent rather than co-surfactant[15,16]. Ethanol-water mixtures are expected to be better solvents for surfactants than pure water and for micelles to form at a higher surfactant concentration. Both this study and others have shown that initially, the CMC lowers as ethanol concentration is increased. Above a threshold concentration of ethanol, the increase in CMC that is predicted is observed[17].

For sodium dodecylsulphate (SDS) a decrease in CMC with increasing ethanol is observed at low ethanol concentrations (co-surfactant effect), which subsequently gives way to the co-solvency effect at higher ethanol concentrations; increasing CMC with increasing ethanol[18]. Hence, the CMC goes through a minimum value at some surfactant-dependant ethanol concentration[13,18].

Many studies have noted that at high alcohol content, the CMC's become increasingly difficult to determine.

The addition of ethanol is expected to decrease the size of the micelle, up to a point where the concentration of ethanol is high enough (>25%) to bring about dissolution of micelles. Decreases in surfactant aggregation number have also been reported.

Changes in shape of micelles are widely accepted to occur upon the addition of alcohol, but the shape of the mixed surfactant-alcohol micelles are difficult to determine with accuracy. Rafati et al[19] have investigated the effect of ethanol (from 10 to 40 v/v%) on the CMC and aggregation number of SDS using ion-selective electrodes. They suggest that after 54.6% v/v% ethanol content, micellisation no longer occurs. The co-solvent effect is noted here and Rafati et al observed the tendency for smaller micellar aggregates to form as the polarity (ethanol content) of solvent increased. Once micelles are saturated by ethanol, each SD^- ion can have approximately 3.7 ethanol molecules associated with it in the micelle.

It has been suggested that in some systems, polydispersity of composition and aggregation number of both surfactant and alcohol may occur[10]. It is possible that there is a co-existence of alcohol-rich and surfactant-rich micelles. Studies of mixed surfactant systems show that two surfactants will only co-micellise if their carbon chain numbers are similar. Since alcohol chain lengths are likely to differ greatly from the surfactant chain length, especially in the case of ethanol as used in this study, co-micellisation is unlikely.

Addition of ethanol to the solvent will affect many of the thermodynamic aspects of micellisation. There are a number of contributions to the free energy of micellisation,

with the standard free energy difference ($\Delta\mu_g^\circ$), of the surfactant monomer in solution being transferred to the micelle, determining whether or not micellisation is favoured. Ethanol will also affect the kinetics of micelle formation and breakdown.

The electrode study of dodecyl tetramethyl ammonium bromide (DoTAB) in ethanol/water mixtures[13] raised the possibility of mixed DoTAB / ethanol micelles that initially increase in size until saturated by ethanol. Beyond this point, a decrease in aggregation number results due to the low dielectric constant. Ultimately, the driving force for micellisation has diminished such that no aggregation occurs[20].

1.3 Polymers

Polymers are long chain molecules that can be naturally occurring or synthetic and consist of a large number of one or more monomer units. Their size falls within the colloidal range of around 10<100nm and may be simple linear molecules, branched or cross linked. Linear polymers were utilised in this study. Numerous polymer classifications exist, and polymers tend to have a high molecular weight. Especially for synthetic polymers, polydispersity or a range of molecular weights will be present. Consequently, mean molecular weight values are used.

Polymers may be described on the basis of the number of different monomers involved in its synthesis and how these are arranged. If a polymer contains more than one monomer unit it is a copolymer. Most polymers have a 'backbone' of carbon but other structures are possible including silicone oxide backbones. Some polymer backbones may have amide, ester or other linkages which will drastically affect the polymer properties. The monomer units may be distributed randomly, alternately, in block fashion, or grafted;

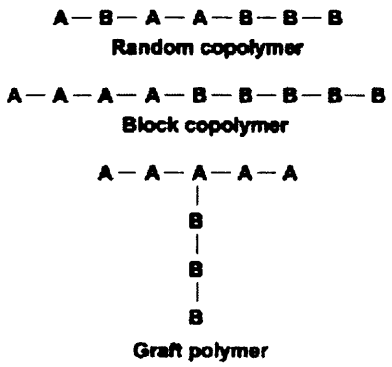

Figure 1.6 A diagrammatic representation of different polymer types

The polymer polyvinylpyrrolidone (PVP) is a linear polymer consisting of one monomer and is known as a homopolymer. The pluronic P104 is a block copolymer

consisting of A-B-A blocks (PEO-PPO-PEO), with each block containing only one type of monomer. A variety of other structures exist, including hydrophobically modified polymers which have had hydrophobic sections grafted on, but this study is only concerned with PVP and P104.

Polymer polarity offers another means of classification. A polymer may be polar and water-soluble e.g. poly(ethylene oxide), slightly polar and sparingly water-soluble e.g. poly(vinyl acetate), ionizable e.g. poly(acrylic acid) or non-polar e.g. polystyrene.

1.3.1 Polymers in solution

Polymers in dilute solutions can be considered by looking at individual molecules surrounded by solvent. When polymers are dissolved in a solvent, an increase to the solution viscosity is observed. Due to their large size, polymers move slowly in solution and slow down the solvent molecules by inhibiting their flow, making the solution measurably more viscous. If attractive secondary interactions exist between solvent and polymer, small solvent molecules may become bound to the polymer.

Flexible polymers have considerable thermal motion compared to the energy barriers associated with the backbone rotation[21]. Such molecules have an associated primary, secondary and tertiary structure. Polymer molecules usually form random coils in solution, three-dimensional in terms of structure and movement, described as a 'walk'. Polymer segments may interact with solvent and with other polymer strands depending on the solvent quality. In a good solvent, polymer segments repel each other, reducing segment-segment interactions. In this case the polymer is in

expanded form. Reducing the quality of the solvent increases segment-segment interactions due to the unfavourable entropic contribution associated with segment-solvent interactions. Consequently, the polymer is in a more contracted conformation, which will affect the viscosity.

1.3.2 Thermodynamics of polymers in solution

In an analogous way to that already described for surfactants, the solvation of a polymer is governed by the magnitude of the free energy of mixing, ΔG_{mix}:

$$\Delta G_{mix} = \Delta H_{mix} - (T\Delta S_{mix}) \qquad \text{Equation 1.11}$$

Where ΔH_{mix} is the enthalpic component, T is the temperature and ΔS_{mix} is the change in entropy upon mixing. ΔG_{mix} must be negative for spontaneous dissolution. Due to solvated chains having increased conformational mobility, the change in entropy upon mixing of the polymer and solvent is large and positive.

1.3.3 Polymer-solvent interactions

The properties of polymers in solution are highly dependent upon solvent quality. A dissolved polymer will experience attractive forces between certain polymer segments that induce cohesion. Energy must be put into the system to keep molecular species away form their nearest neighbours. This is termed cohesive

energy, and is related to ΔH_{mix}, the volume of mixing, the volume fractions and the cohesive energy densities of the components:

$$\Delta H_{mix} = V_{mix}(\delta_1 - \delta_1)^2 \phi_1 \phi_2 \qquad \text{Equation 1.12}$$

V_{mix} is the volume of mixing, δ_1 and ϕ_1 are the solubility parameter and volume fraction of the solvent respectively. δ_2 and ϕ_2 are the solubility parameter and volume fraction of the polymer. Since ΔH_{mix} needs to be small for spontaneous dissolution to occur, the solubility parameters of the solvent and polymer must be as close as possible.

In a good solvent, the solvent molecules have similar properties to those of the polymer and as such the polymer would have similar preference for a solvent molecule as for another polymer molecule. This results in a random configuration of the chains. In a poor solvent, the opposite is true and the chains will contract. This will influence the solution viscosity.

When a polymer is dissolved in an excess of solvent, the polymer-polymer interactions can be neglected. When dissolved, a single flexible linear chain has many internal degrees of freedom and may fold in many ways to minimise polymer-solvent contact. This folding can produce a range of structures such as unperturbed or perturbed coils, wormlike coils and structures resembling Euclidian bodies like spheres.

The size of a polymer coil is characterised by it's radius of gyration, R_g which measures the root-mean-square distance of the segments from the centre of mass.

Three extremes of polymer configuration are the stiff rod, compact (spherical) globule and the coil. The radius of gyration (linked to centre of mass of the polymer), R_g, for a flexible chain is given by;

$$R_g^2 = 1/6\ l^2N \qquad \text{Equation 1.13}$$

Where l is the length between ends, and N the number of randomly oriented bonds. This leads to the probability distribution, P(*r*), of the end point of a chain to be at a distance x from the starting point as being Gaussian, and thus has a distribution as shown below:

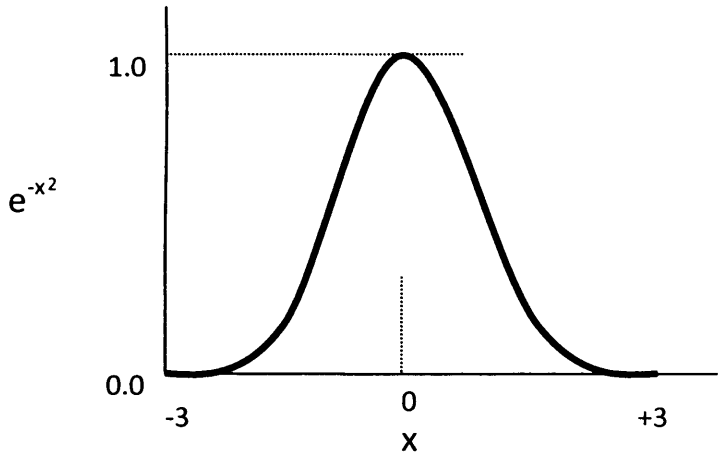

Figure 1.7: A graph of Gaussian distribution[22].

Although polymer segments can overlap in solution, they cannot occupy the same space at the same time i.e. there is an excluded volume. There is also a net attraction between the segments due to van der Waals forces, which is solvent dependent. This is best described by the Flory-Huggins parameter, χ, which is defined as the energy change (ΔkT) associated with the transfer of a segment from pure polymer to pure solvent, or a solvent molecule from solvent to polymer[23].

Depending on the polymer type, polarity or charge on segments of the chain will also influence how easily the polymer chain can form a coil or other structures, or whether large charges along the chain prevent coiling from occurring to any extent due to electrostatic repulsion.

1.3.4 Block copolymers

Homopolymers show consistent properties across the whole chain whereas block co-polymers can act as amphiphiles, like surfactants. This means that they are able to self-assemble, in a similar way to surfactants.

Pluronics® are an example of this. The Pluronic types are block copolymers based on ethylene oxide and propylene oxide. They can function as antifoaming agents, wetting agents, dispersants, thickeners, and emulsifiers, depending on the overall molecular weight and relative sizes of the poly(propylene) (PPO) and poly(ethylene) (PEO) segments[24].

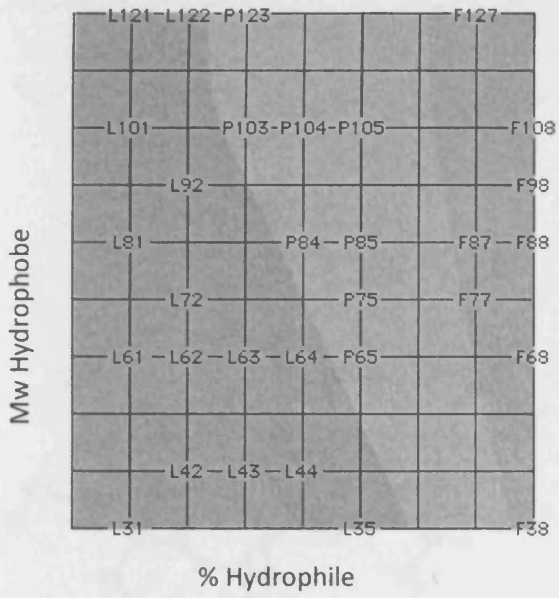

Figure 1.8 (from BASF website[24]) Pluronic grid of molecular weight of hydrophobe (PPO) vs % of hydrophile (PEO). The grid represents the relationship between copolymer structure, physical form and surfactant characteristics by plotting molecular weight ranges of the hydrophobe against percent of hydrophile in the final molecule.

Pluronic P104, used in this study, is a difunctional block copolymer surfactant terminating in primary hydroxyl groups and acts as a non-ionic surfactant with an average molecular weight of 5900. P104 consists of a centre segment of hydrophobic PPO (with 61 monomer units) flanked by two hydrophilic PEO segments, each containing 27 monomer units.

Figure 1.9 shows the structure and geometry of the more hydrophobic pluronic L31 which consists of much shorter hydrophilic segments. It offers a view as to the coiling of pluronics in solution and the bond structure of the EO and PO units.

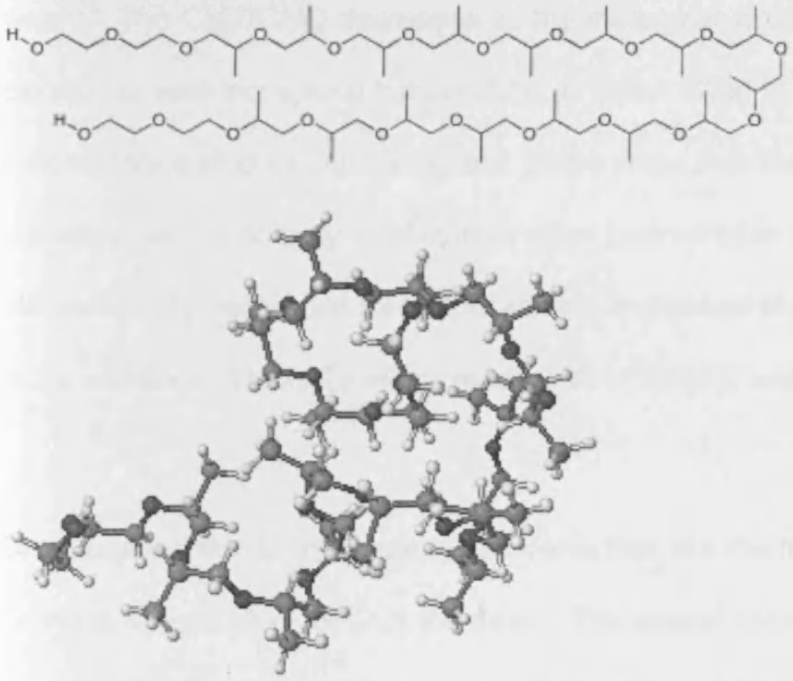

Figure 1.9 Bond structure and 3D molecular representation of Pluronic L31 consisting of PEO-PPO-PEO with unit ratios 2:16:2 (taken from Cambridge University website)[25]

1.3.4.1 Physical properties of pluronics

P104 shows similar physical properties to SDS with respect to there being unimers in solution and on the air-water interface at low concentrations, and with an increase in concentration of P104 until a CMC point occurs. The CMC and (Critical Micelle Temperature) CMT is not as abrupt as that seen for classical surfactants and the micellisation process is not quite a start/stop process. In addition, there is a greater polydispersity of molecules to take into account and the CMC is also sensitive to factors such as temperature, solvent and so on. The CMC of non-ionic polyethylene based surfactants, C_mE_n, varies strongly with m while the variation with n is quite weak[26]. The CMT/CMC decreases as the molecular weight increases. The CMC decreases with increasing temperature as determined by a number of studies[27]. Fluorescence studies using a pyrene probe show that the I_{iii}/I_i ratio intensity increases as the polarity increases ie more hydrophobic microdomains. Microviscosity decreases as temperature is increased since the micelle becomes more compact. Viscosity will increase with molecular weight.

Block copolymers form micelles in solvents that are thermodynamically good solvents for one block but not the other. The closed association model describes the thermodynamics of the unimer to micelle process and provides a good fit with linear results obtained[11], as discussed earlier in this chapter, although it is suggested that the micellisation process is not as clean a start/stop process as for classical surfactants. Micellisation is endothermic and driven by a decrease in polarity of EO

and PO as the temperature increases and by entropy gain when unimers form micelles (hydrophobic effect).

At lower temperatures, copolymers are in solution as unimers. As temperature or concentration of unimers increases, micelles will form at the CMT or CMC. Micellisation is not sharp and tends to occur across a concentration decade or 10K. There is not a sharp CMC/CMT due to polydispersity and sensitivity of different techniques to the unimers in solution.

Surface tension studies show two breaks in the data with the first being at very low polymer concentration (approx 0.001%) and a second break that concurs with dye solubilisation values for the CMC. Wanka et al[28] determined the CMC for P104 through surface tension as occurring at 0.01wt% P104 at 25°C. The first break in the data changes with temperature and is due to a change in structural configuration of the polymer at the air-solvent interface. The copolymer layer becomes more compact due to considerable folding at the interface. The PPO segment adsorbs on the interface with the PEO segments in solution.

SANS experiments show that as temperature decreases and at low polymer concentrations, the unimers are dissolved as gaussian chains of R_g=1.7nm. Upon reaching the CMC/CMT spherical micelles form with a core of approximately 4-5nm, which is temperature dependant[29]. Modelling the micelle shows a micelle structure similar to that previously described for SDS, containing a hydrophobic core

surrounded by a hydrophilic corona. Hydrodynamic radii of P104 is approximately 10nm with N_{agg} approximately 50.

CMC decreases as temperature increases. Water becomes a poorer solvent for both EO and PO segments so enthalpy increases and therefore micellisation is an entropy driven process. The free energy of micellisation is mainly a function of the hydrophobic PPO block. Increasing the size of the PPO segment, decreases CMC/CMT, and increasing temperature causes a decrease in the CMC. The more hydrophilic the polymer, the harder it is to form micelles. The effect of PEO is less than the effect of PPO on micellisation, therefore PPO is the driving force.

1.3.4.2 Configuration of pluronic copolymers

It has been shown that the PEO-PPO-PEO block copolymer backbone chain is coiled at lower temperatures, bringing these groups into closer proximity. At higher temperatures, hydrogen bonding breaks down between water and the hydrophobic PPO segments, and this leads to the backbone reconfiguring and uncoiling. The PPO blocks are hydrated at lower temperatures and lower polymer concentration. Alexandridis et al[26] determined that the micellisation process is entropy-driven with endothermic micellisation enthalpy.

Polyoxyethylene groups can exist in a number of conformations which have a range of energies. A gauche conformation around the C-C bond, and the anti- conformation around the C-O bond has the lowest energy and dominates at lower temperatures. This also has the largest dipole moment and forms strong hydrogen bonds to water. As temperature is increased, conformational changes will lead to anti-anti-anti-conformation and a reduced dipole moment, thus making the polyoxyethlene blocks less polar. Interactions with water then become less favourable, reducing hydration of the groups and leading to closer packing and self assembly e.g. into micelles.

The PEO chain increases the water structure around it (hydration shell). Depending on the bond configuration PEO can exist in two forms, a low-energy and polar form at lower temperatures and a higher-energy, less polar form at higher temperatures which makes the solute-solvent interactions less favourable. Therefore polymer conformation depends on temperature.

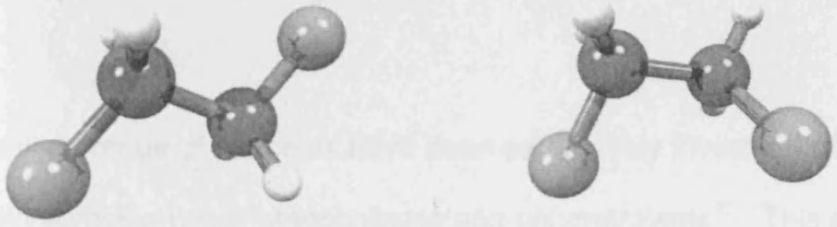

Figure 1.10 Anti conformation around a carbon-carbon (higher energy) bond and a gauche conformation around a carbon-carbon bond (lower energy)

The aggregation number increases with temperature but the radius stays largely the same, hence the micelles become more compact and squeeze out the solvent molecules.

1.3.4.3 Kinetics of pluronic micelles

Pluronic micellar solutions are characterised by two relaxation processes, like micellar solutions of conventional surfactants such as SDS. This is the rapid process of copolymer exchange of micelles to bulk and a slow process of micelle formation and breakup. Characteristic times longer than 0.3μs for exchange of polymers between micelles and intermicellar solution. Relaxation time for formation/breakup of micelles increases as molecular weight increases. Relaxation time increases as the length of the hydrophilic block decreases and as the length of the hydrophobic block increases. Experiments based on the dynamics of micelles shows that the aggregation number is temperature dependant[30].

The wide range of pluronics have been extensively investigated and covered in depth across a range of techniques and polymer types[31]. This section has focused on the papers and work most relevant to this thesis.

1.4 Surfactants and polymers

Mixtures of water-soluble polymers and surfactants have numerous applications in industry. Whereas non-ionic polymers and non-ionic surfactants show only very weak interactions, non-ionic polymers and anionic surfactants, [32,33,34,35,36,37,38,39,40,41] polyelectrolytes and oppositely charged surfactants [42,43,44,45] and hydrophobically modified polymers and anionic surfactants [38,46,47,48,49,50,51,52,53] show strong interactions leading to a variety of uses. Synthetic polymers, proteins, starches, and cellulose derivatives *etc.* interact with surfactants to form complexes. When the surfactant concentration in the complex is high, the polymer-surfactant complex can show solubilisation power often higher than that of the surfactant alone and also at concentrations below the CMC of the surfactant.

Polymers can facilitate the self-assembly of surfactants. The spontaneous aggregation of surfactants to form micelles occurs at a lower concentration when in the presence of a dilute solution of homopolymer. The micelles form in solution and must interact immediately with the polymer once formed, in order to reduce their free energy. The micelles then bind to the polymer, and the concentration at which this occurs is termed the critical aggregation concentration (CAC or CMC1). The CMC1 value depends on the nature of the surfactant and the polymer, and where the polymer aids micellisation, the CMC1 is at a lower concentration than the surfactant-only case i.e. CMC1<CMC.

Whether or not polymers and surfactants form polymer-micelle complexes is determined by the thermodynamics driving the self-aggregation of the surfactant

monomers. Steric constraints between polymer segments and surfactant head groups at the interface of the micelle immobilise the micelle on the polymer, resulting in the loss of translational and configurational entropies. These do not favour an interaction. However, if sufficient water is displaced from contact with the hydrophobic core then the free energy can be lowered enough (CMC1<CMC) for binding to occur. This is the case for surfactants with reasonably small head groups such as the sulphate head group of an anionic surfactant. However, the larger head groups generally present on non-ionic surfactants (such as ethylene oxide oligomers) result in significantly less water being displaced by the polymer and thus no interaction occurs.

1.4.1 Interactions of SDS with PVP

It is widely accepted that micelle-polymer interactions occur for the SDS-PVP system[54,55,56,57,58,59,**Error! Bookmark not defined.**] with the micelles adsorbing to the polymer strands like beads on a string[60]. The interaction between PVP to SDS micelles is exothermic due to the relatively strong interaction between the polymer and the negatively charged micelles[61]. In the case of SDS-PVP, the micelles are thought to be adsorbed to the polymer, with the polymer strand located in the palisade region of the micelle[62], defined as the outer layer of the hydrophobic core, which can be penetrated by water molecules. The presence of the polymer in the palisade region shields part of the hydrophobic core of the micelle from the aqueous phase.

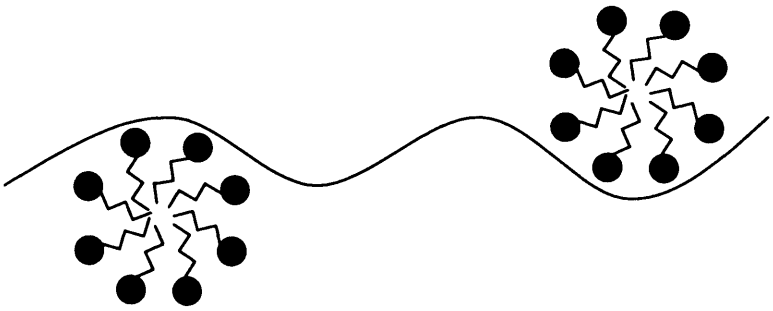

Figure 1.11a A representation of the 'beads on a string' model of surfactant-polymer interactions as present with SDS-PVP

Whereas SDS in a solvent will reach a CMC as surfactant concentration is increased, SDS in the presence of some polymers will experience the equivalent of two CMC's; CMC1 and CMC2. CMC1 is the point at which micelles form on the polymer strands. As the surfactant concentration continues to increase, CMC2 is reached whereby free micelles also form in solution.

Folmer and Kronberg[63] have also modelled the SDS-PVP complex based on surface tension and thin-film stability measurements. In figure 1.11b(a) association at low concentration is illustrated where surfactant molecules are present as unimers and one on one association with the polymer in the presence of the headgroups takes place along the interface. 1.11b(b) shows association at the CMC1 where surfactants begin to micellise along the polymer in the bulk solution. 1.11b(c) shows growth of micelles at the polymer, and the aggregation in the bulk leads to desorption of surfactant-polymer complexes at the surface. 1.11b(d) all polymer present in solution is saturated with surfactant micelles (in the pearl necklace structure previously described). 1.11b(e) shows added surfactants behaving as

unimers in solution until the point at which the non bound bulk micelles begin to form, see figure 1.11b(f). Above CMC2 (T2') micelles complexed to the polymer exist in equilibrium with free micelles in bulk solution.

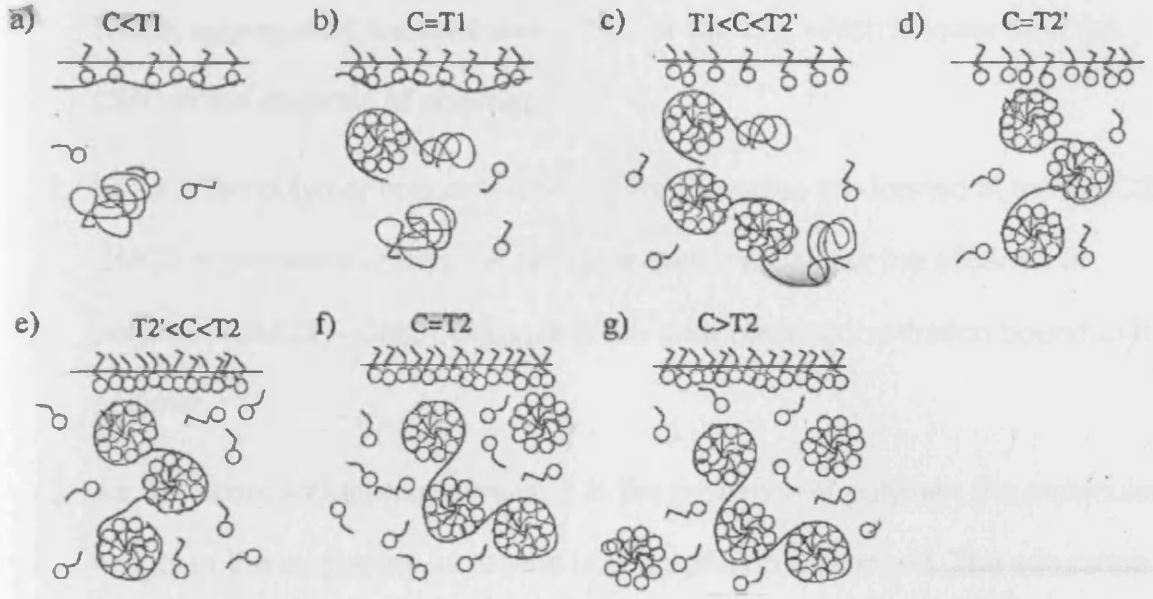

Figure 1.11b Schematic illustration of the complex formation of SDS and PVP in bulk solution and at the liquid –air interface. (T1=CMC1, T2'=saturation of polymer with micelles, T2=CMC2, above which free micelles in solution and saturated polymer exists in equilibrium.)

1.4.2 Features of surfactant – polymer systems

In summary, general features of ionic surfactant - non-ionic polymer systems are[5]:

1. Small micellar-like surfactant aggregates form on the polymer backbone at a critical aggregation concentration (CAC or CMC1), which is lower than the CMC in the absence of polymer.
2. For a given polymer concentration C_P, free micelles are formed at the CMC2. CMC2 in presence of polymer is higher than the CMC in the absence of polymer. CMC2 – CMC1 is equal to the surfactant concentration bound to the polymer.
3. As SDS concentration is increased in the presence of polymer, the molecular weight of the aggregate increases until saturation is reached. The saturation of the polymer is generally observed for low surfactant/polymer ratios.

Two separate breaks are seen in curves such as surface tension and fluorescence which track changes to the surface and probe microenvironment respectively.

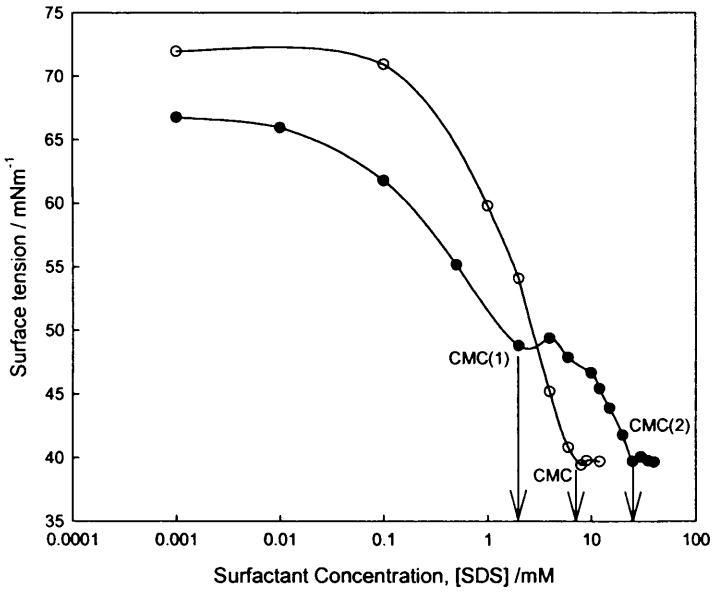

Figure 1.12: Surface tension curves for purified SDS in water, showing the CMC (open circles), and purified SDS with PVP in water showing CMC 1 and CMC 2 (closed circles.)

Since strong interactions between micelle and polymer are mostly confined to ionic surfactant micelles, it follows that polymer-adsorbed micelles are generally (negatively) charged. This causes an electrostatic repulsion between the micelles adsorbed on the same polymer molecule which is a strong function of ionic strength. As such, each polymer chain can only accommodate a certain number of micelles.

Whitesides and Miller[64] discussed the intermicellar electrostatic repulsion which results in stepwise binding of micelles to the polymer. This mechanism also provides an explanation for the "saturation" of the polymer by micelles. The idea has been extended and modelled quantitatively by Nikas and Blankschtein[65].

In order for the (n+1) micelle to bind to the same polymer, the driving force (μ, chemical potential) must be higher than that required to bind micelle n. Consequently, the micelle occupancy on the polymer molecules is stepwise with no polymer molecule having significantly more adsorbed micelles than the next. Another consequence is that the concentration of surfactant unimer in solution increases as the average number of micelles per polymer molecule increases[66].

When the repulsion between micelles is such that forcing another micelle onto the polymer is more difficult than forming a free (non-adsorbed) micelle in solution, then the polymer is said to be "saturated". This defines the second characteristic concentration, CMC2, at which the unimer concentration equals the polymer-free CMC of the surfactant.

Whereas CMC1 is independent of concentration and polymer molecular weight, CMC2 is a linear function of polymer concentration. The type and strength of the electrostatic interactions between the head groups within a micelle and between the micelles themselves will determine the value of CMC1 and CMC2 respectively.

The association between a homopolymer and a surfactant in a gradient of surfactant concentration has been summarized by Cabane *et al*[67].

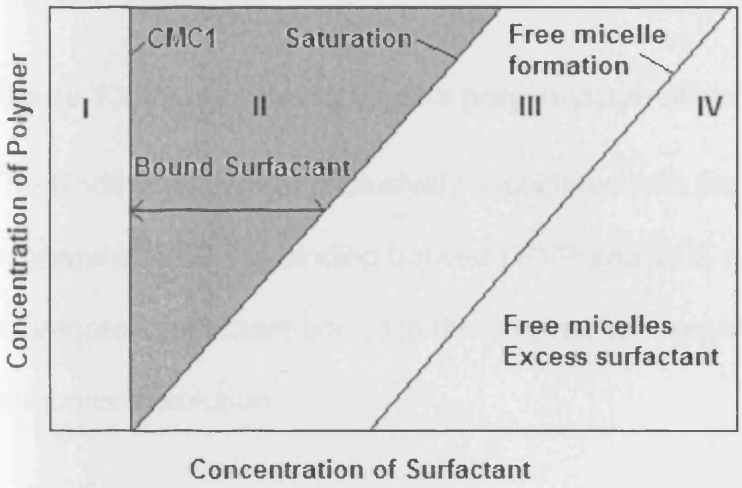

Figure 1.13 Schematic diagram of association between a homopolymer and a surfactant across a concentration range. *I. At low surfactant concentration there is no association. II. Above CMC1 association increases up to a surfactant concentration which increases linearly with polymer concentration. III. Association is saturated and surfactant unimer concentration increases. IV. There is co-existence of surfactant aggregates at the polymer chains, and free micelles (adapted from Cabane[67]).*

In SDS-PVP systems it is well established that SDS exists on the polymer as micellar type aggregates which grow in size and number during the binding process[6]. Interaction occurs through electrostatic interaction between the mildly cationic nitrogens on the pyrrolidone rings of PVP and the negative charge on the head groups of SDS.

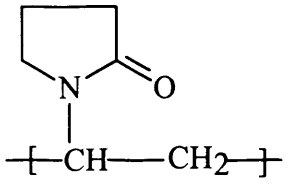

Figure 1.14 Bond structure of a polyvinylpyrrolidone monomer unit

The binding process is exclusively associated with the formation of bound aggregated SDS i.e. binding between PVP and SDS monomers does not occur. The aggregated surfactant bound to the polymer is in equilibrium with surfactant monomer in solution.

1.4.3 Factors affecting surfactant-polymer association

Several factors influence the association of surfactant on the polymer chain:

1. At high temperatures, association is less favourable.
2. The addition of salt affects the critical aggregation concentration.
3. The association depends on the surfactant structure. The CMC1 value decreases with increasing chain length with a homologous series.
4. The molecular weight and the amount of polymer in solution. The critical aggregation concentration decreases slightly with the amount of polymer.

SURFACTANT	POLYMER	CMC1 /mM	CMC /mM
$C_{12}H_{25}$-OSO_3Na	Poly(ethylene oxide)	5.7	8.3
	Poly(vinyl pyrrolidone)	2.5	8.3

Table 1.2 [68], showing the critical aggregation concentration, CMC1 for the surfactant-polymer complexes and CMC for surfactant alone. The CMC1 values are smaller than the CMC values.

If solvent polarity is altered then this will cause change to the dielectric constant which in turn has a profound effect on the electrostatic interactions and hence on the values of CMC, CMC1 and CMC2.

There are very few studies concerning polymer-surfactant systems in polar solvents other than water[69]. The electrode study by Shirahama et al[70] shows that the co-operative nature of the binding and indeed the binding affinity of poly(styrene sulfonate) to dodecylpyridinium chloride is reduced as ethanol is added.

References

[1] Rosen, M.J., *Surfactants and Interfacial Phenomena*, Wiley Interscience, **1989**
[2] **dbs.umt.edu/.../lectures/005/lecture.html**
[3] Evans and Wennerstrom, *The Colloidal Domain*, Wiley-VCH. 1999
[4] Bury, R., Desmazières, B., and Treiner, C. *Colloids and Surfaces A*, **1997,** *127*, 113-124
[5] Corkhill, J.M., Goodman, J.F., and Harrold, S.P., *Trans. Faraday Soc.* **1964,** *60*, 202,
[6] Nemethy, G., and Scherega, H.A., *J. Chem. Phys.* **1962,** *36*, 3401,
[7] Blankschtein, D., *et al., Langmuir*, **1998,** *14*, 7166,
[8] Evans, D.F., Wennerstrom, H., *"The Colloidal Domain: Where physics, chemistry, biology and technology meet."*, 2nd Ed. Wiley-VCH, **1999**
[9] "Bicontinuous Liquid Crystalline Mesophases — Solubilization Reactivity and Interfacial Reactions", in *Bicontinuous Liquid Crystals*, M. L. Lynch & P. T. Spicer (eds.), Surfactants Science Series, CRC Publishers, Vol. 127 pp 387-425 (2005)
[10] Zana, R., *Advances in Colloids and Interface Science*, 57 (1995) 1-64
[11] Jonsson, N., Lindman, B., Holmberg, K. and Kronberg, B., *Surfactants and polymers in aqueous solution,* Wiley, **1998**
[12] Huang, J-B., Mao, M., Zhu, B-Y., *Colloids and surfaces A*, **1999**, *155*, 339-348
[13] Gharibi, H., Razavizadeh, B.M., Rafati, A.A., *Colloids and surfaces A,* **1998,** *136*, 123-132
[14] Manabe, M., Tokunaga, A., Kawamura, H., Shiomi, M., Hiramatsu, K., *Colloid Polym. Sci.* **2002**, *280,* 929-935
[15] Cinelli, S., Onori, G., Santucci, A., *Colloids and Surfaces A*, **1999**, *160,* 3-8
[16] Zana, R., *Aqueous Surfactant-alcohol systems: A review. Advances in Colloid and Interface Science*, **1995**, *57*, 1-64
[17] Aramaki, K., Olsson, U., Yamaguchi, Y., Kunieda, H., *Langmuir*, **1999,** *15*, 6226-6232
[18] Safarpour, M.A., Rafati, A.A., Gharibi, H., *J. Chin. Chem. Soc.* **1999**, *46*, 6, 983-992
[19] Rafati, A.A., Gharibi, H., Rezaie-Sameti, M., *J. of Molecular Liquids*, **2004**, *111*, 109-116
[20] Aramaki, K., Olsson, U., Yamaguchi, Y., Kunieda, H., *Langmuir*, **1999**, *15*, 6226-6232
[21] Fleer, G. J., Chen Stuart, M. A., Scheutjens, J. M. H. M., Cosgrove, T., and Vincent, B., *Polymers at Interfaces*, Chapman and Hall, **1993**.
[22] Atkins, P. W., *Physical Chemistry*, Oxford University Press, **1992**.
[23] Flory, P. J., *Principles of Polymer Chemistry*, Cornell Univ. Press, Ithaca NY, **1953**.

[24] *http://worldaccount.basf.com/wa/NAFTA~en_US/Catalog/ChemicalsNAFTA/pi/BASF/Brand/pluronic*, BASF product information
[25] **www-jmg.ch.cam.ac.uk/data/molecules/misc/l31.html**
[26] Alexandridis, P., Hatton, A.T., *Colloids and Surfaces A.*, **1995**, *96*, 1-46
[27] Alexandridis, P., Nivaggioli, T., Hatton, A.T., *Langmuir*, **1995**, *11*, 1468-1476
[28] Wanka, G., Hoffman, H., Ulbricht, W., *Macromolecules*, **1994**, *27*, 4145-4159
[29] Liu, Y., Chen, S-H., Huang, J., *Macromolecules*, **1998**, *31*, 2236-2244
[30] Michels B., Zana, R., *J. Colloid and Interface Sci.* **1999**, *212*, 593-596
[31] Alexandridis, P., Hatton, A.T., *Colloids and Surfaces A.*, **1995**, *96*, 1-46 and references therein.

[32] Chari, K., Antalek, B., Lin, M.Y., Sinha, S. K., *J. Chem. Phys.*, **1994**, *100*, 5294-5300.
[33] Goddard, E.D., *J.Am.Oil Chem.Soc.*, **1994**, *71*, 1-16.
[34] Goddard, E.D., 'Interactions of surfactants with polymers and proteins', **1993**, Boca Raton, Fla, CRC Press.
[35] Lin, M. Y., Sinha, S. K., Chari, K., *J.Phys.IV.*, **1993**, *3*, 6.
[36] Cabane, B., Duplessix, R., *J.Phys.*, **1987**, *48*, 651-662.
[37] Cabane, B., *Colloids Surf.*, **1985**, *13*, 19-33.
[38] Francois, J., Dayantis, J., Sabbadin, J., *Eur.Polym.J.*, **1985**, *21*, 165-174.
[39] Nikas, Y. J., Blankschtein, D., *Langmuir.*, **1994**, *10*, 3512-3528.
[40] Schick, M. J., 'Nonionic Surfactants: Physical Chemistry, Surfactant Science', series Vol. 23, Marcel Dekker, Inc., **1987**, USA.
[41] Li, Y.J., Xia, J.L., Dubin, P.L., *Macromolecules.*, **1994**, *27*, 7049-7055.
[42] Li, Y. J., Dubin, P. L., Havel, H. A., Edwards, S. L., Dautzenburg, H., *Macromolecules.*, **1995**, *28*, 3098-3102.
[43] Guillemet, F., Piculell L., Nilsson, S., Djabourov, M., Lindman B., *Prog.Colloid Polym. Sci.*, **1995**, *98*, 47-50.
[44] Guillemet, F., Piculell L., *J.Phys.Chem.*, **1995**, *99*, 9201-9209.
[45] Gelman, R. A., Barth, H. G.,: *Adv.Chem.Ser.*,**1986**, *213*, 101-110.
[46] Gelman, R. A., Barth, H. G., *Polym.Mater.Sci.Eng.*, **1984**, *51*, 556-560.
[47] Varelas, C. G., Steiner, C. A., *Stud.Polym.Sci.*, **1990**, *8*, 259-273.
[48] Dualeh, A. J., Steiner, C. A., *Macromolecules.*, **1990**, *23*, 251-255.
[49] Loyen, K., Iliopoulos, I., Olsson, U., Audebert, R., *Prog.Colloid Polym. Sci.*,**1995**, *98*, 42-46.
[50] Magny, B., Iliopoulos, I., Audebert, R., Piculell, L., Lindman, B., *Prog.Colloid Polym. Sci.*, **1992**, *89*, 118-121.
[51] Magny, B., Iliopoulos, I., Zana, R., Audebert, R., *Langmuir.*, **1994**, *10*, 3180-3187.
[52] Sarrazin-cartalas, A., Iliopoulos, I., Audebert, R., Olsson, *Langmuir.*, **1994**, *10*, 1421-1426.

[53] Whitesides, T. H., Miller, D. D., *Langmuir.*, **1994**, *10*, 2899-2909.
[54] Li, Y., Ghoreishi, S.M., Warr, J., Bloor, D.M., Holzwarth, J.F., *Langmuir*, **1999**, *15*, 6326 - 6332
[55] Li, Y., Bloor, D.M., Penfold, J., Holzwarth, J.F., Wyn-Jones, E., *Langmuir*, **2000**, *16*, 8677-8684
[56] Purcell, I.P., Lu, J.R., Thomas, R.K., Howe, A.M., Penfold, J., *Langmuir,* **1998**, *14,* 1637
[57] Lu, J.R., Thomas, R.K., Penfold, J., *Advances in Colloid and Interface Science:* **2000**, *84*, 143-304
[58] Cabane, B., Duplessix, R., *Colloids Surf.*, 1985, **13**, 19.
[59] Cabane, B., Duplessix, R., *J. Phys.*, 1987, **48**, 651.
[60] Cabane, B., and Duplessix, R., *J. Phys.* **1987**, *48,* 651
[61] Bury, R., Desmazières, B., Treiner, C., *Colloids and Surfaces A*: **1997,** *127*, 113-124
[62] Griffiths, P.C., Stilbs, P., Howe, A.M., Cosgrove, T., *Langmuir,* **1996**, *12*, 2884-2893
[63] Folmer, B.M., Kronberg, B., *Langmuir,* **2000**, *16,* 5987-5992
[64] Whitesides, H., and Miller, D., *Langmuir*: **1994**, *10*, 2899
[65] Nikas, Y.J., Blankschtein, D., *Langmuir*: **1994**, *10*, 3512
[66] Sesta, B., D'aprano, A., Segre, A.L., Proietti, N., Langmuir, **1997**, *13*, 6612-6617
[67] Cabane, B., Duplessix, R., *J. Phys. (Paris),* **43**, 1529, **1982**
[68] Fennell Evans, D., Wennerstrom, H., 'The Colloidal Domain', VCH Publishers Inc., 1994.
[69] Smitter, L.M., Torres, M.E., Miller, A.J., Sáez, A.E., *J. Coll. Int. Sci.* **2001**, *244*, 164-172
[70] Shirahama, K., Liu, J., Aoyama, I., Takisawa, N., *Colloids and Surfaces A*: **1999**, *147*, 133-138

Chapter 2

2.1 Context

A number of methods can be used to investigate the properties of surfactants and polymers in solutions, utilising the different features of such systems in solution, such as the presence of hydrophobic domains, or interfaces. Since techniques utilise different properties, the correlation between results derived from different methods may not be precise. In this study a wide range of methods were employed to map the physical properties of the surfactant and polymer solutions in water and water/ethanol mixtures and comparison of the use and correlation of each technique is given within the analysis.

2.2 Surface tension theory

Behaviour of molecules at the surface of a liquid provides a useful and accurate insight into the properties of the molecules under investigation, as conditions such as temperature, concentration and solvent are changed.[1]

Molecules located at the surface of a liquid are subject to different forces from those that are located in the bulk of a solution. Bulk molecules are subject to equal forces of attraction acting in all directions, whereas molecules on a liquid-air interface experience an inbalance in attractive forces which result in a net inwards pull to the solution. This 'film' on the surface makes it more difficult to move an object through the surface than through the bulk solution.

The surface therefore has a higher free energy than the bulk solution and this can be quantified as a measurement of energy/area. The surface tension can be quantified as a force/length measurement.

A surface consists of two phases, such as liquid-liquid or liquid-gas. The liquid-air interace is considered in this study. Polar liquids such as water have strong intermolecular interactions and thus a high surface tension. Various factors will influence surface tension, for example, an increase in temperature, or addition of organic molecules will lower the surface tension.

2.2.1. Addition of solutes

When surfactants or other amphiphilic molecules such as polymers are added to solution, they will adsorb at the air-liquid interface. This will change the energies of the interface and thus it's surface tension.

As discussed in chapter 1, the work, dW needed to change the surface area, A of a sample by an infinitesimal amount dA is given by,

$$dW = \gamma dA \qquad \text{Equation 2.1}$$

The relative adsorption, Γ, of a solute at the liquid-air interface is related to surface tension through the Gibbs equation.

The proportionality constant, γ is the surface tension.

$$\Gamma = -\frac{1}{RT}\frac{d\gamma}{d\ln a_2} \qquad \text{Equation 2.2}$$

Where a_2 is the activity of the solute in the bulk. Since surfactant concentration below the cmc is very low, the solute activity can be replaced by the solute concentration, c_2.

$$\Gamma = -\frac{1}{RT}\frac{d\gamma}{d\ln c_2} \qquad \text{Equation 2.3}$$

The surfactant adsorption can be obtained from the slope of the surface tension vs the logarithm of the concentration[2].

Addition of a solute such as ethanol decreases the surface tension of water steadily with increasing concentration. This is due to the preferential adsorption of ethanol molecules on the liquid-air interface. This effect was important in this study since there reaches a point where the ethanol content is high enough to lower the surface tension of the solvent so much that the addition of polymer or surfactant does not reduce the surface tension much further. This means that at higher ethanol content, it is not possible to track CMC points (if they are occurring) because the surface tension curves are too shallow. Thus this limits the use of surface tension as a technique for measuring the CMC across a range of water/ethanol mixtures.

Addition of surfactants or amphiphilic polymers to a solvent such as water shows a large decrease in the surface tension, at very low concentrations up to the Critical Micelle Concentration (CMC). After reaching the CMC, the surface tension remains approximately constant. The presence of contaminants in solution such as organic impurities, can cause a dip in the curve around the CMC, rather than a clean break.

Electrolytes increase surface tension by the negative adsorption of ions at the air-liquid interface. This is often seen with SDS where dodecyl impurities (a by-product of SDS synthesis) are more surface active than the surfactant, until the point where they are absorbed into micelles, resulting in an increase in the surface tension before it plateaus off.

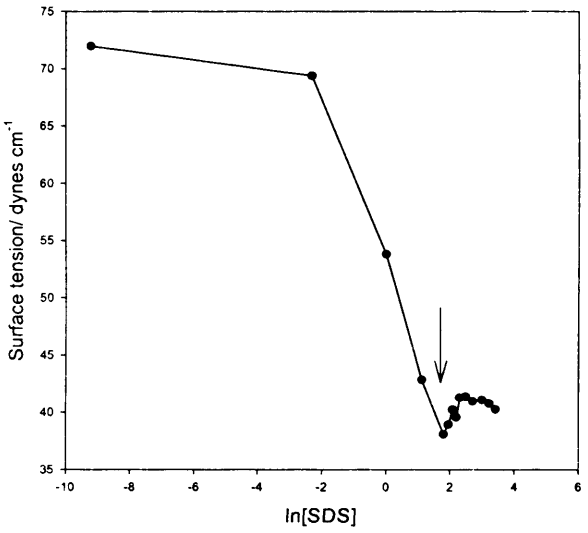

Figure 2.1: A surface tension curve for SDS in water containing a dodecanol impurity, resulting in a dip around the CMC.

2.2.2. Measurement of Surface tension

There are a number of methods for measuring surface tension, with the two most common[2] being the Wilhelmy Plate and the De Nöuy ring. The De Nöuy ring method is employed in this study. This essentially consists of a small (1cm diameter) platinum ring hung from a zero displacement balance. After allowing time for the solution to equilibrate, the liquid is slowly lowered.

A meniscus forms around the circumference of the ring and a downwards force is felt by the ring due to the surface tension. The ring raises the meniscus of the liquid as it moves, until the meniscus tears from the ring.

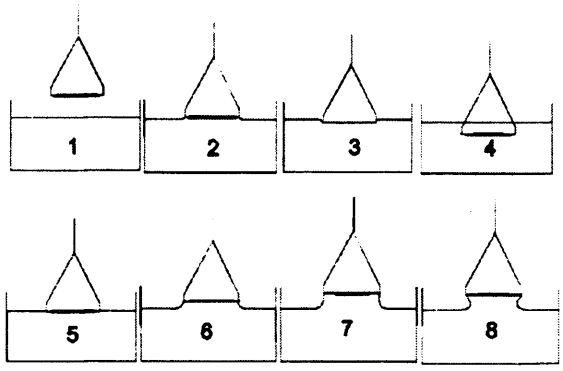

Figure 2.2: The De Nöuy ring method for measuring surface tension.

A zero displacement feedback loop maintains the position of the ring and, force on the balance is measured in millivolts and this is then converted into mNm^{-1} or dynes cm^{-1}.

During this process, the force exerted on the ring as the meniscus pulls it downwards, goes through a maximum and then begins to decrease shortly before the ring is released from the liquid.

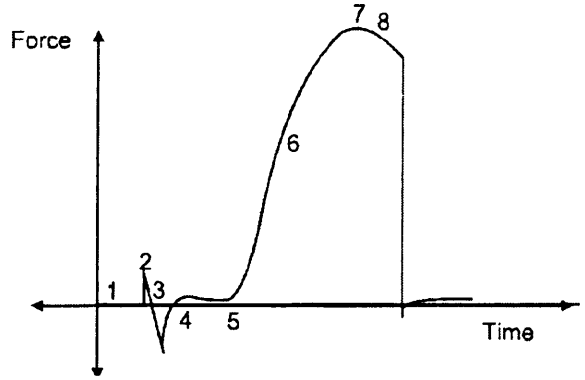

Figure 2.3: Force vs time as a De Nöuy ring is lowered into a liquid and then removed.

The voltammeter reading passes through a maximum shortly before the ring is released from the liquid, which can then be converted to the surface tension, γ, by;

$$\gamma = \frac{\beta F}{4\pi R} \qquad \text{Equation 2.4}$$

where β is the correction factor, which allows for non-vertical tension forces within the liquid and the distorted shape of the liquid at the point of ring release, F is the force acting on the ring and R is the mean radius of the ring. The nature of β depends on the dimensions of the ring and nature of the interface[3].

The requirement for such a correction factor is removed by using a zero-displacement balance, which was employed in this study. When using a zero-displacement balance, the voltammeter records the voltage required to maintain the position of the ring as the liquid is lowered on a moveable platform i.e. it prevents the ring from being drawn down with the liquid as it moves.

The surface tension, γ, of pure water is known to be 71.97 dynes cm^{-1} at 25°C. A standard measurement in mV is taken for pure water and multiplied by a constant to give the correct value of γ. All subsequent solution measurements are also multiplied by this constant. All measurements were taken at room temperature.

The balance is calibrated by using water and a number of water/ethanol mixtures of known surface tension values. The maximum voltage is recorded for each water/ethanol mixture and plotted against their known surface tension values (dynes cm^{-1} or mNm^{-1}), giving a straight line with a slope equal to the normalisation factor specific to the instrument. In this study the normalisation factor is in the order of 326

+/- 10. The conversion factor of dynes cm^{-1} and mNm^{-1} is unity, so these units are interchangeable.

The surface tension measurements commenced with a stock solution. A $10cm^3$ aliquot was used for each data point and the solution diluted to the appropriate concentration in a single volumetric flask to minimise errors. The surface was given time to equilibriate before measurements were taken. Each data point represents the average of 2-3 concordant results (within 1-3%).

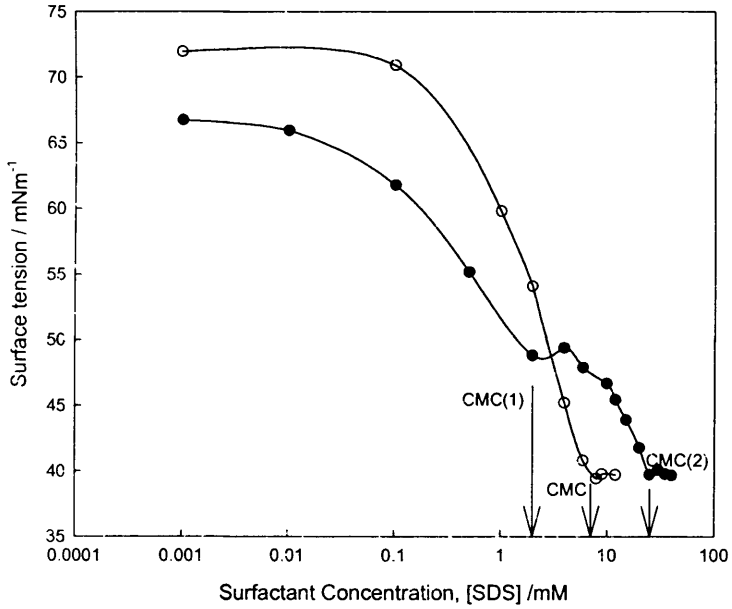

Figure 2.4: Surface tension curves for purified SDS in water, showing the CMC (open circles), and purified SDS with PVP in water showing CMC 1 and CMC 2 (closed circles.)

2.3 Viscometry

Rheology is the study of deformation of matter resulting from the application of force. Whereas solids deform and regain their shape when force is removed, gases and

liquids will flow upon application of force. Within certain parameters, this property is measureable and provides a useful technique for cross referencing values obtained through other techniques. Viscosity is described as Newtonian when the shearing force per unit area, σ, between two parallel planes of liquid in relative motion is proportional to the shear strain rate, γ. The proportionality constant is known as the viscosity.

$$\sigma = \mu\gamma \qquad \text{Equation 2.5}$$

Two common methods used for rheometric measurements on fluid systems are capillary (tube) and rotational. For a simple Newtonian material as described above, an Ostwald U-tube capillary viscometer[4,5,6] is used, as in this study.

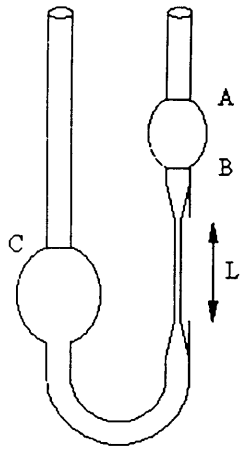

Figure 2.5: An Ostwald U-Tube Viscometer. A and B are timing marks, C is a filling mark.

The liquid is added to the viscometer until it reaches point C, (figure 2.5). The liquid is then drawn up the right arm using a pipette bulb until it is *above* point A. The bulb is then removed and as the liquid moves down the viscometer, the meniscus is timed

as is crosses point A until it reaches point B, (L is the length of the internal capillary section).

The pressure 'driving the liquid through the capillary' at any time during the experiment is directly proportional to the density of the substance. Poiseulle's Law relates flow time *t*, to the liquid's viscosity, η.

$\eta = k\rho t$ Equation 2.6

where η is the viscosity of the solution, *k* is the viscometer constant (calculated by calibration with pure water), ρ is the density of the solution and *t* is the flow time.

The dimensionless "relative viscosity" is the ratio of the sample viscosity to the solvent's viscosity;

$$\eta_r = \frac{\eta}{\eta_s} = \frac{t}{t_s}$$ Equation 2.7

Where η_s is the solvent viscosity and t_s is the time of flow of the solvent from A to B.

The specific viscosity is a measure of the thickening effect (or increase in viscosity) of the addition of polymer to the solution as compared to the pure solvent. From the measured viscosity of polymer solutions at various concentrations the specific viscosity is calculated using equation;

$$\eta_{sp} = \frac{\eta - \eta_s}{\eta} = \frac{(t - t_s)}{t}$$ Equation 2.8

where η_{sp} is the specific viscosity, η is the viscosity of the polymer solution (measured), η_s is the viscosity of the solvent, t is the efflux time of the polymer

through the capillary in the Ostwald viscometer and t_s is the efflux time for the solvent.

2.4 Fluorescence techniques

A range of techniques and probes were used to explore the systems through fluorescence. Exploring the microenvironment of the 8-anilino-1-naphththalene sulfonic acid (ANS) or pyrene probes was used to gauge the CMC[7], whilst quenching with $[Ru(bipy)_3]Cl_2$ probe and 9-methyl anthracene quencher was used to estimate the aggregation number[8] of the SDS and SDS-PVP systems. The addition of probes does not significantly alter the composition of the system or the process of micellisation and provides an accurate and useful way to investigate micellar solutions. The theoretical background of these techniques will be discussed in this section.

2.4.1 Theory of fluorescence spectroscopy

Spectroscopic methods utilise the characteristic absorption or emission frequencies of molecules to extract information on molecular states or the environment of irradiated molecules that are used as probes.

Where a molecule is irradiated with electromagnetic radiation within the ultraviolet to visible region, the energy of the incident photon may be transferred to the atoms or molecules in a number of ways, raising them from their ground state to an excited state of higher energy. The absorbed energy may then be lost in a number of ways, for example through vibrational, rotational, or electronic transitions[9].

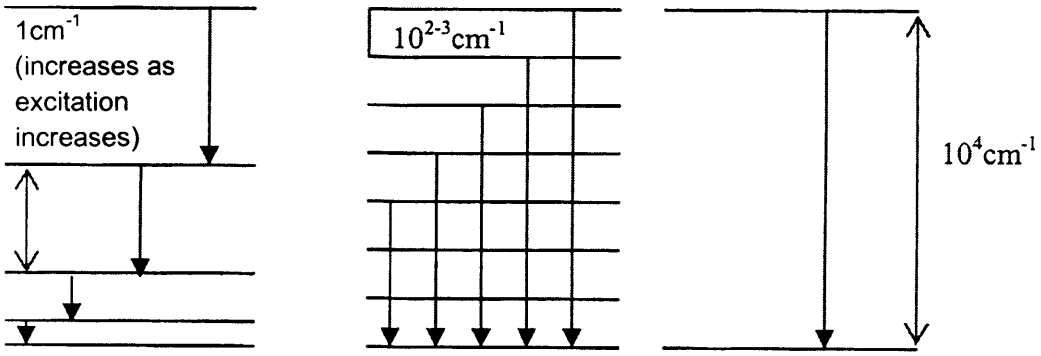

Figure 2.6a A diagrammatic representation of the quantized energy transitions; rotational, vibrational and electronic transitions, respectively.

The Jablonski diagram below (figure 2.6b) depicts the possible energy transitions between energy levels of an atom or molecule that lead to the characteristic absorption or emission spectra. A Jablonski diagram is essentially a Potential Energy (Ep) diagram which shows the relative positions of the electronic energy levels in a molecule[5].

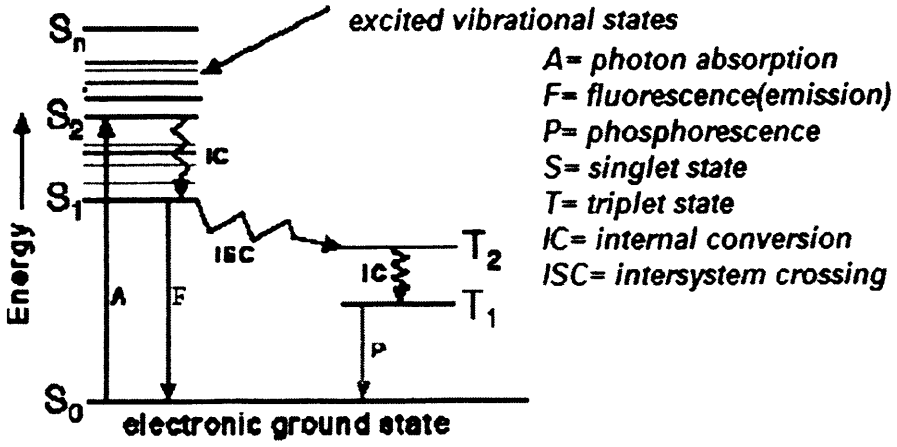

Figure 2.6b: A Jablonski diagram showing possible transitions between different electronic levels. This study focuses on fluorescence.

The fluorescence emission is characterised by the transition from the lowest vibrational mode of the electronically excited state to the ground state, ie through relaxation of the molecule. Selection rules state which transitions are allowed or forbidden (i.e. an indication of how likely it is that such transitions will occur).

Vibrational relaxation occurs in accordance with the Boltzmann Distribution. Molecules in a high vibrational state will lose energy to regain thermal equilibrium as the molecule cascades down the vibrational energy levels to the lowest vibrational state.

Four basic steps are involved in fluorescence[5]:

- Initial absorption of radiation, promoting a molecule to an excited state
- The excited molecule undergoes collisions with neighbouring molecules and loses energy
- The energy loss induces the molecule to drop down the vibrational energy levels by radiationless decay
- When the molecule reaches the lowest vibrational level of the excited state, further collisions cannot release energy in defined quanta so it will spontaneously emit it's energy as radiation i.e. it will fluoresce.

Energy may only be absorbed and emitted in discrete quanta,specific to individual molecules or atoms according to their structure or environment, thus allowing interpretation of the characteristic frequencies of molecules or probes, identifying any changes to the environment.

A limited number of molecular species are capable of relaxing by fluorescence and these are mainly rigid organic and aromatic structures which have relatively slow radiationless relaxation mechanisms. The intensity of the fluorescence emission is dependant upon a quantum efficiency factor, determined by a number of structural factors, including the solvent and environment of the molecule. It has been shown that fluorescence, using a number of probes is a useful and accurate method for measuring surfactant-surfactant and polymer-surfactant interactions and provides results analagous to those given by other methods[10].

2.4.2 Fluorescent probes and π^*–π^* transitions

Fluorescent probes such as pyrene and aniline derivatives consist of mainly conjugated molecules, allowing delocalisation of π electrons around the molecule. Absorption of radiation by a carbon=carbon double bond excites an electron from a π orbital to π^* antibonding orbital. This absorption usually lies in the UV region. Since molecular orbitals in a conjugated molecule are closer together than unconjugated molecules, less energy is required to complete the transition. Thus, longer wavelengths within the visible spectrum are usually sufficient for transitions to occur.

The probes used in this study were pyrene and 8-anilino-1-napthalenesulphonic acid, ANS.

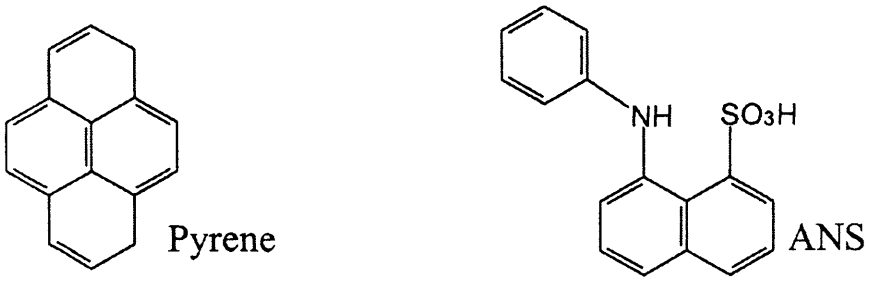

Figure 2.8: Pyrene and ANS probes

2.4.3 Pyrene probe

Pyrene has a number of photophysical properties which are well documented. Pyrene's suitability as a probe is due to it's long life time of pyrene monomers and the efficient formation of eximers. The fluorescence intensities for various vibronic fine structures in the pyrene monomer fluorescence show a strong dependence[11] on the solvent environment. The distinct features of the vibronic fine structure signify accurately changes to the surroundings of the pyrene molecules. Since pyrene is a strongly hydrophobic probe and has very poor solubilisation in water (2-3μM at 25°C), it will preferentially solubilize in the hydrophobic core of micelles.

Pyrene possesses five vibrational bands that exhibit a strong sensitivity to the polarity of the environment.

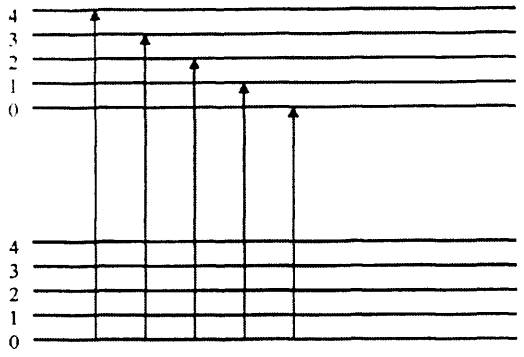

S_1, excited state

S_0, Ground state

Figure 2.9: Electronic transitions possible on absorption in a pyrene molecule

The ratio of the fluorescence intensity of the highest energy vibrational band (I_i) at approximately 372nm, to the intensity of the third highest band (I_{iii}) at 385nm, undergoes significant changes as the environment of the molecule is altered[10]. The band I_{iii}/I_i ratio has been shown to correlate with solvent polarity for a range of solvent structures including hydrocarbons (ca. 0.6), ethanol (ca. 1.1) and water (ca. 1.6). The intensity enhancements in polar solvents of some vibronic band frequencies that are normally forbidden by selection rules suggest some specific solute-solvent dipole-dipole mechanisms playing a role due to the influence of the solvent as a dielectric medium. This is well understood and widely documented and thus the I_{iii}/I_i ratio of pyrene serves as a good measure of the solvent polarity and is especially useful in tracking the point of CMC in micellar systems.

At concentrations below the CMC, no micelles are formed and the spectrum is derived from pyrene in solvent, giving a ratio of around 0.5-0.6. The five vibronic peaks on the pyrene spectra are due to electron transitions from excited vibrational states back to their ground states[12].

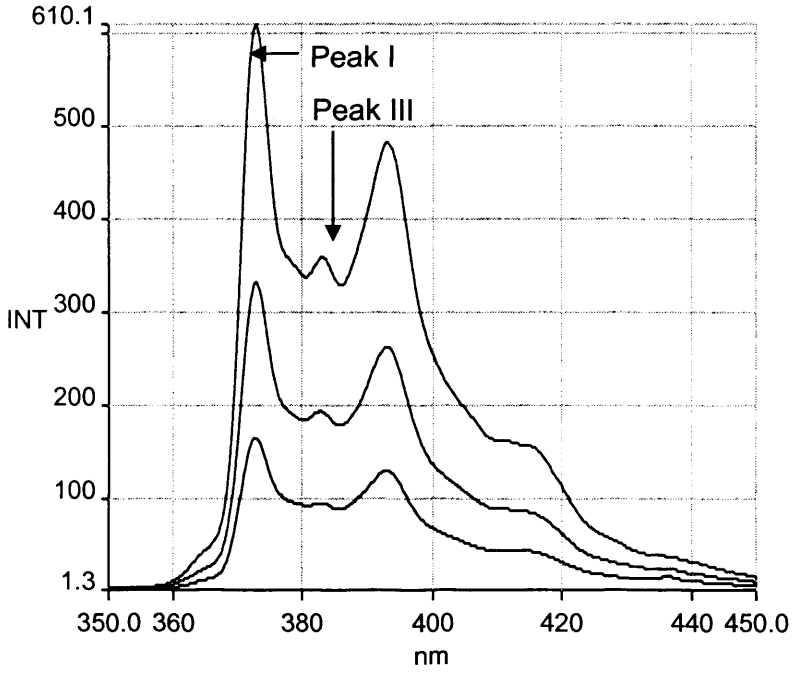

Figure 2.10: Direct spectrum of intensity vs wavelength for pyrene in water (bottom), 5% ethanol (middle) and 10% ethanol (top), showing the increase in polarity of the solvent as ethanol content increases.

As surfactant concentration increases, a sharp increase in the I_{iii}/I_i ratio marks the CMC as the pyrene moves from solution into the micelles[13]. That is, the I_i peak decreases as the I_{iii} peak increases. Depending on the amphiphile under investigation the ratio can increase to around 0.8 – 0.95.

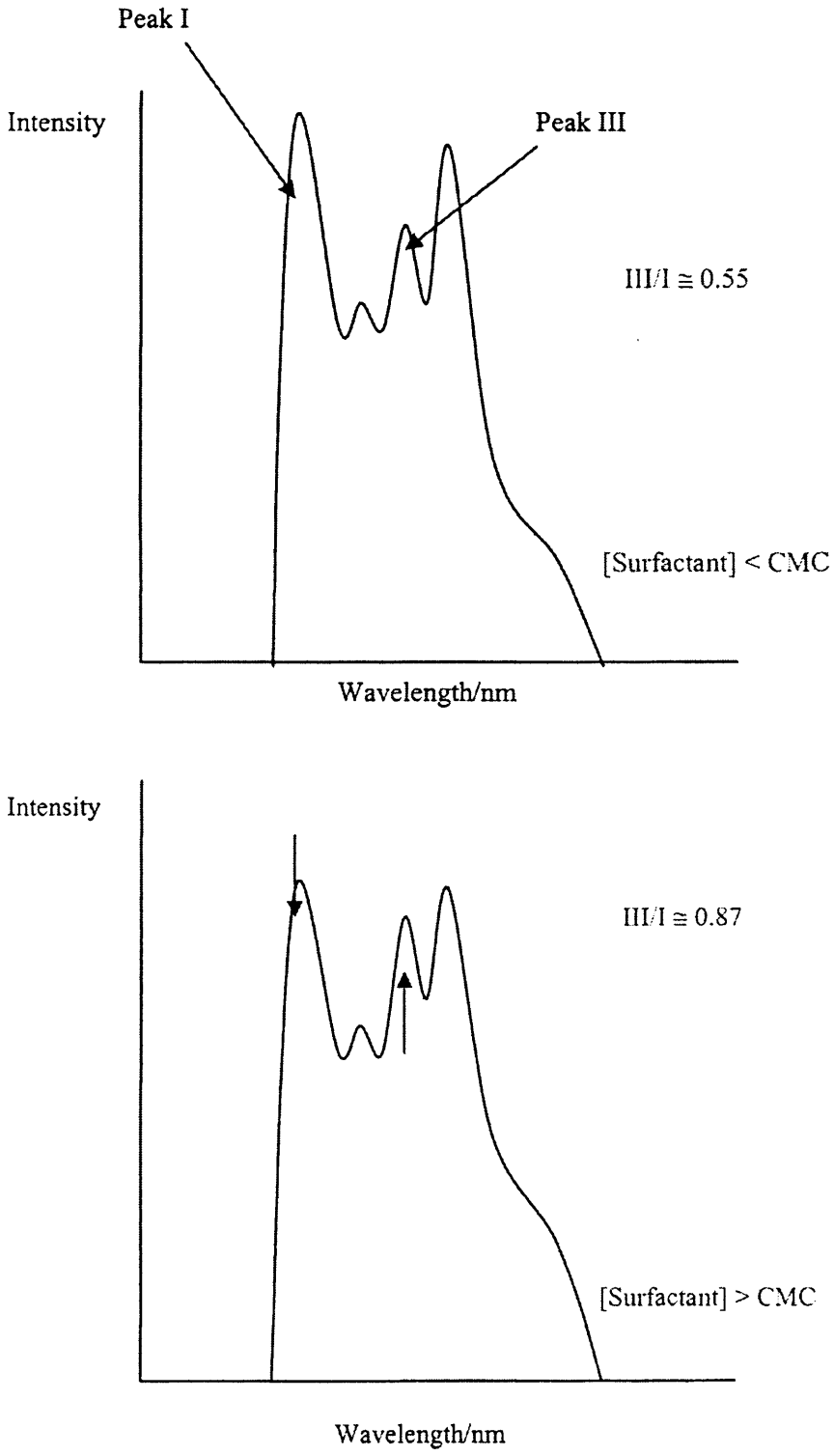

Figure 2.11:Representation of the change in I_{iii}/I_i ratio at concentrations below the CMC and concentrations above the CMC

2.4.4 ANS – 8-anilino-1-naphththalene sulfonic acid probe

The fluorescence probe 8-anilino-1-naphththalene sulfonic acid (ANS) is frequently used in micellar systems. ANS behaves in such a way as to provide a qualitative indication of the polarity of the probe environment[14]. The probe is not considered to perturb the structure of the micelle significantly[15] since estimates of the CMC of SDS measured by ANS fluorescence compare favourably with those determined by other techniques.

For alkyl chain lengths greater than the octyl, ANS associates predominantly with the micelle and executes rapid motion between the polar shell of the palisade layer and the surrounding aqueous pseudophase (i.e. it associated mainly with the region of the micelle occupied by hydrated headgroups)[16]. The fluorescence intensity of ANS increases with increasing hydrophobicity, and thus, the measured fluorescence is an average of the intensity within the polar shell and in the aqueous pseudophase[17]. At concentrations below the CMC, the fluorescence intensity is low and independent of concentration of both surfactant and polymer. As the surfactant concentration passes through the CMC, micelles form, and a sharp increase in fluorescence intensity is seen. This has been shown to be due to the preferential solubilisation of the ANS into the polar shell of the micelle.

All fluorescence measurements were carried out using a Perkin-Elmer LB 50 Luminescence spectrophotometer with a temperature controlled sample holding area. In this study the fluorescence probe 8-anilino-1-naphthalene sulphonic acid

(ANS) was used to probe the SDS-PVP systems in order to obtain the CMC(1) and CMC(2) values, and to probe the SDS systems to obtain the CMC. The equilibriated sample was excited at 320nm and the fluorescence emission intensity measured as a function of surfactant concentration by integration of the emission intensity between 490 and 520nm[16].

Pyrene probe was used for P104 and SDS in order to obtain the CMC values. When using pyrene, the equilibriated sample is excited at 310nm and the ratio of the peaks I_{iii}/I_i is used to investigate the hydrophobicity of the system, allowing measurement of the CMC.

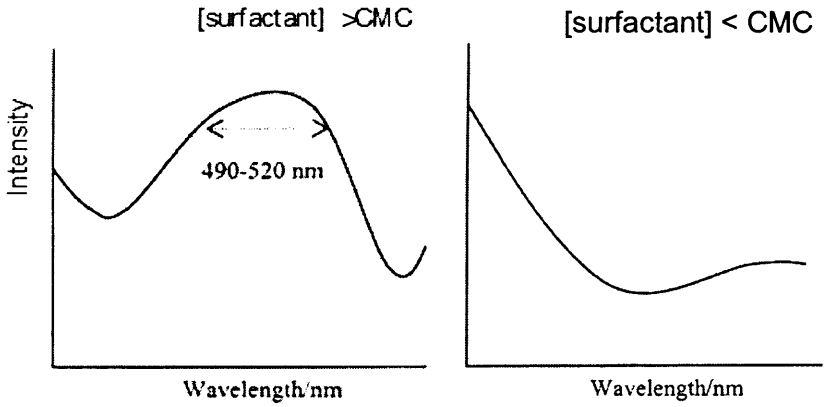

Figure 2.12a: A diagramatic representation of an ANS spectrum above and below the CMC

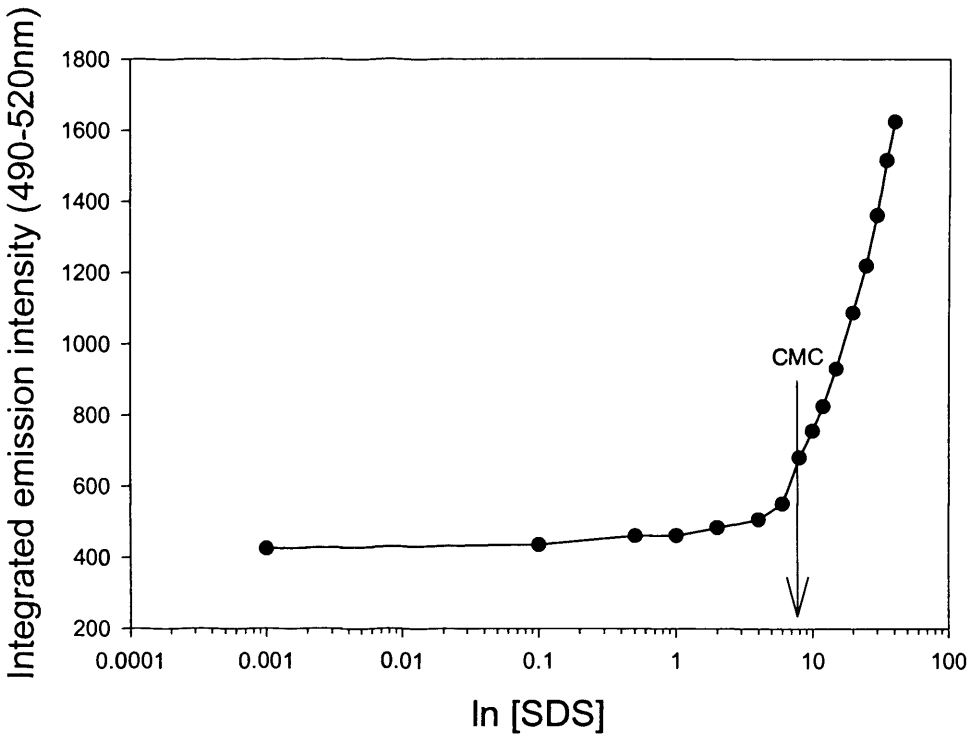

Figure 2.12b: ANS spectrum of integrated emission intensity across a range of [SDS] showing the break of the curve coinciding with the CMC

2.4.5 Fluorescence Quenching

The technique of fluorescence quenching provides a method for measuring micellar aggregation numbers. The emission from a fluorescent probe (P) is quenched using a quencher (Q). To allow for straightforward results and analysis, P and Q are chosen to have a high affinity for the micelles in the system being studied. The quencher is added to a system containing known amounts of surfactant and probe.

Quenching will only occur when P and Q are in close proximity i.e. when both P and Q are located within a micelle.

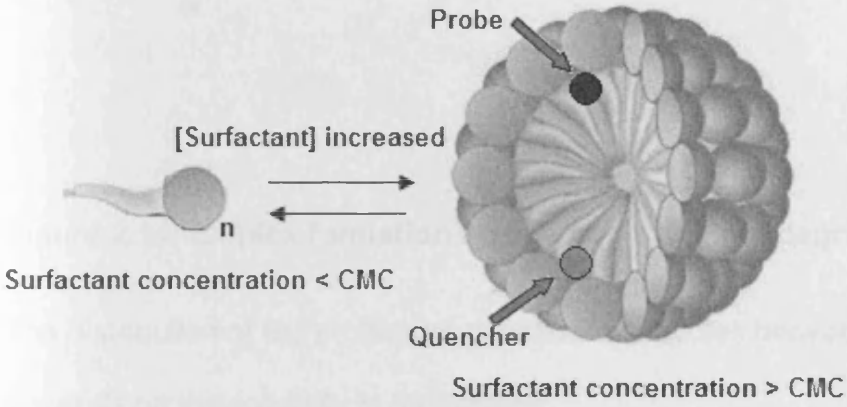

Figure 2.13 Representation of probe and quencher within micelles.

There are two main pathways through which quenching may occur. One is where the probe and quencher collide resulting in an energy transfer.

$$P^* + Q \rightarrow P + Q^* \qquad \text{Equation 2.9}$$

The * indicates that the molecule is in the excited state. This energy transfer may only occur if the quencher is at a lower energy state that the probe.

The second pathway involves an intermediate, an excited complex, or exiplex, consisting of the probe and the quencher. The exiplex may exist as a new complex of the probe and quencher molecules or it may be transient in which case the two will then separate.

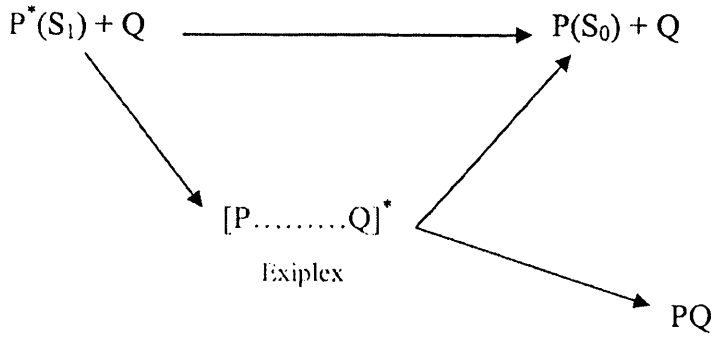

Figure 2.14: Exiplex formation and its two routes of degradation

The distribution of the probe and quencher molecules between solvent and micelles depends on the solubility in the solvent.

For simplicity, a number of assumptions have been made:

1. At concentrations above the CMC both molecules are entirely solubilised in the micelles and are insoluble in the solvent.

   Hence, $[Q]_{mic} \cong [Q]_{total}$

2. The probe is quenched instantaneously in the presence of quencher and will not fluoresce.

   ∴ decrease in fluorescence is directly proportional to the number of micelles containing P and Q.

3. A Poisson distribution amongst the micelles is assumed, with some containing only P, some only Q, some P and Q and some with multiple occupancy of both.
4. The PQ complex does not exist in the ground state.

In these circumstances the ratio of fluorescence intensity, I_o/I_Q is related to the quencher concentration, [Q] and the micellar concentration, C_{mic}.

$$\ln\left(\frac{I_o}{I_Q}\right) = \frac{[Q]}{C_{mic}} \qquad \text{Equation 2.10}$$

Where, I_o is fluorescence intensity in the absence of quencher and I_Q in the presence of quencher.

The micelle concentration is given by the following equation. N_{agg} is the aggregation number and [S] the total surfactant concentration.

$$C_{mic} = \frac{([S]-CMC)}{N_{agg}} \qquad \text{Equation 2.11}$$

Combining these equations gives;

$$\ln\left(\frac{I_o}{I_Q}\right) = \frac{[Q]N_{agg}}{[S]-CMC} \qquad \text{Equation 2.12}$$

Hence a plot of $\ln\left(\frac{I_o}{I_Q}\right)$ vs $\frac{[Q]}{[S]-CMC}$ will have a gradient of N_{agg}.

The aggregation number of the SDS micelles and SDS with PVP was obtained in this study by utilising this method of fluorescence quenching with the probe tris(bipyridyl ruthenium (II) chloride), and hydrophobic quencher 9-methyl anthracene.

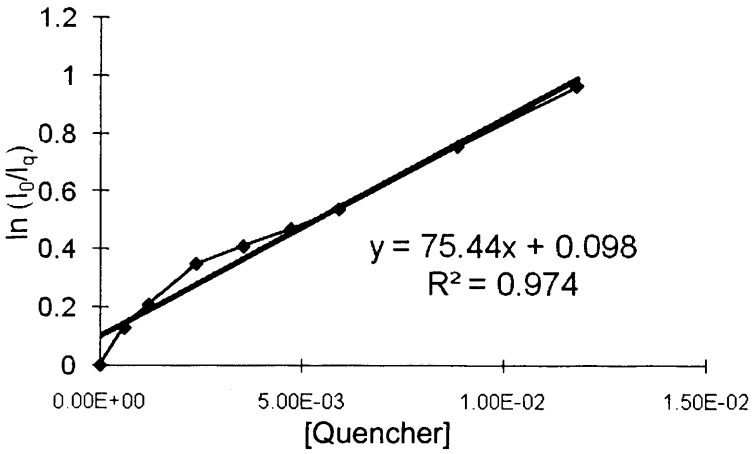

Figure 2.15: Plot of I_o/I_q vs [quencher] for 75 mM SDS in water using quenching of 1μM tris(bipyridyl ruthenium (II) chloride) probe with 9 methyl anthracene. N_{agg} approximately 75.

A solution containing a known amount of surfactant (and polymer) containing 1μM of the probe was quenched with 22mM quencher added in 10 μL aliquots[18,19,20].

It is likely that at higher ethanol concentration the assumption that probe and quencher are insoluble in solvent will not hold, due to the increased hydrophobicity of the solvent. Thus the error involved in calculating the aggregation number will increase with ethanol content.

2.5 Nuclear Magnetic Resonance (NMR)

NMR is an extremely powerful and versatile analytical technique[21]. The characteristic spectrum yields very detailed information on both structural and dynamic features of a system, correlating to individual atoms within a molecule. NMR is advantageous with regard to there being no need to add probes or isotopic labels in order to examine the system under investigation, and is a non-invasive technique.

A number of multi-pulse experiments exist which excite the sample with an intense pulse of radiation, followed by Fourier Transform analysis of the emitted signals. Advantages of pulse techniques over continuous wave techniques include time efficiency and accumulation of scans to reduce signal to noise ratio.

2.5.1 Nuclear Magnetic Moments

Nuclear magnetic resonance occurs because the nuclei of certain atoms possess *spin*. The spin is characterised by the nuclear spin quantum number, ***I***, which may take integer or half integer values i.e. $I = \frac{1}{2}, 1, \frac{3}{2}, 2, \ldots$ according to the expression;

$$I = \sqrt{I(I+1)}\left(\frac{h}{2\pi}\right) = \sqrt{I(I+1)}\ units \qquad \text{Equation 2.13}$$

h is planck's constant.

Nuclei with $I = 0$ are not amenable to NMR observation, although there may be isotopes of atoms with spin that can be observed using NMR. The most useful is $I = \frac{1}{2}$ and as such, the most commonly studied atoms are ^{1}H and ^{13}C.

Nuclei that possess spin therefore have angular momentum and all nuclei have a charge. The spinning charge will have a weak magnetic field associated with it i.e. they possess a magnetic moment, μ.

When these nuclei are placed in an external magnetic field, they will experience a torque, which forces them into precession about the axis of the external field (consequently the magnetic moment vector cannot lie exactly in the direction of the field). This is known as Larmor precession and occurs at the Larmor frequency, ω_o, which is directly proportional to the strength of the applied field, $\boldsymbol{B}$.

$$\omega_o = \gamma B \qquad \text{Equation 2.14}$$

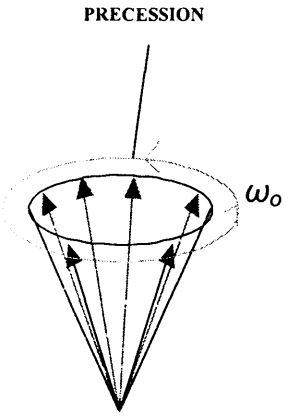

Figure 2.16: When a field is applied, the nuclei will precess about the axis of the field at the Larmor frequency.

The nuclei posessing a magnetic moment is acted upon by the external magnetic field and can take up $2I+1$ possible orientations in this field. Thus atoms with $I = \frac{1}{2}$ may align themselves in two ways; parallel to the field, (the lower energy state, α) or anti-parallel, (higher energy state, β). In the absence of an external magnetic field,

the $2I+1$ components are degenerate i.e. they have the same energy. When a field is appled, $2I+1$ energy levels result, those aligned parallel to the field have a slightly lower energy, according to the Boltzman distribution. This results in a bulk magnetisation vector, *M*, parallel to the direction of the applied field and referred to as the *z*-axis.

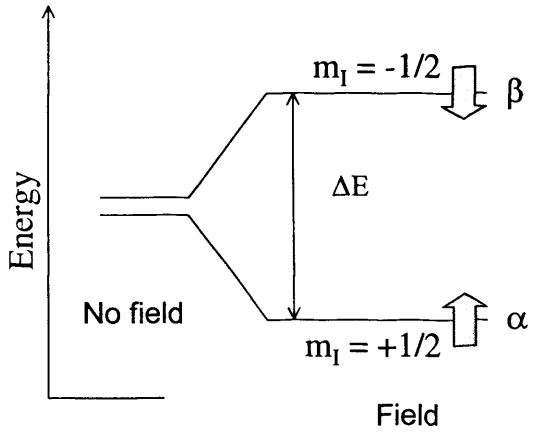

Figure 2.17: Energy levels of a spin ½ nucleus. Nuclear magnetic resonance occurs when the energy of the separation of the levels equals that of the energy of the photons in the electromagnetic field.

These discrete orientations are the only ones allowed due to the quantization of energy levels. The difference in energy levels is expressed by:

$$\Delta E = h\omega_o \qquad \text{Equation 2.15}$$

The difference in population between α and β levels is extremely small (about 1 part in 10^4), and thus a reasonable size of sample of a few miligrams is needed to overcome the lack of sensitivity.

When a field is applied, the spinning nucleus will precess about the direction of the applied field. The nucleus can interact with a beam of electromagnetic radiation, so long as the beam is of the same frequency as the precessing nucleus i.e. nuclear magnetic *resonance* occurs.

Vectors can be used to describe the processes that occur following pulse excitation of a sample. Magnetisation along the z-axis is longitudinal magnetisation. If a second magnetic field is applied for a certain duration perpendicular to the first field (along the x-axis) then the this field, B_x, will cause the net magnetization vector to precess into the x-y plane.

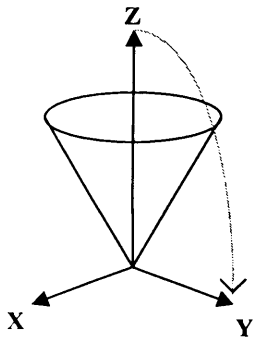

Figure 2.18: Net magnetization is placed in the x-y plane

This is known as a 90° pulse and equalises the populations of the α and β states. Conventionally, the transmitter is aligned along the x-axis and the receiver along the y-axis with the main field in the z-axis. The magnetisation in the x-y plane will rotate at it's Larmor Frequency and this fluctuating magnetic effect induces an oscillating voltage in the receiver coil, creating a signal.

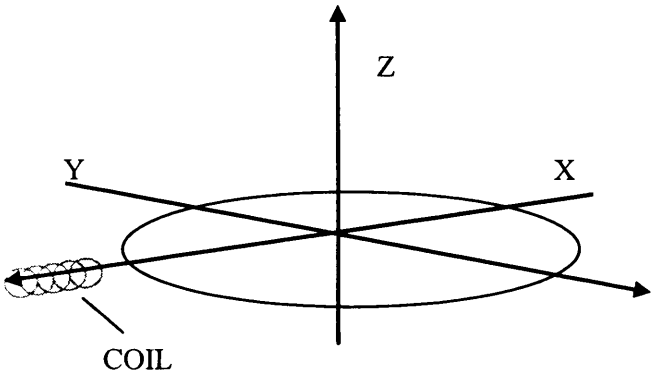

Figure 2.19a During pulsed NMR the transverse magnetization rotates about the Z-axis, and a current in a coil is around the X-axis.

As time passes, the individual spins move out of step (since they precess at different rates) and gradually move back to the z-axis by relaxation. Thus the magnetisation vector shrinks exponentially with a time constant T_2 and induces a weaker signal. The form of signal is the oscillating-decaying free induction decay (FID) which can be Fourier transformed and displayed as the frequency spectrum of the nuclei.

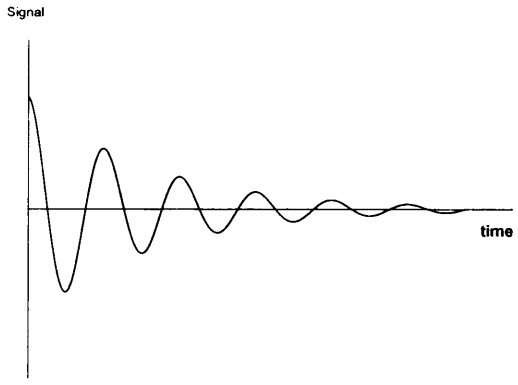

Figure 2.19b The Free Induction Decay signal is formed as the spins dephase during relaxation. This is then converted to an NMR spectrum using fourier transform

Longitudinal relaxation restores the equilibrium populations between high and low energy spin states and hence z-magnetisation. The z-component of magnetisation

reverts to it's equilibrium value M_o with a time constant, the longitundinal relaxation time, T_1.

$$M_z(t) - M_o \propto e^{-t/T_1} \qquad \text{Equation 2.16}$$

This is known as spin-lattice relaxation since it distributes energy to the surroundings (the lattice).

A second aspect of spin relaxation is known as transverse relaxation and this corresponds to loss of bulk magnetisation in the x-y plane (which does not relate to the restoration of equilibrium populations.)

$$M_y(t) \propto e^{-t/T_2} \qquad \text{Equation 2.17}$$

Following the 90° pulse, bulk magnetisation exists in the x-y plane and aligned spins have phase coherence on a macroscopic level. However there will be some variations in the local magnetic environments, leading to small changes in the precessional frequencies, causing 'fanning out' of the magnetisation vector as phase coherence is lost. This results in a spread of frequencies in the final spectrum so that individual resonances have a defined linewidth, instead of being infinitely narrow lines.

2.5.2 Chemical Shift and proton NMR experiments

The strength of the local magnetic field experienced by a proton as a result of an applied magnetic field, depends on the details of the electronic structure near the proton of interest. The nucleus is surrounded by an electron cloud which also circulates in the magnetic field around the nucleus, generating a magnetic field of

their own. This influences the resultant field at the nucleus, *shielding* the nucleus from the applied magnetic field. A small change to the shielding alters the rate at which the nucleus precesses (the Larmor frequency) and thus the frequency required to make the nucleus resonate. These changes to the resonance frequency are in the order of a few kilohertz (compared to an external field strength of hundreds of megahertz). Since the detail required is regarding the difference in frequency between nuclei in differing environments, it is convenient to define the frequency scale as a relative scale.

The chemical shift δ, for any resonance is defined as:

$$\delta = \frac{\nu - \nu_{ref}}{\nu_{ref}} \qquad \text{Equation 2.18}$$

Although this is dimensionless, since the result is of the order 10^{-6}, units of parts per million (ppm) are used. The chemical shift is independent of the applied field strength. The reference compound for ^{1}H and ^{13}C is tetramethylsilane (TMS) although in this study the chemical shifts were referenced to the residual water peak.

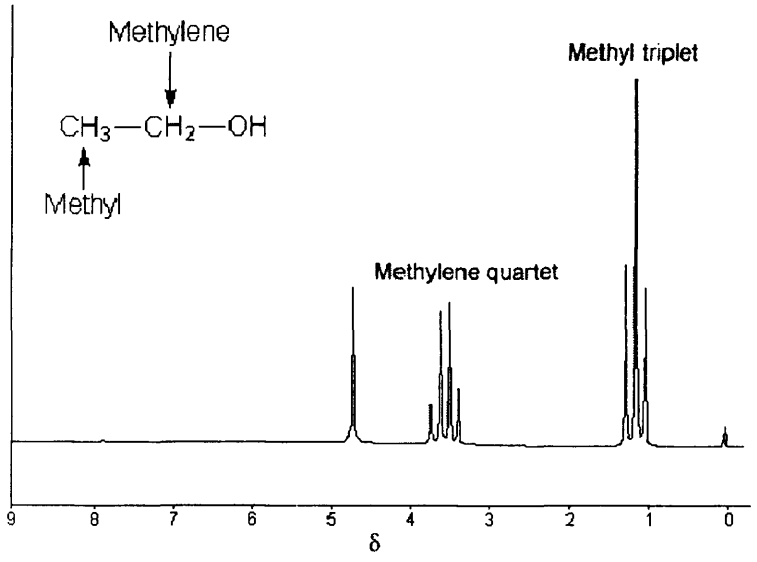

Figure 2.20 NMR spectrum of ethanol showing splitting patterns.

The intramolecular effects of shielding result in substantial changes to the chemical shifts, in most cases, traceable to the structural features of a single molecule. As the shielding experienced by a single proton gets smaller (e.g. by an electronegative neighbour drawing electron density away from the proton), the chemical shift increases.

2.6 Small Angle Neutron Scattering (SANS)

This is a powerful and non-destructive method for the study of micellar systems[22,23]. It has a wide range of applications, including investigation of surfactant micelles, structure and interaction potentials, contrast variation for structure and composition of colloidal solutions, block co-polymer micelles for size and density profile, and polymer/surfactant interactions. SANS can be applied to dilute particles and to concentrated systems to give a view of nanostructure and internal features. Small angle neutron scattering is used to study structures on the 1-100nm scale. SANS contrast variation, particularly substituting deuterium for hydrogen, reveals details in the structure that are not accessible by other techniques.

SANS involves the firing of neutrons at a sample and measuring the angle through which the neutrons are scattered. The neutrons are scattered elastically i.e. the incident energy E_i and final energy E_f, are equal. Neutrons have a wavelength (~10 Å) of the same order of magnitude as the dimension of colloidal systems (10~100nm). Since they are neutral and have negligible dipole moment, they are capable of penetrating matter and interact purely with the nuclei in the sample. SANS is analogous to X-ray diffraction, since neutrons also act as waves, but they are scattered by nuclei rather than electrons.

The SANS measurements were performed on the fixed geometry, time of flight LOQ diffractometer at the ISIS Spallation Neutron Source, Didcot, UK (Picture courtesy of ISIS website.)

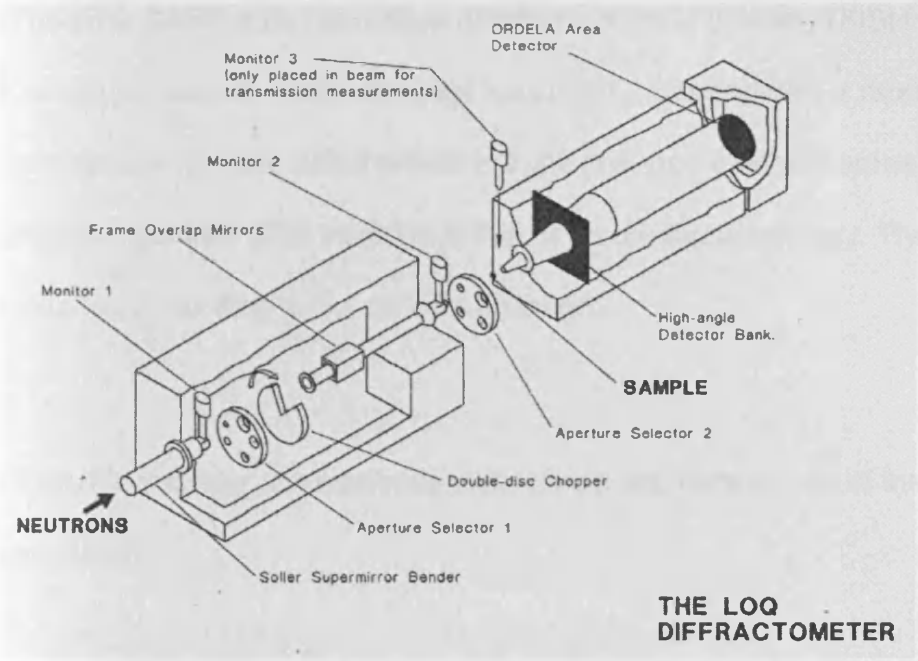

Figure 2.21 The time of flight LOQ diffractometer[24]

Neutron wavelengths of 2→ 10 Å were used. Samples were held in 2mm pathlength quartz cuvettes (Hellma) mounted in Aluminium holders on top of an enclosed computer controlled sample changer. Temperature was kept at 25°C ± 0.2°C and temperature control achieved by use of a thermostatted circulating bath pumping fluid through the base of the sample changer. Measuring times were between 80-120 minutes.

Scattering is normalised for sample transmission and incident wavelength distribution and background corrected using an empty quartz cell. It is also corrected for linearity and efficiency of detector response and the data is put on an absolute scale by reference to a partially deuterated polystyrene blend sample. Deuterated solvent was used for all solvent mixtures.

When the SANS data have been obtained, a fitting strategy (FISH written by R.K. Heenan) is used to obtain the best feasible fit. Starting with a model of the simplest solid sphere, greater detail is built in if the previous model is unreasonable. The chosen model for SDS micelles is that of a core-shell topology. The radius can be assumed according to the chain (tail) length.

From this strategy, the most probable shape and dimensions of the micelle can be concluded.

2.6.1 Neutron production and instrumentation

There are two main methods for producing neutrons, one being fission of Uranium-235 producing a continuous neutron source. The second method of neutron production is spallation as used at ISIS in Oxford where the SANS experiments for this study took place. This uses particle accelerators and synchrotrons to generate intense, high-energy proton beams. The proton beam is directed at a metal target composed of heavy nuclei, in this case tantalum, which blasts the target nuclei apart, producing a pulse of neutrons. A cryogenic moderator slows the neutrons down to provide a suitable range of wavelengths and a well defined pulse structure. This pulsed neutron flux is ideal for the time-of-flight neutron diffraction technique. This measures the time-of-flight, t, taken for a neutron to travel the total flight path, L, from the moderator to the detector, via the sample. Assuming elastic scattering:

$$t = \frac{m_n}{h} L\lambda \qquad \text{Equation 2.19}$$

Where, m_n is neutron mass, h is Plank's constant, L the flight path length and λ the wavelength. $t = 252.82L\lambda$ in the units of Angstroms, allowing the determination of neutron wavelength.

A SANS beam line has a 2D detector in a vacuum tank 2-20m after the sample position, which records the diffraction pattern of the scattered neutrons. A beam stop prevents damage to the central detector elements caused by unscattered neutrons. A pulse shaping 25Hz disc chopper selects wavelengths of 2.2 to 10 Å which are used simultaneously by time-of-flight, allowing for a much greater simultaneous scattering vector, (Q) range. Before reaching the sample, the neutron beam is shaped by apertures to approximately 10mm and a monitor measures the rate at which neutrons are reaching the sample and produces an output proportional to the incident beam and flux structure.

Instrument control, data acquisition and normalisation is all computer based. The scattering angle is calculated by geometry and the wavelength determined by time of flight. Software controlled radial averaging calculates the signal intensity (I(Q,λ)) as a function of scattering angle and wavelength. I(Q,λ) is typically the sum of 10^4 pulses. The λ-dependent transmission of each sample is measured by taking the ratio of the output of two time sensitive monitors placed in front of and behind the sample.

2.6.2 Principles of neutron scattering

The differential scattering cross-section, $(\delta\Sigma/\delta\Omega)(Q)$, is the dependant variable measured in a SANS experiment and contains all of the information on size, shape, and interactions between the scattering centres in the sample. Atomic nuclei are

some 10^4 - 10^6 times smaller than typical neutron wavelengths, and so act as point scatterers for the beam of neutrons. The result of this is that the nuclear scattering remains constant as the scattering angle increases, allowing scattering patterns to be collected over the full range from forward to backward angles. The scattering is spherically symmetric.

Considering two nuclei, A and B, located by vector *r,* for elastic scattering, the quantity Q (the scattering vector or 'wavevector) is the modulus of the resultant wavevector between the incident k_i and scattered k_s wavevectors and its value in nm^{-1} or $Å^{-1}$ is given by;

$$Q = |Q| = |k_s - k_i| = \frac{4\pi n}{\lambda} \sin\left(\frac{\theta}{2}\right) \qquad \text{Equation 2.20}$$

Where *n* is the refractive index of the medium (≈1.0 for neutrons). Thus the modulus Q is the independent variable in a SANS experiment.

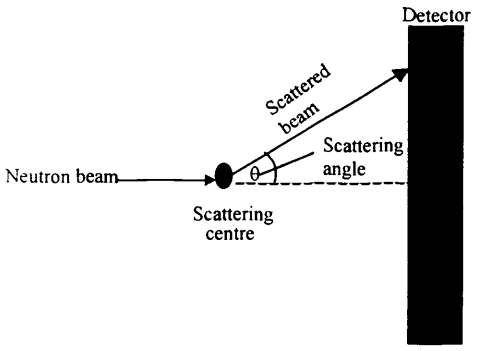

Figure 2.22: Scattering vector, Q

Incident radiation of intensity I_o and wavelength λ, is directed at the sample. Some of the beam with intensity *I*(θ) is then scattered through angle θ to give structural information according to the character of the sample.

Scattered waves from pairs of points in the sample will interfere with each other. Where this is equal to an integer number of wavelengths, this constructive interference meets the Bragg condition.

Substituting equation (X) into Bragg's Law of diffraction (equation 2.21) obtains an expression that allows the size of scattering bodies to be calculated.

$$\lambda = 2d \sin\left(\frac{\theta}{2}\right) \qquad \text{Equation 2.21}$$

$$d = \frac{2\pi}{Q} \qquad \text{Equation 2.22}$$

Where d is a molecular level length scale of approximately 0.6-100nm accessible through the Q-range of the experiment[24]. Q is a reciprocal distance, so at low Q the distances are large compared to high Q.

Nuclei absorb as well as scatter neutrons, so the intensity is normalized to obtain the actual neutron scattering intensity, or flux. This is expressed in terms of wavelength λ, and angle θ:

$$I(\lambda,\theta) = I_o(\lambda)\Delta\Omega\eta(\lambda)T(\lambda)V\left(\frac{\delta\sigma}{\delta\Omega}\right)(Q) \qquad \text{Equation 2.23}$$

Where $I_o(\lambda)$ is the incident flux, $\Delta\Omega$ is the solid angle element, $\eta(\lambda)$ is the detector efficiency (all instrument specific); $T(\lambda)$ is the sample transmission, V is the volume of the sample and $\left(\frac{\delta\sigma}{\delta\Omega}\right)(Q)$ is the differential cross section (all sample dependant [illegible])

The first objective of a SANS experiment is to determine the differential scattering cross section (in cm^{-1}) as a function of the scattering vector since this contains all the

information on size, shape and interactions between the scattering centres (subscript 'p' for particles);

$$\left(\frac{\delta\sigma}{\delta\Omega}\right)(Q) = N_p V_p^2 (\Delta\rho)^2 P(Q) S(Q) + B_{inc} \qquad \text{Equation 2.24}$$

Where N_p is the number concentration of particles, V_p is the volume of one particle, $(\Delta\rho)^2$ is the **contrast** (square of the difference in neutron scattering densities), P(Q) the single particle form, or shape factor and S(Q) the interparticle structure factor, B_{inc} is the incoherent background signal.

2.6.3 Scattering length density, ρ, and contrast

The scattering length density, ρ, gives the degree of interaction between the neutron and nucleus of an atom and may be calculated from the chemical structure of the material:

$$\rho = \sum b \frac{\rho_{bulk} N_A}{M_w} \qquad \text{Equation 2.25}$$

Where ρ_{bulk} is the bulk density of the scatterer, N_A is Avogadro's number, M_w is the molecular weight and b is the coherent neutron scattering length of the nucleus. Only coherently scattered neutrons carry structural information about the sample. ρ has dimensions of (length)$^{-2}$ and units of 10^{10} cm^{-2} or 10^{-6} Å^{-2}.

The contrast is the difference in ρ values between that part of the sample (scatterer) of interest, ρ_p, and the surrounding medium or matrix, ρ_m, all squared; i.e., $(\Delta\rho)^2 = (\rho_p - \rho_m)^2$. If $(\Delta\rho)^2$ is zero then there is no scattering and the scattering bodies are said to be at *contrast match*. Since the SANS from a multi-component

sample is essentially a contrast-weighted summation of the SANS from each individual component, the technique of contrast matching can be used to dramatically simplify the scattering pattern. Different isotopes possess different scattering lengths and thus neutrons are good for studying colloidal systems.

The selective labelling or changing of contrast is a significant advantage of SANS. For example in the study of a two-component system in a solvent, contrast matching one component to the solvent, means that the only scattering observed is that from the second component in the system. Scattering length densities of different components can be adjusted using deuterated analogues thus adjusting contrast. Hydrogen and deuterium differ in sign and magnitude.

Nucleus	Coherent scattering lengths, **b /10^{-15} Metres**
^{1}H	-3.741
^{2}D	+6.671

Table 2.1 Coherent scattering lengths of hydrogen and deuterium

This enables ρ to be manipulated by replacing hydrogen in a molecule with deuterium. The typical density scattering values range from -0.5×10^{-10} cm^{-2} for protonated compounds to 7×10^{-10} cm^{-2} for deuterated compounds. So it is easy to 'see' or study the proton-containing hydrocarbon-type materials which are dissolved in heavy water (D_2O).

The isotopic exchange does not affect the chemical or physical properties of the system. Scattering can be "emphasised" from certain parts of the surfactant

molecule by labelling this part of the surfactant molecule and using an appropriate composition of H_2O/D_2O mixture.

Below is a representation of obtaining contrast for separate phases using the core-shell model.

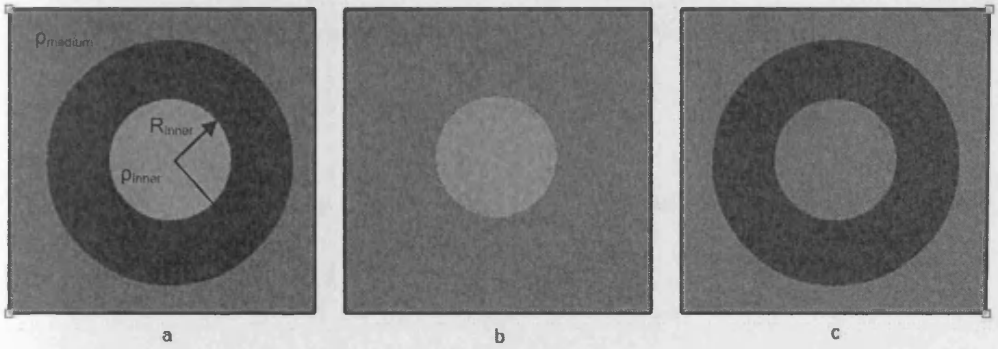

Figure 2.23: Schematic representation of contrast variation of a multi-component system. Contrast matching between (a) neither regions (b) solvent and palisade layer (c) solvent and core.

The blue area of figure (a) is the solvent and the orange area contains the hydrocarbon tail core of a micelle. The maroon ring can be likened to shell or corona of a micelle. R_{outer} is the radius of the outer circle, and R_{inner} is the radius of the inner circle. The core-shell model assumes that the system can be modelled as two homogenous, concentric spheres, for example, a spherical copolymer micelle has a poorly solvated core but surrounded by a well solvated corona. The scattering will be from the outer sphere of radius (R_{outer}) and outer scattering length density (ρ_{outer}), subtract the scattering from the inner sphere of radius (R_{inner}) and inner scattering length density (ρ_{inner}). In other words, when $\rho_{outer} = \rho_{medium}$, the corona is contrast matched to the dispersion medium or solvent, hence only the scattering from the core is observed (Figure (b)). When $\rho_{inner} = \rho_{medium}$, the scattering is from the spherical shell or corona (Figure (c)). The core-shell model can be used to determine the radius of the core, the thickness of the corona, and their respective scattering length densities.

2.6.4 Form Factor, P(Q)

The form or shape factor is a dimensionless function describing the angular distribution of scattering due to the particle radius and is *dependent on the size and shape of the scattering centre*. Expressions for the form factor are known for a range of particle shapes including spheres, shells, polyelectrolytes, gaussian coils and cylinders or rods.

Most useful in this study are the following: Gaussian coil (ideal polymer), Ellipsoid and solid sphere models.

2.6.5 Structure Factor, S(Q)

The structure factor is a dimensionless function describing how the scattering is modulated by interference effects between neutrons scattered by different scattering centres i.e. *it is dependent on the interparticle interactions*. It is given by the equation:

$$S(Q) = 1 + \frac{4\pi N_p}{QV_s}\int_0^\infty [g(r) - 1] r \sin(Q_r)\, d_r \qquad \text{Equation 2.27}$$

Where r is the radial distance outward from the centre of any scattering body in the sample and g(r) is the density distribution function obtained by Fourier inversion. S(Q) tends towards unity at high Q as the concentration of scattering bodies becomes dilute.

SANS data typically has the form of a curve. A maximum occurs at low Q and the intensity decreases as Q increases. At low Q, the wavelength of the neutron radiation is similar to that of a colloidal particle meaning that the scattering produced

is high. However, as Q increases, the wavelength of the radiation is reduced, decreasing the amount of scattering and the signal tends towards the incoherent background level noise.

As the charge decreases, the peak becomes broader. As S(Q) decreases the curve shifts to the right and the peak is smaller.

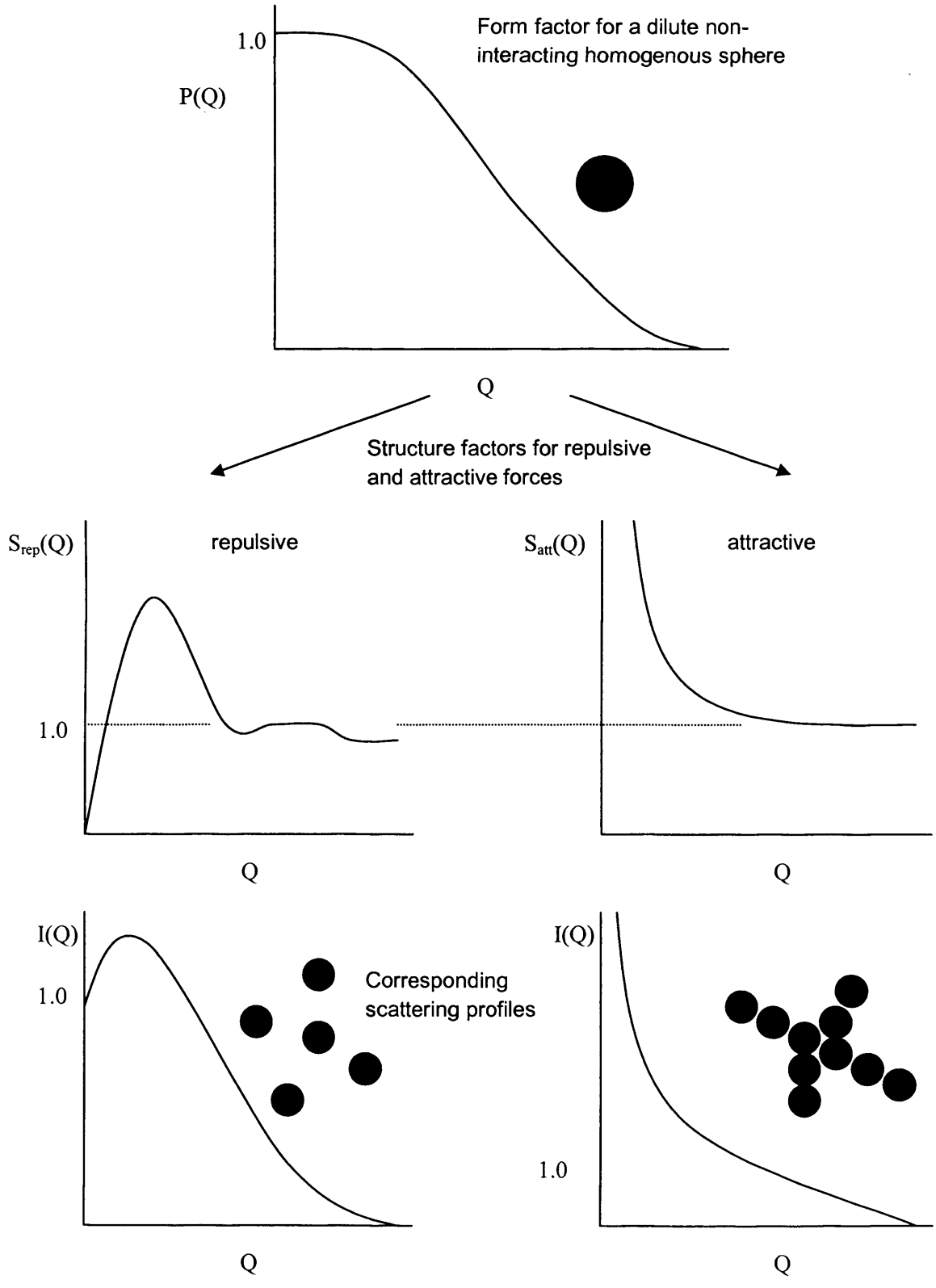

Figure 2.24: Diagrammatic representation of the single particle form factor P(Q) and the interparticle structure factor S(Q) for homogenous spheres (A.Winnington Thesis[27])

2.6.6 The Neutron scattering experiment

For each sample, a minimum of four different measurements are required:

1) The empty sample position (the direct or straight-through beam) from which $I(\lambda)\Delta\Omega\eta(\lambda)$ can be obtained.
2) The sample.
3) The sample solvent and cell *i.e.* 'backgrounds'.
4) The calibration standard or sample.

For example, a sample containing two components such as sodium dodecyl sulphate (SDS) in a 5 wt% PVP, both dissolved in D_2O, this would be the sample to be measured. The background solvent would be the D_2O. The calibration sample is a partially deuterated homopolymer blend (the molecular weight of the deuterated species is known).

For each sample and background, it is necessary to measure both the scattering behaviour and the transmission, $T(\lambda)$. Transmission runs are generally of a shorter duration (typically 5-10 minutes) than most scattering runs.

2.6.7 Data reduction

As previously discussed, the differential cross-section, $(d\Sigma/d\Omega)(Q)$, is measured indirectly, and this function is recovered by the process of data reduction from what the detectors actually records.

Scattered neutrons generate a series of diffraction rings (due to the detector taking conic sections of the spheres of scattering). The diffraction rings complicate the data reduction procedure as the detector pixels are arranged on a square array, which must be divided into a series of concentric rings, each with the same width (of the same order as the size of a pixel). Within each ring a radial integration over some range of solid angles is performed.

Where scattering is isotropic all solid angles are taken into consideration, as was the case in this study.

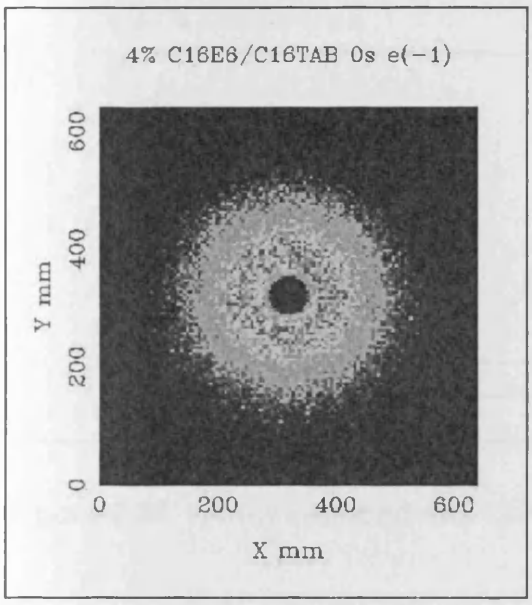

Figure 2.25 shows an image of the isotropic type of scattering pattern of surfactants C16E6 and C16TAB (obtained during SANS training). They are intensity line contour plots.

The radially integrated data are then normalised (placed on a per neutron basis) using the transmission and the integrated counts which are recorded by the monitor detector, and the area detector efficiency ratio. Any similarly processed background data, is subtracted ring by ring. The position of each ring is converted to Q using equation $\boldsymbol{Q} = |\boldsymbol{Q}| = |\boldsymbol{k}_s - \boldsymbol{k}_i| = \frac{4\pi n}{\lambda} \sin\left(\frac{\theta}{2}\right)$ to give the final and fully reduced dataset (Figure 2.26)[25,26,27,28,29].

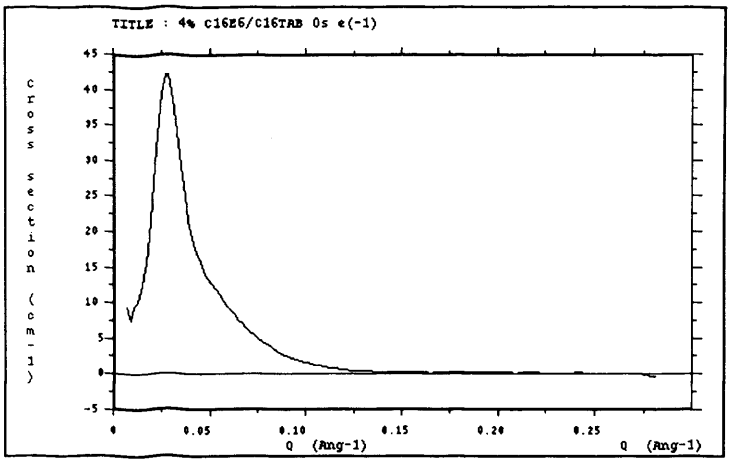

Figure 2.26 A fully reduced and normalised dataset of C16E6/C16TAB

2.6.8 Data normalisation

The transmission is measured:

$$T(\lambda) = \frac{\Sigma(\lambda)}{\Sigma_{EB}(\lambda)} \qquad \text{Equation 2.28}$$

where $\Sigma(\lambda)$ is the sum of counts on the post sample detector for the sample (*i.e.* transmitted beam flux) and the 'empty beam' subscript EB the incident beam flux.

The relative intensities, $I(\theta,\lambda)$, are expressed in the following equation:

$$I(\theta,\lambda) = \frac{s(\theta,\lambda)}{T(\lambda)M_s} \qquad \text{Equation 2.29}$$

$s(\theta,\lambda)$, the raw scattering data, is corrected for the number of incident neutrons (M_s) and the proportion that reach the detector ($T(\lambda)$). $I(\theta,\lambda)$ is then converted to I(Q) using equation 5.4.1. As mentioned earlier, it is necessary to subtract scattering contributions from the sample environment such as solvent and other parts of the sample. Scattering from the background is measured and the intensity is corrected for the respective transmission. With reference to a calibration standard the absolute scattering cross-section for the sample I(Q), can be calculated.

$$I(Q) = A\left(\frac{I_{sample}(Q) - I_{sample-background}(Q)}{I_{standard}(Q) - I_{standard-background}(Q)}\right)$$ Equation 2.30

A is the cross-section of the standard (cm^{-1}).

2.6.9 Data Fitting

The FISH program written by R.K. Heenan from ISIS, was used to analysis the SANS spectra. The core shell model was used for fitting the data to the SANS curves. This assumes a core particle with a shell or skin around it, allowing parameters such as radius, ellipticity and shell thickness to be determined. Utilising the contrast-matched method as described previously allows the different layers or sections of a micelles to be investigated. The aim is to obtain the best fit for I(Q), P(Q) and S(Q) and then other values can be calculated using equation 2.24. This model works best if the adsorbed layer is reasonably uniform and homogenous i.e well defined.

2.7 Electron Paramagnetic Resonance

The basic concept of EPR is analogous to that of NMR except in this case it is the electron spins that are excited and not the spins of atomic nuclei. The technique is used for studies on species with unpaired electrons, by observing the magnetic fields at which they come into resonance. The majority of stable molecules are held together by bonds in which spins are paired and do not give any interaction between the electron spin and an applied field. Solvents usually fall into this category and thus do not give an EPR signal. Atoms or molecules with unpaired spins are also paramagnetic.

Species such as NO, O_2 and NO_2 are stable and easily studied by EPR. Unstable species such as ions or free radicals may form as intermediates in a chemical reaction or by irradiation of a molecule. So long as the lifetime of radicals is greater than $\sim 10^{-6}$ seconds then they can be studied using EPR.

2.7.1 Properties of EPR spectral lines

Four properties of the spectral lines of the EPR spectra are important; the intensity, width, position and multiplet structure (similarly for NMR).

2.7.1.1 The position or g-value of the spectral lines

As with the principle of NMR, when unpaired electrons spins exist, in the absence of a field, they will be aligned at random (as are neutrons with spin). When placed in a magnetic field, the electron spin will each interact with the field.

$$h\nu = g\mu_B B \qquad \text{Equation 2.31}$$

Where g is the g-value of the radical or complex, μ_B the Bohr magneton, and v the frequency of electromagnetic radiation in an electromagnetic field, B. The g_e factor for a free electron is 2.0023 (at 0.34 Tesla in a field of 9506.69MHz). The g factor in equation 2.31 is the value for electrons that are able to move more or less freely over molecules and varies for different types of radicals and ionic crystals. g-values are used to identify species present in a sample.

The quantum number of an electron is ½ and each electron can be thought of as spinning clockwise or anticlockwise about the field direction. EPR spectroscopy measures the energy required to reverse the spin of an unpaired electron.

2.7.1.2 Intensity of spectral lines

The intensity of an EPR absorption is proportional to the concentration of the paramagnetic species being studied. This is advantageous in estimating the amount of free radical present, making EPR a sensitive technique.

2.7.1.3 Width of spectral lines

The width of an EPR resonance depends on the relaxation time of the spin state being studied. Spin-spin relaxation has a relaxation time of 10^{-6}-10^{-8} seconds. Spin-lattice relaxation is efficient at room temperature at about 10^{-6} seconds. Relaxation time becomes progressively less as temperature is decreased. The spectral lines are the first derivative of the absorption spectrum.

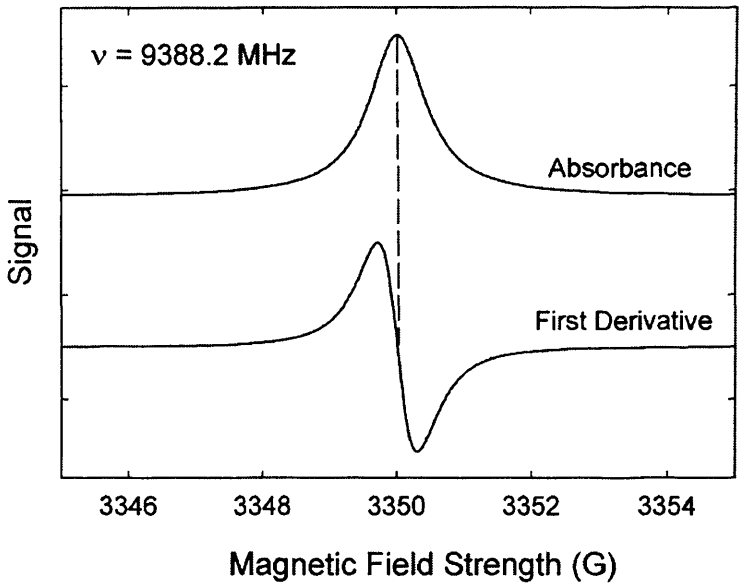

Figure 2.27 The absorbance signal and first derivative, as recorded on an EPR spectrum

2.7.1.4 Multiplicity and hyperfine structure of spectral lines

The hyperfine structure is the splitting of individual resonance lines into components. The source of the splitting is the magnetic interaction between the electron spin and the magnetic dipole moments of the nuclei present in the radical.

Electron-nucleon coupling constants are much larger than nucleon-nucleon coupling constants since electrons can get closer to nuclei than a nucleus can. Equation 2.13 describes the nuclear angular momentum. Depending on the orientation of the nuclear spin, it can add or subtract from the applied field. The total local field is;

$$B_{loc} = B + am_1 \quad m_1 = \pm\frac{1}{2}$$ Equation 2.32

Where *a* is the hyperfine coupling constant. Since half of the radicals of spin ½ will have a + sign and half a – sign the spectrum will show two lines separated by *a,* and centred on the field determined by *g*. For radicals with a greater number of spin

orientations, the spectrum is split into 2I+1 hyperfine lines of equal intensity. Where several magnetic nuclei are present, each one contributes to the hyperfine structure and equivalent protons will produce some coincident lines. This is similar to the way in which NMR spectra display splitting patterns. The intensity distribution of the lines will follow Pascal's triangle.

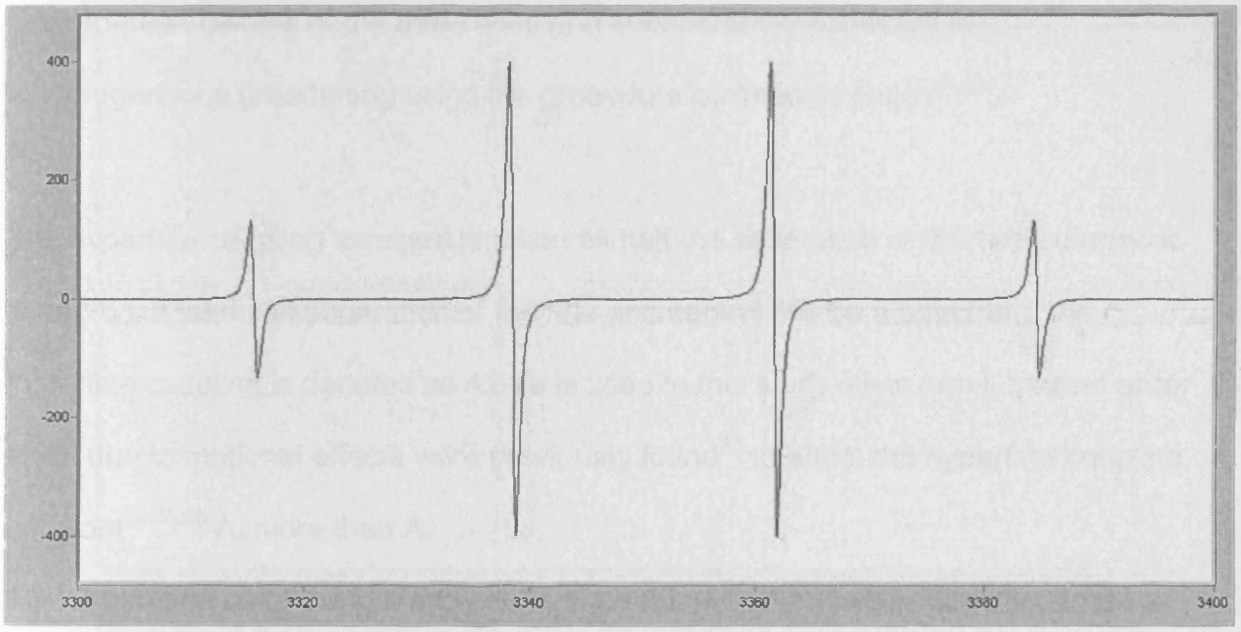

Figure 2.28 Simulated EPR spectrum of the CH_3 radical showing the hyperfine splitting caused by three equivalent protons.

A stock solution of the surfactant with a spin-probe/surfactant molar ratio of 1/400 was mixed with an appropriate polymer solution to yield the desired solution composition. These nondegassed samples were sealed with a gas-oxygen torch into melting point capillaries, which were housed within a quartz EPR tube for the measurements. The temperature was controlled to 25°C ±1°C by a Bruker Variable Temperature Unit BVT 2000. Five spectra were recorded at X-band on a Bruker ESP-300 spectrometer[30].

2.7.2 EPR lineshape fitting and analysis

The lineshapes were fitted to a Voigt approximation to separate the Gaussian and Lorentzian components of the spectral lines and to locate the resonance fields of the three EPR lines of a nitroxide radical to a precision of a few mG. Rotational correlation times are computed from the overall linewidth of the centre line and the peak-to-peak heights of the three lines and subsequently corrected for inhomogeneous broadening using the procedure outlined by Bales[31,32].

The hyperfine coupling constant is taken as half the separation of the two outermost lines (A_o). If taken as separation of the first and central line on a spectrum, the hyperfine coupling is denoted as A_+. A_+ is used in this study since small second order shifts due to motional effects were previously found[33] to affect the hyperfine coupling constant[34,35,36] A_o more than A_+.

The separation A_+ of the low and centre lines (M_I=+1 and M_I=0) is directly related to the polarity index H(25°C), defined as the molar ratio of OH groups in a given volume relative to water, φOH. For simple SDS solutions, H(25°C) corresponds to the volume fraction of water in the polar shell, φ*water*. The presence of ethanol in the polar shell will also contribute to the value of φOH but it is not possible to decouple these two contributions.

References

[1] Hamley, I.W. "Introduction to Soft Matter-Polymers, Colloids, Amphiphiles and Liquid Crystals". Wiley, **2000**

[2] Jönsson, B., Lindman, B., Holmberg, K., and Kronberg, B., *Surfactants and polymers in aqueous solution*, John Wiley and Sons, Inc., New York, **1998**.

[3] Shaw, D., *Introduction to Colloid and Surface Chemistry*, 4th edition.

[4] Hackley, V.A., Ferarris, C.F., *Guide to rheological nomenclature: Measurements in Ceramic Particulate Systems,* National Instutite of Standards and technology Special Publication 946, January **2001**

[5] Atkins, P. W., *Physical Chemistry*, Oxford University Press, **1992**, fifth edition

[6] Barnes, H. A., Hutton, J. F., and Walters, K., *An Introduction to Rheology*, Rheology Series, 3, Elsevier Science B. V., **1989**

[7] Guan, J.Q., and Tung, C.H., *Langmuir*, ***15, 1011, 1999***

[8] Jover, A., Meijide, E., Rodriguez Nunez, E., and Vazquez Tato, J., *Langmuir,* **13,** 2935, **1997**

[9] Winnick, M.W., and Regismond, S.T.A., *Fluorescence methods in the study of the interactions of surfactants with polymers,* Colloids and Surfaces Review, **1996**

[10] Turro, N.J., Baretz, B.H., Kuo, P-L., *Macromolecules*, **1984,** *17,*1321-1324

[11] Kalyanasundaram, K., Thomas, J.K., *Environmental effects on Vibronic Band Intensities in Pyrene Monomer Fluorescence and Their Application in Studies of Micellar Systems,* Journal of the American Chemical Society, 99:7, **1977**

[12] Kalyanasundaram, K., and Thomas, J.K., *J. Am. Chem. Soc.* **99,** 2039 (**1999**)

[13] Campbell, I.D., and Dwek, R.A., *Spectroscopy,* p97-100

[14] Griffiths P.C., Roe J.A., Bales B.L., et al; *Langmuir,* **2000,** 16, 8248-8254

[15] P.C. Griffiths, J.A. Roe, R.J. Abbott, A.M. Howe: *Imaging Science Journal*: **1997**, *45*, 224-228

[16] Whitesides, T.H., and Miller, D.D., *Langmuir.* **10,** 2899-2909, **1994**

[17] Griffiths, P.C., Hirst, N., Paul, A., King, S.M., Heenan, R.K., Farley,R., Murphy, D.M., *Langmuir*, **2004**, *20,*6904-6913

[18] Dorrance, R.C., and Hunter, T.J., *J. Am. Chem. Soc. Faraday Trans.,* **1,** 1572, **1974**

[19] Turro, N,. and Yekta, A., *J. Am. Chem. Soc.,* **100,** 5951, **1978**

[20] Koglin, P., Miller, D., Steinwandal, J., and Hauser,M., *J. Phys. Chem.,* **85,** 2363, **1981**

[21] Harwood, L. M., Claridge, T.D.W., *Introduction to Organic Spectroscopy,* Oxford University Press, 1997

[22] Eastoe, J., *Small-Angle Neutron Scattering and Neutron Reflection,* Chapter 12, University of Bristol, UK, **2000**

[23] King, S.M., *Small Angle Neutron Scattering*, ISIS report, Large-scale structures group, 1995

[24] ISIS website, www.isis.rl.ac.uk, **2002**

[25] Eastoe, J., 'Small-Angle Neutron Scattering and Neutron Reflection in New Physico-Chemical Techniques for the Characterization of Complex Food Systems', (ed Dickinson, E.), Chapter 12, Chapman and Hall, UK, **1996**

[26] King, S.M., 'Small-angle neutron scattering in Modern techniques for Polymer Characterisation', (ed. Pethrick, R.A., Dawkins, J.V.), John Wiley and Sons, Ltd, New York, **1999**

[27] Winnington, A., *Fluorescence studies of polymer/surfactant complexes*, Ph.D Thesis, Cardiff University, **2003**

[28] Cheung, A.,*Gelatin-Surfactant interactions,* Ph.D Thesis, Cardiff University, **2003**

[29] Davies, J.A., Ph.D Thesis, Cardiff University, **2005**

[30] Bales, B.L., Ranganathan, R., Griffiths, P.C., *J. Phys. Chem. B,* **2001**, *105,* (31), 7465-7473

[31] Bales, B.L., In *Inhomogeneously Broadened Spin-Label Spectra*: Berliner, L.J., Reuben, J., Eds.; Biological Magnetic Resonance 8; Plenum Publishing Corporation: New York, **1989**; p.77

[32] Bales, B.L., Stenland, C., *J. Phys. Chem.* **1993**, *97,* 3418

[33] Bales, B.L., Messina, L., Vidal, A., Peric, M., Nascimento, O.R., *J. Phys. Chem.* **1998**, 102, 10347

[34] Polnaszek, C.F., Freed, J.H., *J. Phys. Chem.* **1975**, 79, 489

[35] Hwang, J.S., Mason, R.P., Hwang, L.P., Freed, J.H., *J. Phys. Chem.* **1975**, 79, 489

[36] Rao, K.V.S., Polnaszek, C.F., Freed, J.H., *J. Phys. Chem.* **1977**, 81, 449

Chapter 3

This chapter sets out the experimental methods used for the characterizations of SDS-PVP systems in ethanol-water mixtures and pluronic P104 with SDS in ethanol-water mixtures.

Concentration ranges of polymer and surfactant varied between systems depending on where the CMC lay and any limitation of experimental technique due to very high or low concentration. The concentration ranges for each system studied can be seen in the results analysis.

3.1 Materials

3.1.1 Surfactants

Sodium dodecyl sulphate (SDS), (Aldrich, purity 98%) was purified by repeated recrystallisations from ethanol until the impurity "dip" in the surface tension *vs.* log(concentration) curve could no longer be observed.

Deuterated sodium dodecyl sulphate (d-SDS) for use in SANS experiments was obtained from Aldrich (99.9% atom) and used as received.

3.1.2 Polymers

Poly(vinylpyrrolidone) (PVP), (Aldrich, M_W 1.3 x 10^6) was used as received.

The Pluronic, $H(-OCH_2CH_2-)_z[-OCH(CH_3)-CH_2-]_y(-OCH_2CH_2-)_zOH$ (Aldrich, average M_w 5800) was used as received and is a paste at room temperature. This was not obtained from BASF, which uses its own nomenclature for pluronics. Based on analysis of key properties it is shown that the pluronic used from Aldrich correlates closely with both P104 and P123. For the purposes of this thesis, the pluronic shall be referred to as P104.

3.1.3 Solvents

Analytical grade ethanol (Aldrich) and doubly distilled water was used to prepare all solutions. Where applicable, deuterium oxide, D_2O, 99.9% atom (Aldrich) was used as received and deuterated ethanol, d-ethanol, 99.9% atom (Aldrich) was used as received.

3.1.4 Fluorescence Probes

The fluorescence probe 8-anilino-1-naphthalene sulphonic acid ANS (Aldrich) was used as received, and dissolved in small quantities (ie in <1ml) of ethanol before use.

The fluorescence probe, pyrene, (Aldrich) was used as received and dissolved in very small quantities of acetone (approximately 5ml) before making up the stock solution.

The fluorescence probe, Ruthenium tris(bipyridine) Chloride ($[Ru(bipy)_3]Cl_2$), (Aldrich) was used as received and dissolved in very small quantities of acetone before making up the stock solution.

In cases of probe being dissolved in acetone, the quantity of acetone making its way into the sample was negligible in terms of affecting the properties of the system.

3.1.5 Fluorescence Quencher

The quencher 9-methyl anthracene (Avocado) was used as received and dissolved in ethanol to add in microlitre aliquots to the sample containing the Ruthenium tris(bipyridine) Chloride ($[Ru(bipy)_3]Cl_2$) probe[1,2].

3.2 Methods

3.2.1 Surface tension

The surface tension was determined by the Du Nouy ring method consisting of a small (1cm diameter) platinum ring hung from a zero displacement balance (CI Electronics, UK), calibrated by reference to distilled water / ethanol mixtures. All solutions were prepared from a stock solution of distilled water with the appropriate concentration of ethanol. All measurements were taken at room temperature after allowing equilibration

of the solution. The average of 6 consecutive measurements within 0.002mV was taken. Concentrated solutions were diluted down using aliquots pipetted into volumetric flasks.

3.2.2 Fluorescence

For samples utilising ANS probe, all solutions were prepared from a stock solution of distilled water with the appropriate concentration of ethanol, containing a stock ANS probe at a concentration of 2×10^{-5} M and where appropriate, stock level of polymer or SDS. Emission intensities were determined by integration of the fluorescence intensity over the range 490 and 520 nm, with excitation at 320nm using a scan speed of 240 nm s^{-1} and slit widths of 5.0 nm.

For samples utilising pyrene probe, all solutions were prepared from a stock solution of distilled water with the appropriate concentration of ethanol, containing a stock pyrene probe[3] at a concentration of 2×10^{-6} M and where appropriate, stock level of polymer or SDS. Emission intensity is recorded over the range 350 and 450 nm, with excitation at 310nm using a scan speed of 240 nm s^{-1} and slit widths of 2.5 nm. The ratio of the peaks I_{iii}/I_i (at approximately 385nm and 374nm[4]) is taken to observe changes to the hydrophobicity of the probe environment as described in chapter 2 (the trend has altered over time from taking the I_i/I_{iii} to I_{iii}/I_i ratio).

All emission spectra were obtained on samples equilibrated at 25°C or 35 °C ±1°C as stated in the results analysis.

3.2.3 Fluorescence quenching

Static fluorescence quenching was carried out using tris(bipyridyl ruthenium (II)) chloride as a luminescent probe and 9-methyl-anthracene (9-MA) as a hydrophobic quencher. 9-methyl-anthracene was obtained from Avocado and used as received. All solutions were prepared using distilled water with the appropriate concentration of ethanol, containing 1 x 10^{-6} M tris(bipyridyl ruthenium (II)) chloride. The quencher (0.1M 9-MA in ethanol) was introduced in microlitre aliquots, so that the additional volume fraction of ethanol never exceeded 1wt%. All emission spectra were obtained on samples equilibriated at 25 °C ±1°C, with excitation at 450nm. Emission intensities were determined by integration of fluorescence intensity between 575 and 675 nm. All measurements were carried out using a scan speed of 240 nms^{-1} and slit widths of 5 nm.

All fluorescence measurements were carried out using a Perkin-Elmer LB 50 Luminescence spectrophotometer.

3.2.4 Small Angle Neutron Scattering, SANS

The SANS measurements were performed on the fixed geometry, time of flight LOQ diffractometer at the ISIS Spallation Neutron Source, Didcot, UK. Neutron wavelengths of 2→ 10 Å were used. Samples were held in 2mm pathlength quartz cuvettes mounted in Aluminium holders on top of an enclosed computer controlled sample changer.

Temperature was kept at 25°C ± 0.2°C. Measuring times were between 80-120 minutes.

Scattering is normalised for sample transmission and incident wavelength distribution and background corrected using an empty quartz cell. It is also corrected for linearity and efficiency of detector response and the data is put on an absolute scale by reference to a partially deuterated polystyrene blend sample. Deuterated solvent was used for all solvent mixtures.

3.2.5 Viscometry

Viscosity of samples was measured using a calibrated Ostwald U-tube capillary viscometer suspended in a temperature regulated water bath, at temperatures 25°C and 35°C± 1°C. The viscometer was washed with distilled water, acetone and then oven dried before each use. The measurements were repeated three times and an average reading taken.

3.2.6 Nuclear Magnetic Resonance (NMR) Spectroscopy measurements

A Bruker 400Mhz high resolution NMR machine was used to determine the proton resonance at 300K (27°C). Samples of approximately 3ml were placed in glass samples tubes and stoppered and sealed.

3.2.7 Electron Paramagnetic Resonance (EPR) Spectroscopy measurements

All of the EPR measurements were carried out at a temperature of 25°C ±1°C. The samples, not degassed, were sealed with a Bunsen burner into melting point capillary tubes. These in turn were put into a quartz EPR tube during measurements. Measurements were performed using a Bruker ESP-300 spectrometer. For each sample, the measurements were made five times. The microwave power was 2.02mW, sweep width 50 Gauss, time constant 10.24ms and sweep time of 41.943s. The spectra were transferred to a computer and fitted with a software program called LOWFIT, coded in C. The program fits the spectra by separating the Gaussian and Lorentzian components of the spectral lines and locating the resonance fields of the three EPR lines to a precision of a few mG[5,6].

The spacings between hyperfine lines are defined as $A_+ = H_o - H_{+1}$, and $A_o = (H_{-1} - H_{+1})/2$ where H_{M_I} denotes the resonance fields of the three lines, $M_I = +1$, 0, and -1, which corresponds to the low, middle and high-field lines respectively. A_+ was preferred to A_o since A_o was found in previous studies to cause small second order shifts due to motional effects resulting in the hyperfine coupling constant being affected[7].

References

[1] Turro and N.J., Yekta, A., *J. Am. Chem. Soc.*, **1978,** *100*, 5951

[2] Koglan, P.K.F., Miller, D.J. Steinwandel, J., Hauser, M., *J. Phys. Chem.*, **1981**, *85*, 2363

[3] Winnik, F., *Chem. Rev.,* **1993,** *93*, 587

[4] Grubbs, R.H., Pancoast, T.A., *J. Am. Chem. Soc.* **1977,** *99*, 7

[5] Halpern, H.J., Peric, M., Yu, C., Bales, B.L., *J. Magn. Reson.,* **1993**, *103*, 13

[6] Bales, B.L., Inhomogenously Broadened Spin-Label Spectra, in *Biological Magnetic Resonance*, Berliner, L.J., Reuben, J., Eds., Plenum Publishing Corporation, New York, **1989**, *8*, 77

[7] Bales, B.L., Messina, L., Vidal, A., Peric, M., Nascimento, O.R., *J. Phys. Chem.,* **1998**, *102*, 10347

Chapter 4

4 Context

The findings of the investigation into SDS and SDS/PVP systems in water and ethanol mixtures has been published in Langmuir (2004) as "Effect of Ethanol on the Interaction between Poly(vinylpyrrolidone) and Sodium Dodecyl Sulfate"[1]. The results are discussed in this chapter and the paper attached as appendix I. This work also contributed to the production of a second paper, published in Chemical Society Review (2006) as "Electrophoretic NMR Studies of Polymer and Surfactant Systems"[2].

This section of the research investigated how the addition of ethanol to a PVP/SDS solution affects the polymer/surfactant interaction. This chapter discusses the experimental data regarding the onset of the interaction and its effects on size and shape of the polymer/surfactant complex.

A number of experimental methods were used, each exploiting different properties of the system, for example, surface tension to assess changes taking place on the air/solution interface, fluorescence to view changes to the microscopic probe environment and viscosity to view changes to macroscopic properties of the solution.

4.1 Onset of Surfactant Micellisation.

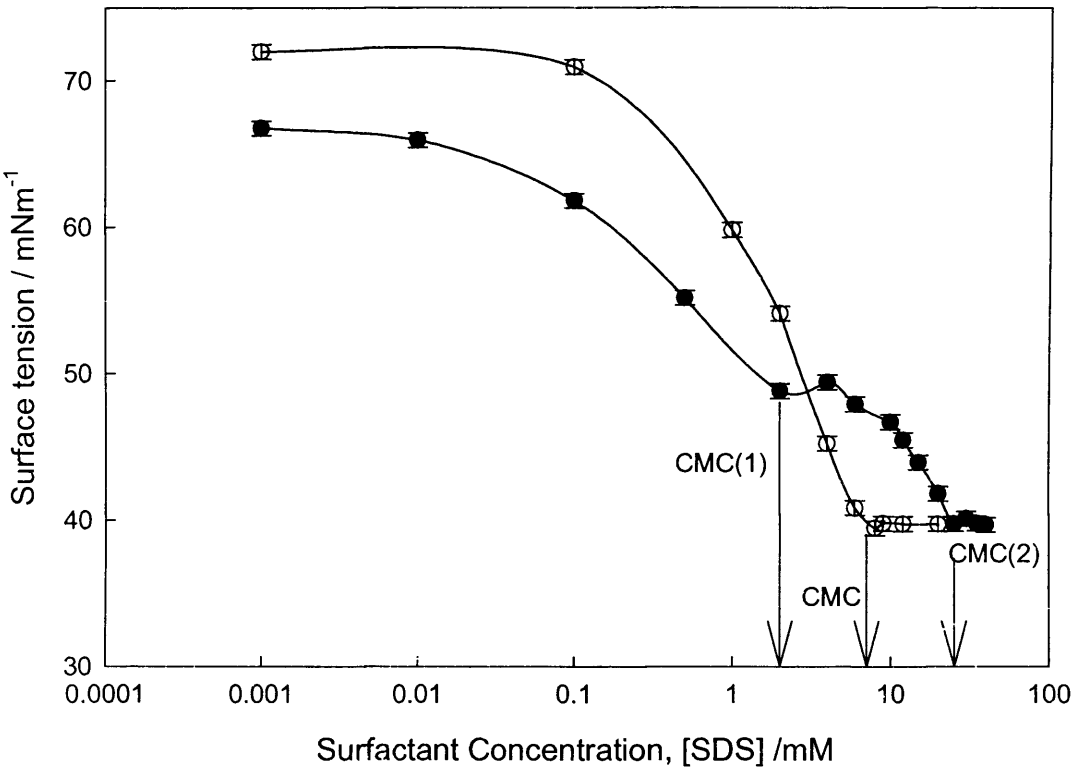

Figure 4.1(a) Surface tension behaviour of SDS in water (open circles) and SDS with 0.5%w/w PVP in water (filled circles). The CMC of SDS in water is clearly visible, as are CMC1 and CMC2 for SDS in the presence of PVP.

Figure 4.1(a) shows the surface tension versus surfactant concentration of SDS in the absence and presence of 0.5 wt % PVP. For the SDS only case, there is clearly one break in the curve yielding CMC = 8 $\pm$ 0.2 mM, in excellent agreement with the literature value. In the presence of the PVP, two breaks are observed on the surface tension data indicating CMC1 and CMC2. As discussed in Chapter 1, this corresponds to the formation of micelles on the polymer strand (CMC1) and the formation of

unbound micelles in solution (CMC2). The estimate of CMC1 in water from this study is in good agreement with the earlier work by Turro et al.[3] At CMC2, the unimer concentration of SDS corresponds to that at the CMC of SDS in the absence of PVP, so CMC2-CMC gives a measure of the amount of polymer bound surfactant, C_{bound}.

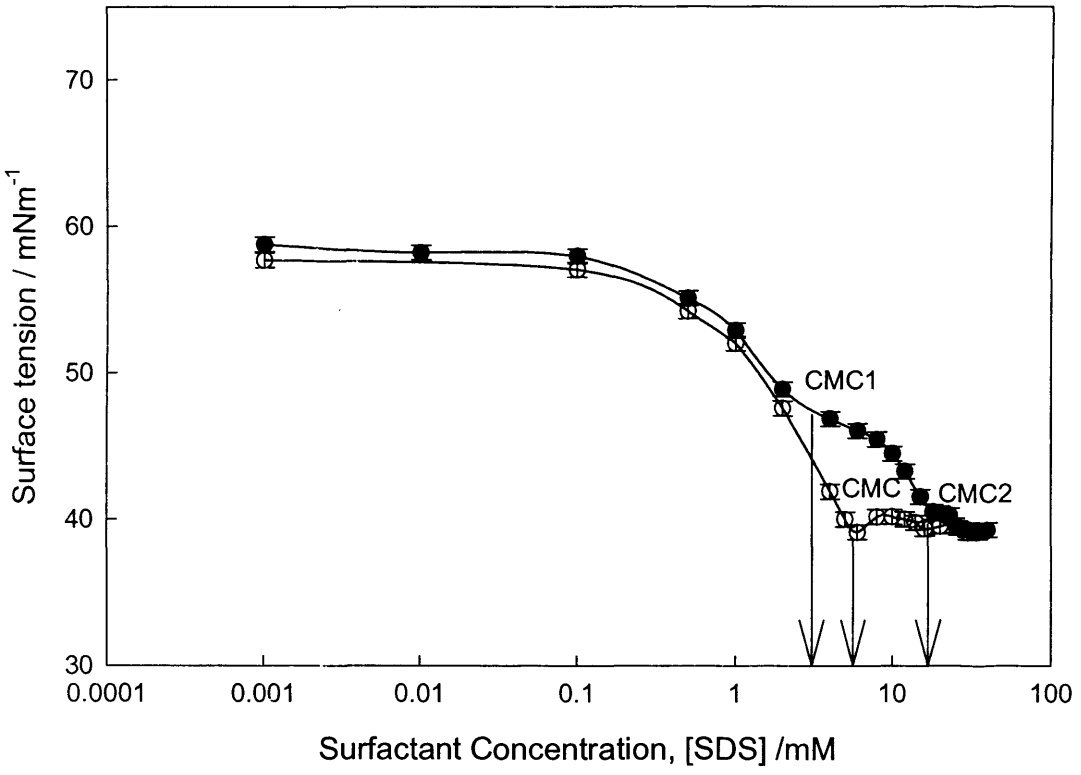

Figure 4.1(b) Surface tension behaviour of SDS in 5wt% ethanol / water mixtures (open circles) and SDS with 0.5%w/w PVP in 5wt% ethanol / water mixtures (filled circles).

In the presence of 5wt% ethanol (Figure 4.1b), the surface tension of SDS both with and without PVP is significantly reduced, due to the surface activity of ethanol. The break in the surface tension curve for the SDS case (with no-PVP) in the presence of ethanol

occurs at lower SDS concentrations compared with the no-ethanol case, confirming that micellisation is promoted (the CMC decreases) by the presence of these amounts of ethanol. This is referred to as the co-surfactant effect. This behavior is in good agreement with the work of Safarpour et al[4]. Similar behavior is observed for the polymer/surfactant/ethanol mixture to that observed in the aqueous SDS/PVP case (with no ethanol), two breaks corresponding to CMC1 and CMC2, respectively.

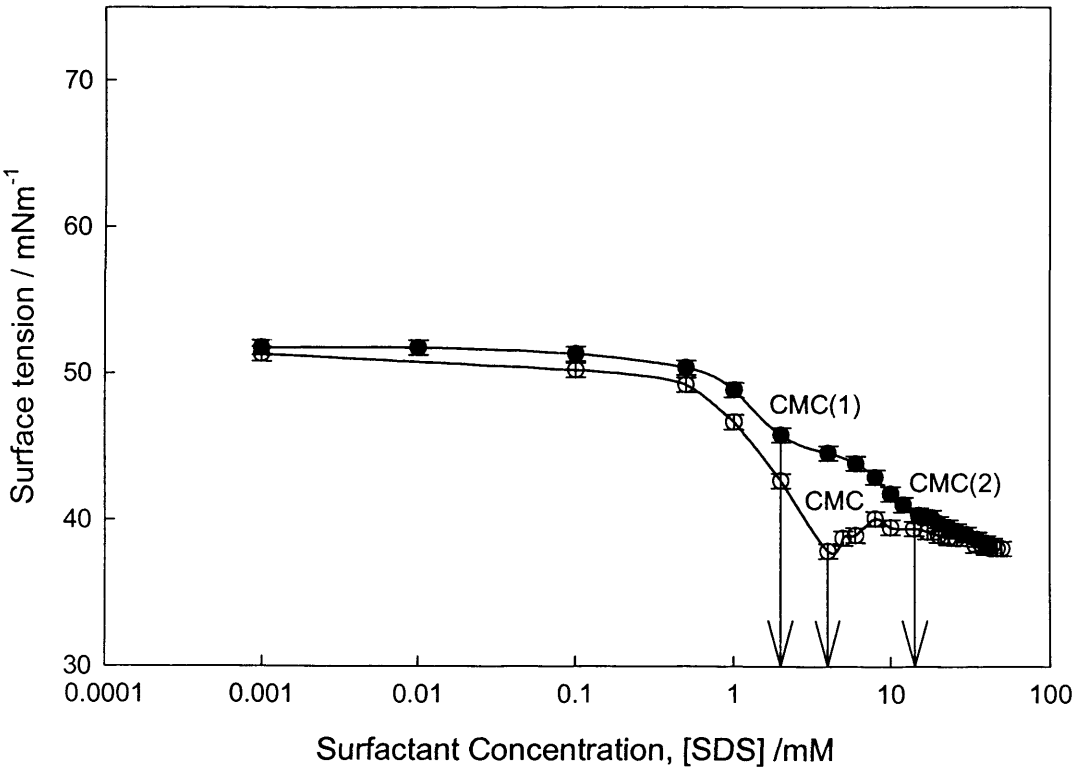

Figure 4.1(c) Surface tension behaviour of SDS in 10wt% ethanol / water mixtures (open circles) and SDS with 0.5%w/w PVP in 10wt% ethanol / water mixtures (filled circles).

At 10% wt ethanol, it can be seen that the curves are less well defined, increasing the error in estimating the values of CMC1 and CMC2. A more pronounced dip around the

CMC in the absence of PVP is noted, not due to impurities but connected to the presence of ethanol in solution. It is not clear how ethanol causes a dip around the CMC point. If impurities had existed, then a larger impact would have been seen in water, rather than in the presence of ethanol.

CMC1 is largely invariant with ethanol concentration, at least to ~10% ethanol. In contrast, CMC2 is dependent on the ethanol content, at least at the lower ethanol concentrations. CMC2 decreases monotonically to a minimum around 15 wt % ethanol outlined in table 4.1. Subsequent increases in ethanol content further reduce the surface tension of the solutions, causing the curves to become less well defined which makes accurate determination of the CMC values somewhat difficult, a conclusion reached in other studies[5,4,6]. Nonetheless, CMC, CMC1, and CMC2 increase with subsequent increases in ethanol beyond 15 wt %.

Ethanol /wt%	**CMC / mM**	**CMC(1) / mM**	**CMC(2) / mM**
0	8.0 ±0.2	2.0 ±1	23.0 ±4
5	5.0 ±0.5	2.0 ±2	16.0 ±3
10	3.5 ±2	2.0 ±2	11.0 ±2
15	4.0 ±3	5.0 ±3	11.0 ±3
20	7.0 ±3	10.0 ±3	25.0 ±3

Table 4.1 Surface tension derived CMC, CMC(1) and CMC(2) values for sodium dodecylsulphate SDS and poly(vinyl pyrollidone) (PVP) as a function of ethanol concentration; [PVP]=0.5wt%

It should be noted that surface tension is a measure of the surface characteristics of the solution, and thus, there are limitations on the interpretation of these data to explain bulk characteristics[7]. To supplement these data, (static) fluorescence was used to obtain a separate measurement of the critical micelle concentrations.

The fluorescence probe used in this study is 8-anilino-1-naphththalene sulphonic acid (ANS), as described in Chapter 2. Such probes support the determination of CMCs by detecting changes in polarity. The probe is not considered to perturb the structure of the micelle significantly[8], since estimates of the CMC of SDS measured by ANS fluorescence compare favourably with those determined by other techniques.
As the surfactant concentration passes through CMC1, micelles form, and a sharp increase in fluorescence intensity is seen as ANS is solubilised into the polar shell of the micelle.

4.1.1 SDS in ethanol/Water

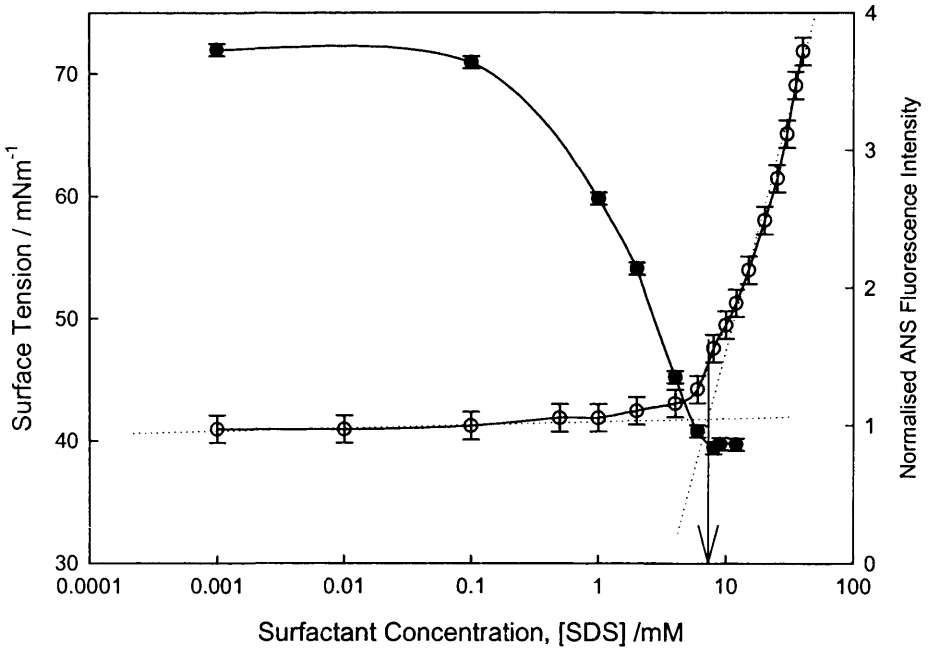

Figure 4.2(a) Fluorescence intensity of ANS in SDS in water (open circles) as a function of SDS concentration. Also shown is the corresponding surface tension data showing the correlation between the two techniques (filled circles).

The ANS fluorescence intensity versus surfactant concentration is shown in Figure 4.2(a-c) for SDS solutions as a function of ethanol concentration. The fluorescence intensity increases significantly above the CMC as the surfactant concentration passes through the CMC. When compared to surface tension, the correlation is clear. The intersection of the limiting slope and the initial slope gives a reasonable estimate of the CMC, although, for the higher ethanol content systems, some curvature of the data is apparent.

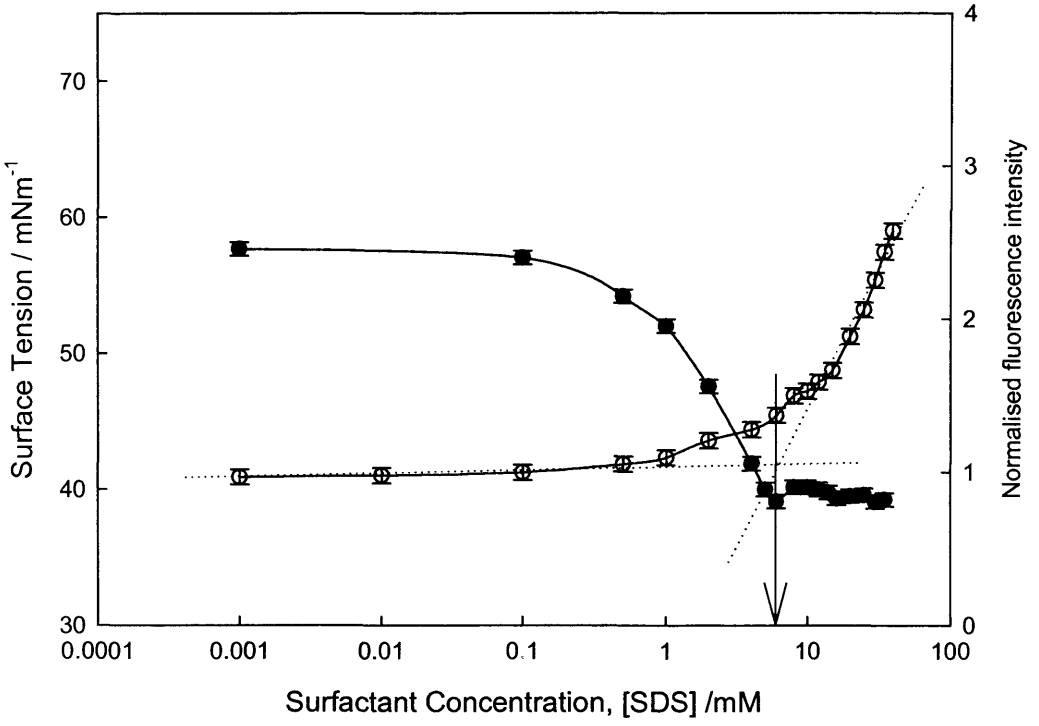

Figure 4.2(b) Fluorescence intensity of ANS in SDS in 5wt% ethanol / water mixtures (open circles) as a function of SDS concentration. Also shown is the corresponding surface tension data showing the correlation between the two techniques (filled circles).

Nonetheless, there is a clear correlation between the surface tension derived CMC's, which are also shown, and those extracted from the fluorescence study.

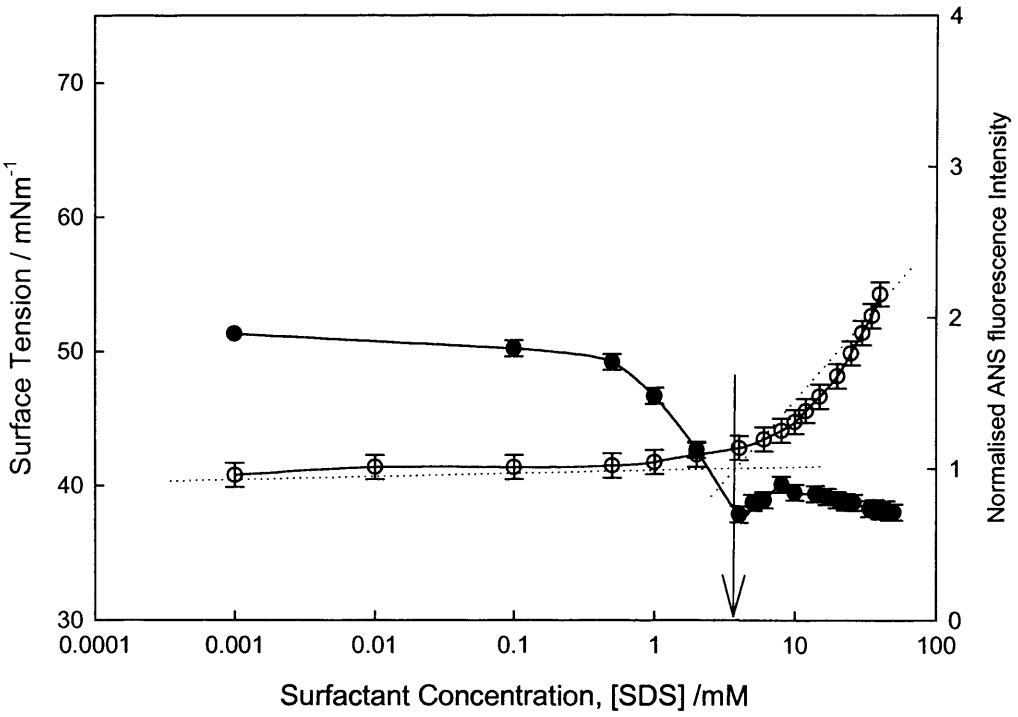

Figure 4.2(c) Fluorescence intensity of ANS in SDS in 10wt% ethanol / water mixtures (open circles) as a function of SDS concentration. Also shown is the corresponding surface tension data showing the correlation between the two techniques (filled circles).

4.1.2 The effect of ethanol/water on the SDS and PVP interactions

For the SDS/PVP systems, two breaks in the curve are seen, corresponding to CMC1 and CMC2. While not always numerically coincident due to the quite different inherent natures of the two techniques, the overall behavior is analogous. Therefore, ANS fluorescence studies compliment surface tension studies. 0.5wt% PVP was chosen in order to avoid the solution becoming too viscous (requiring long equilibrium times to

allow for probe and micelle kinetics) and still providing a range in which the CMCs can be easily tracked.

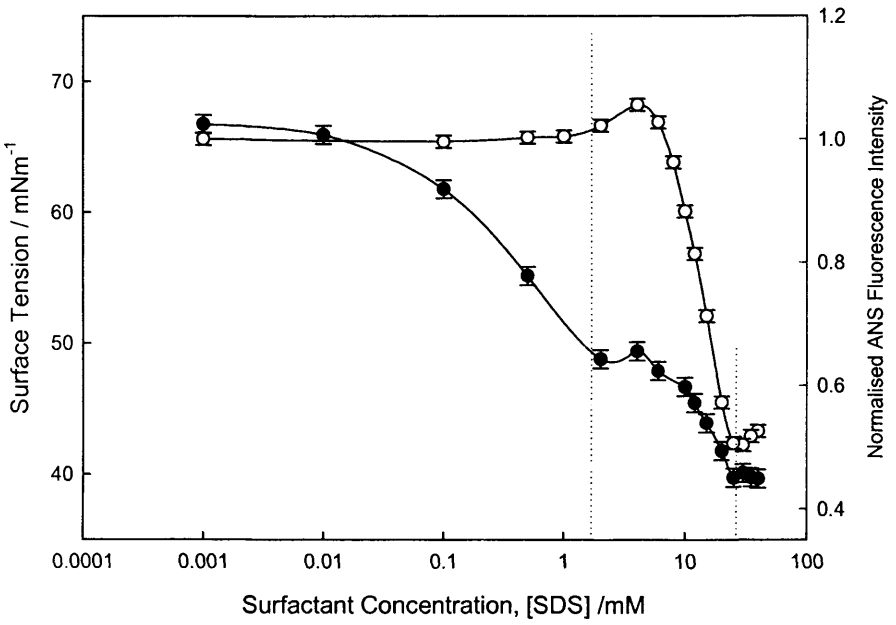

Figure 4.3(a) Fluorescence intensity of ANS for 0.5%w/w PVP-SDS in water (open circles) as a function of SDS concentration. Also shown is the corresponding surface tension data showing the correlation between the two techniques (filled circles).

There are a number of interesting differences between the ANS data for the SDS and SDS/PVP systems. The ANS intensity data in Figure 4.3(a-c) have been normalized by the measured intensity in the absence of SDS.

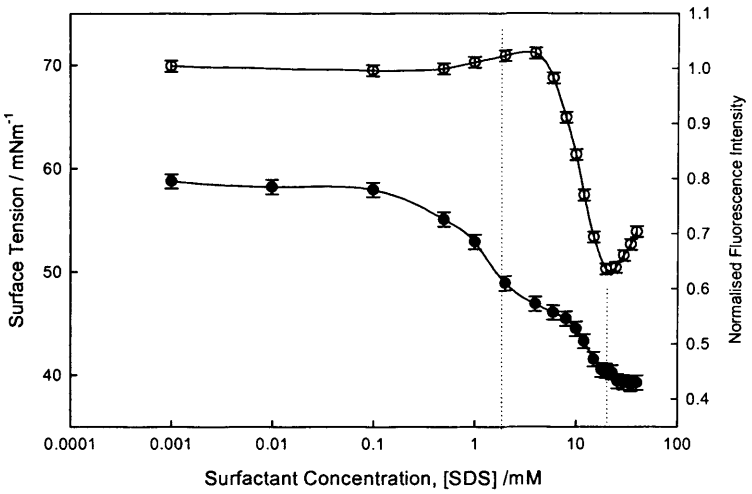

Figure 4.3(b) Fluorescence intensity of ANS for 0.5%w/w PVP-SDS in 5wt% ethanol / water mixtures (open circles) as a function of SDS concentration. Also shown is the corresponding surface tension data showing the correlation between the two techniques (filled circles).

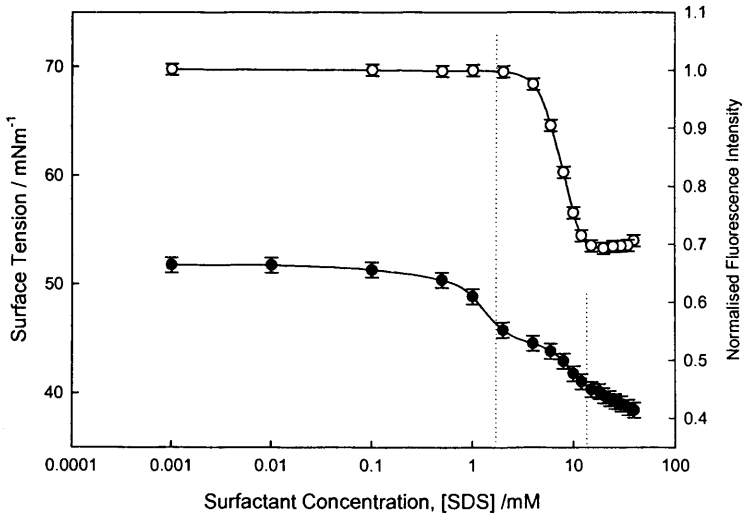

Figure 4.3(c) Fluorescence intensity of ANS for 0.5%w/w PVP-SDS in 10wt% ethanol / water mixtures (open circles) as a function of SDS concentration. Also

shown is the corresponding surface tension data showing the correlation between the two techniques (filled circles).

In the absence of PVP, the (normalized) fluorescence intensity has a low value which increases significantly around the CMC as the probe relocates into the micelles. In the presence of PVP (below the CMC1), the fluorescence intensity is substantially higher. At around CMC1, there is a small further increase in intensity, (at low ethanol concentrations) and then a significant decrease as surfactant concentration is increased further. The ANS intensity then reaches a minimum and begins to increase a second time upon increasing surfactant concentration, and previous work has shown this to coincide with CMC2.

The substantial fluorescence intensity of ANS in the presence of PVP is not seen for poly(ethylene oxide) (PEO) or gelatin[9,8]. Therefore, the conclusion is that some ANS binds to the PVP. The substantial *de*crease in fluorescence intensity with increasing SDS concentration is attributed to polymer-bound ANS being displaced by the surfactant micelles. Hence, the ANS experiments still give a measure of the onset of the interaction between the polymer and the surfactant.

The initial rise in intensity around CMC1 arises due to the polymer collapsing onto the micelle surface[10,11,12] creating a more hydrophobic environment without displacing significant quantities of the ANS. The reduction of the peak with increasing ethanol content would then suggest a less hydrophobic environment, that is, a smaller amount

of polymer binding and the preferential solubilisation of the ANS into the increasingly hydrophobic micellar phase.

Ethanol /wt%	CMC / mM	CMC(1) / mM	CMC(2) / mM
0	8.0 ±1	2.0 ±1	29 ±3
5	5.0 ±1.5	1.0 ±2	20 ±2
10	4.0 ±2	1.0 ±2	17 ±5
15	4.0 ±2	1.8±1	11 ±4
20	5.0 ±3	2.0±1	10 ±5

Table 4.2 ANS fluorescence derived CMC, CMC(1) and CMC(2) values for sodium dodecylsulphate SDS and poly(vinyl pyrollidone) (PVP) as a function of ethanol concentration; [PVP]=0.5wt%

With increasing ethanol concentration and in the absence of both surfactant and polymer, the fluorescence intensity of the ANS increases as a result of increased hydrophobicity for the solvent. The data presented in Figure 4.3(a-c) have been normalized to account for this by dividing through by the appropriate intensity in the absence of SDS. It can also be seen that as the ethanol concentration increases, the fluorescence curves become shallower, (in a similar manner to the shallower curves of surface tension upon addition of ethanol). The hydrophobic character sensed by the ANS upon association with the micelle surface is becoming increasingly similar to that of the corresponding bulk solution as ethanol content increases. Accordingly, there is less polymer associated with the micelle surface and/or the probe molecule and, by inference, the micelle surface is more accessible to the solvent. The polarity

(hydrophobicity) reported by the fluorescent probe at the CMC and CMC1 is presented in Figure 4.4 as a function of ethanol concentration.

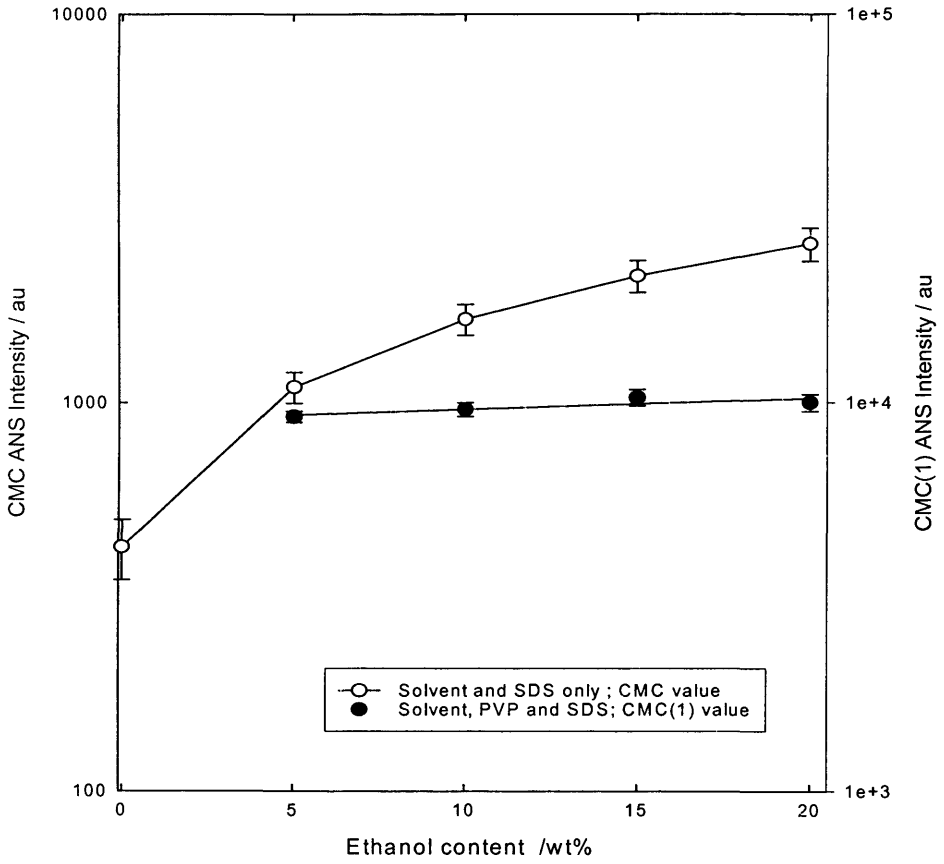

Figure 4.4 Fluorescence intensity of ANS at a surfactant concentration corresponding to the CMC for SDS (left hand scale) and at CMC(1) for 0.5%w/w PVP-SDS (right hand scale) as a function of ethanol concentration.

In the presence of the polymer, the hydrophobicity is significantly greater and less dependent on ethanol content compared with the no-polymer case. This suggests that the ethanol participates to a far smaller degree in the micellisation process when the

polymer is present. This is in agreement with the behaviour of CMC1 which does not vary with ethanol content.

The surface tension data for systems with ethanol contents of > 20% ethanol are particularly featureless and do not allow for determination of CMCs nor for confirmation of absence of CMCs. This limits the analysis primarily with the concentration region 0 wt % < ethanol < 15 wt %. Changes in the ANS fluorescence intensity (and also the SANS which will be covered later) suggest that micellisation does take place beyond 20 wt % ethanol.

4.2.1 Structure of SDS micelles upon addition of ethanol

The SDS/ethanol system was investigated using SANS to characterise the effects of ethanol on the size and shape of the simple SDS micelle.

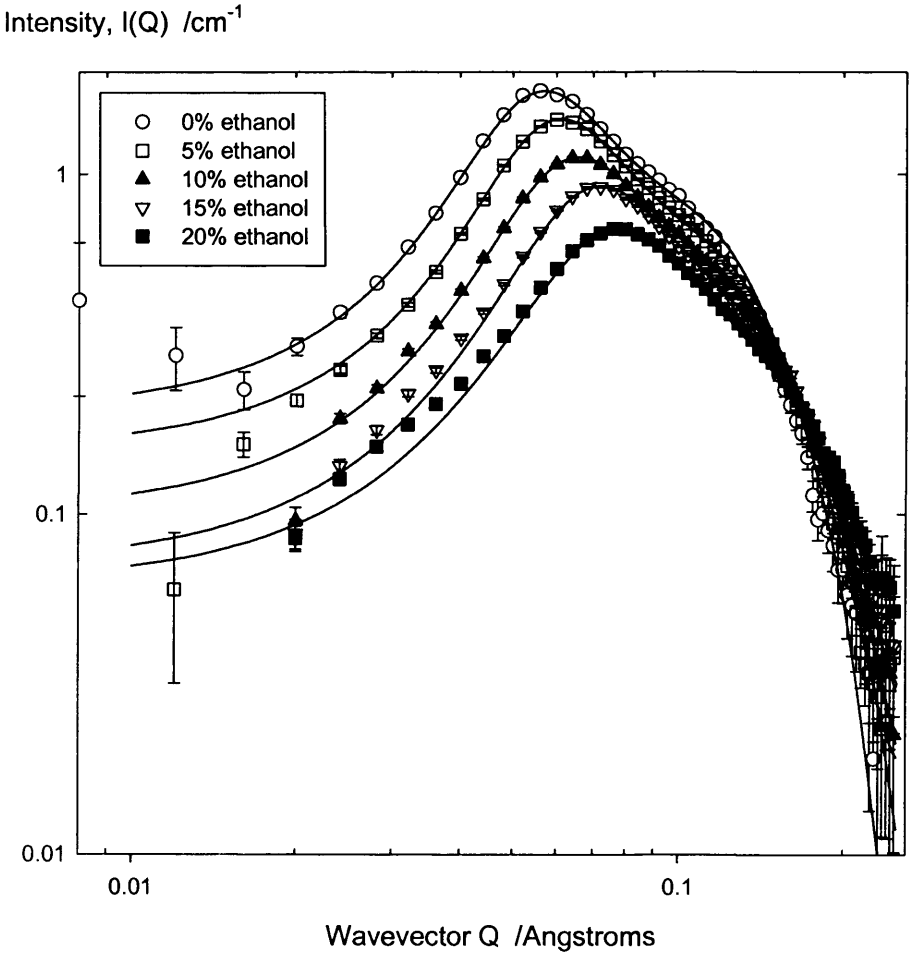

Figure 4.5 SANS from 75mM h-SDS in D_2O solutions as a function of d-ethanol content. (h-SDS is the normal hydrogenated version as opposed to the deuterated version, d-SDS). The solid lines correspond to fits to the core-shell model.

Figure 4.5 presents SANS data from 75 mM SDS solutions (without PVP) as a function of ethanol content. In these studies, deuterated ethanol has been used. The scattering length density of CD_3CD_2OH is sufficiently similar to that of D_2O that over the range of ethanol concentration studied here, 0 wt % < [ethanol] < 20 wt %, the scattering length density of the solvent changes by < 5%. Nonetheless, these small variations are implicitly included in the fitting procedure and subsequent analysis.

At this surfactant concentration, the data exhibit a strong structure factor peak as a result of the electrostatic interaction between adjacent micelles. With increasing ethanol content, this peak becomes progressively weaker, suggesting that the ionic character of the micelle is decreasing, although the electrostatic interaction is a strong function of the dielectric constant of the medium.

The peak also moves toward a higher *Q* value, associated with a closer proximity of the micelles. At a fixed surfactant concentration, this implies that the micelles are becoming smaller. The data have been fitted to the charged core-shell ellipse model.

Ethanol Wt %	R_{core} / Å	Shell thickness, δ/Å	Axial ratio	Polar shell – OH volume fraction	Aggregation number N_{agg}
0	16.7	3.2	1.25	0.70	65
5	15.8	2.9	1.25	0.66	58
10	15.8	2.5	1.0	0.64	46
15	15.7	2.3	0.95	0.61	44
20	15.4	2.2	0.90	0.60	38

Table 4.3 SANS fitting parameters for SDS/ethanol systems

Key parameters obtained through fitting the data are presented in Table 4.3. The aggregation numbers thus calculated are in very good agreement with those presented by Caponetti[13] and Almgren et al[14]. The addition of ethanol to the solvent alters the dielectric constant of solution and the solvent hydrophobicity. A more hydrophobic solvent decreases electrostatic repulsion between the head groups, allowing closer packing and a reduction in aggregation number[15].

4.2.2 Structure of the PVP/SDS/Ethanol Complex

Having characterized the effects of ethanol on the surfactant micelle, the range of data available has been used to quantify the effects of ethanol on the polymer conformation in the absence of surfactant. Viscosity (figure 4.6) and SANS (figure 4.7) have been used to this end.

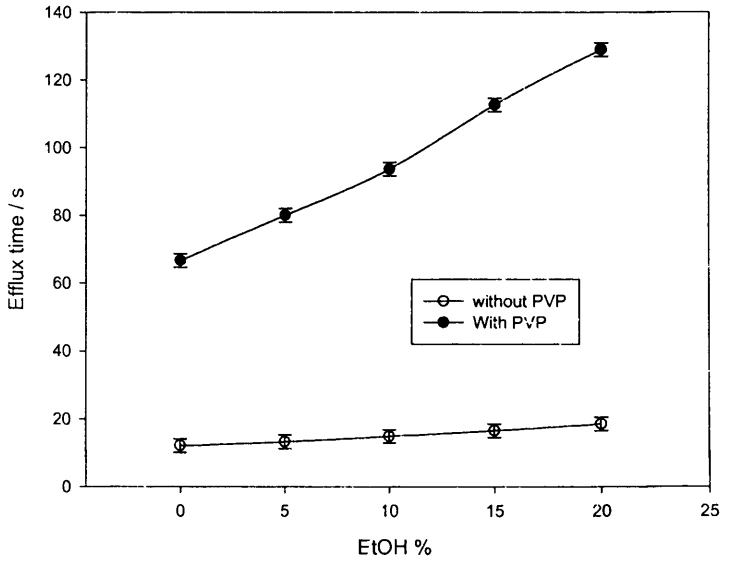

Figure 4.6 Solvent viscosity (efflux time) in the absence (open circles) and presence of PVP (closed circles)

The SANS data clearly show that the polymer scattering is unaffected by the presence of ethanol, and the scattering may be described by a simple Lorentzian with a correlation length of ξ= 55 Å. The viscosity of simple PVP solutions however does change upon addition of ethanol, but since the polymer conformation is unaffected (shown by figure 4.7, SANS) by the addition of ethanol, the changes observed in the viscosity merely reflect the change in the solvent viscosity rather than a change in the polymer conformation.

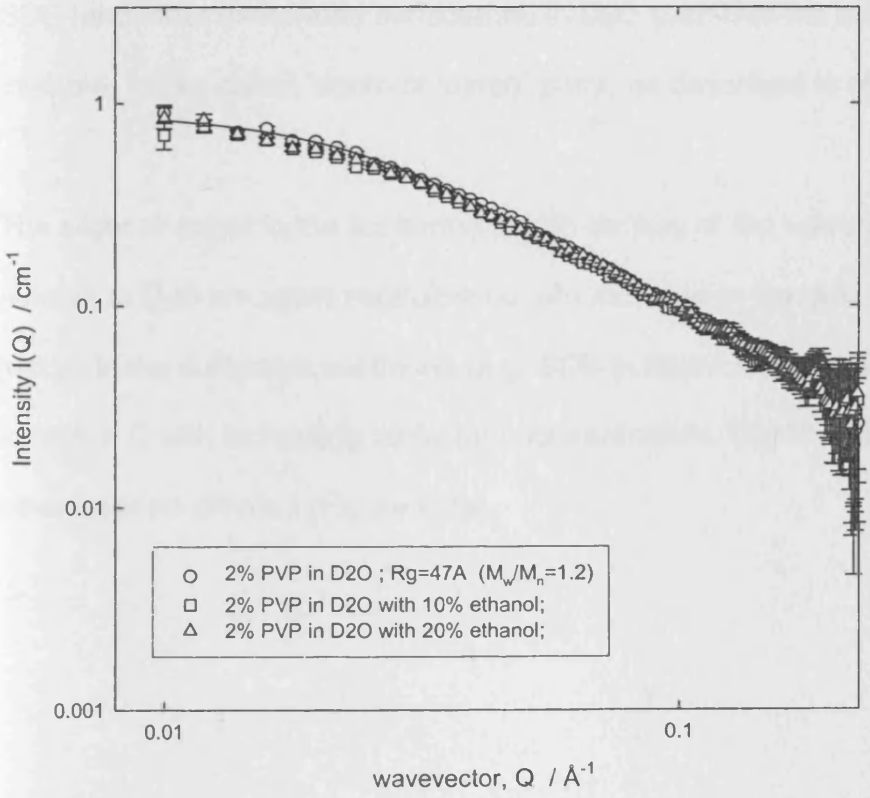

Figure 4.7 SANS from 2wt% PVP in D_2O solutions as a function of d-ethanol content. The solid lines correspond to fits to a simple Lorentzian to account for scattering from a polymer network.

It has become well-established from SANS studies that when an anionic surfactant is added to an aqueous non-ionic or polyampholytic polymer solution at low ionic strengths, the polymer scattering adopts some character of the micelle scattering.

This principally involves the appearance of the peak characteristic of surfactant scattering in the *polymer* scattering; in other words, the polymer coil wraps around the surfactant micelle, adopting a significant character of the micelle morphology, at least over the *Q* range being investigated. This is very easily demonstrated using deuterated SDS (and other deuterated surfactants) in D_2O such that the surfactant is rendered invisible, the so-called "contrast match" point, as described in chapter 2.

The slight changes in the scattering length density of the solvent induced by adding *d*-ethanol to D_2O are again negligible but are included in the data analysis. Accordingly, just as in the surfactant scattering (e.g. SDS in figure 4.5), the structure peak will move to higher *Q* with increasing surfactant concentration. The PVP/SDS system (without ethanol) is no different (Figure 4.8a).

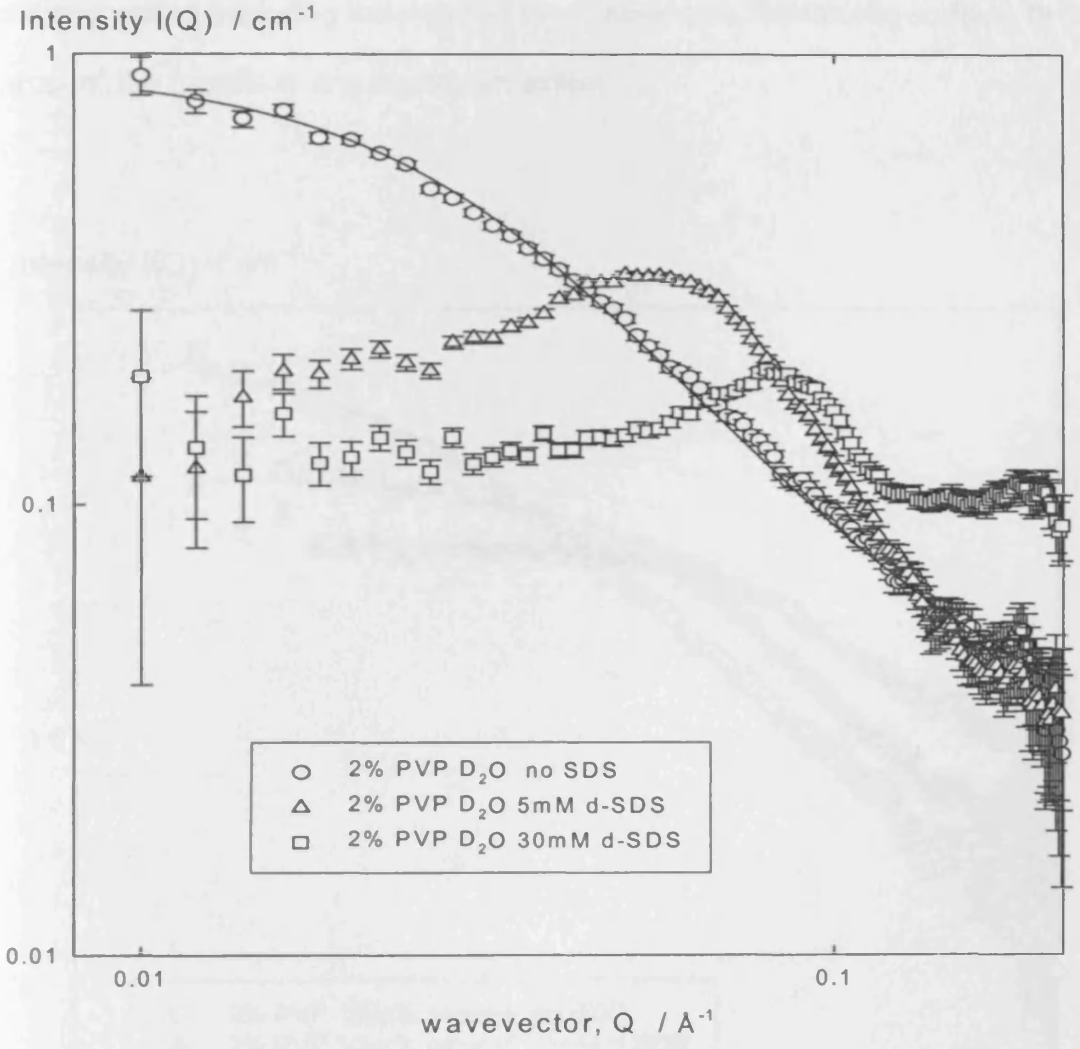

Figure 4.8(a); SANS from 2% PVP in D2O as a function of the concentration of d-SDS; i.e. conditions of "contrast match" for the surfactant

However, in the presence of, for example, 10 wt % ethanol (Figure 4.8b), the situation is quite different to the simple aqueous case with only small changes observed in the scattering and no pronounced structure peak. This implies that the intermicellar repulsion is significantly reduced in the presence of ethanol, in an analogous manner to the addition of salt. In the presence of ethanol, the surfactant micelle adsorbs to the

polymer without causing the polymer to collapse onto the micelle surface, or "wrap around" the micelle to any significant extent.

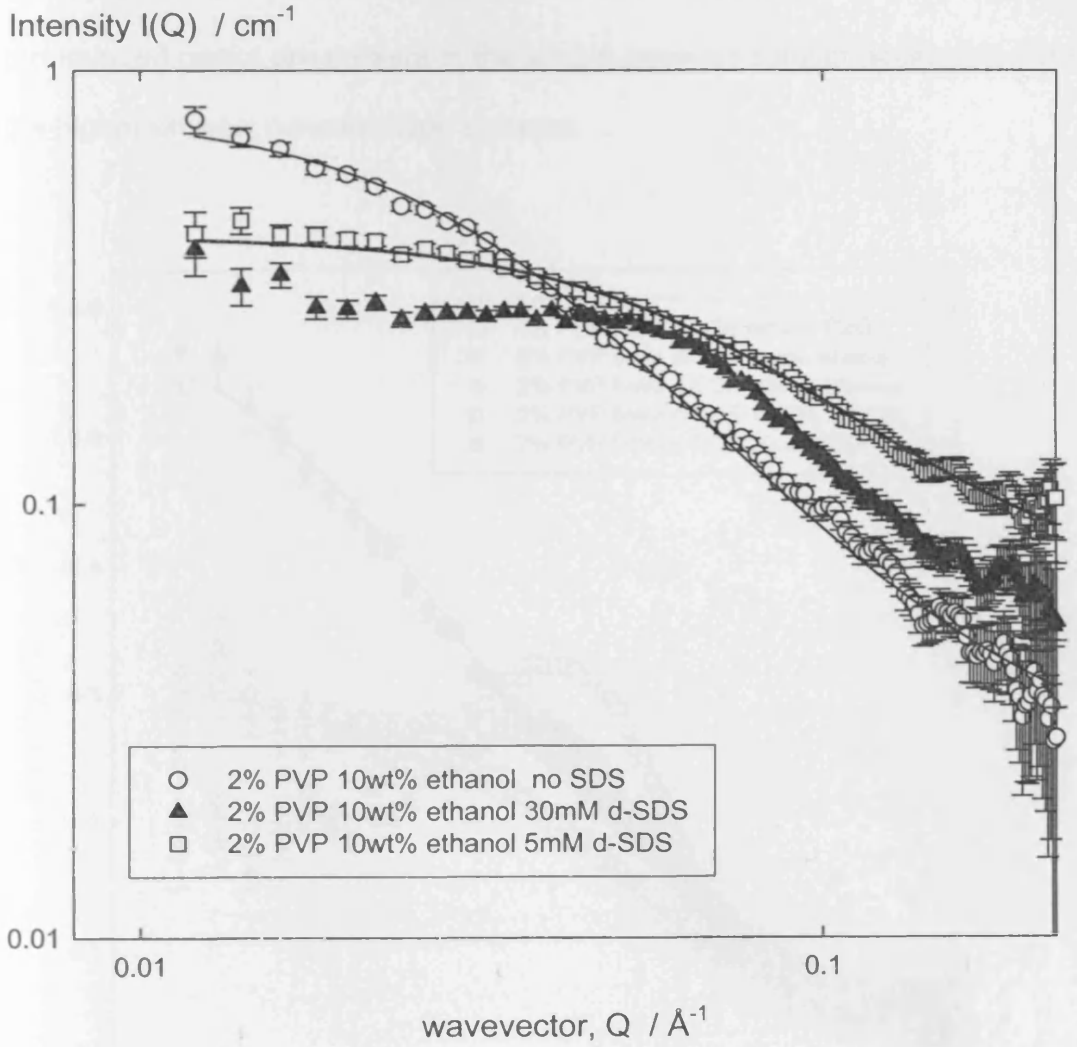

Figure 4.8(b); SANS from 2% PVP in D_2O/10% d-ethanol solutions as a function of concentration of deuterated SDS; the surfactant in contrast matched.

The effect of bound surfactant on the size and shape of the polymer can be studied by recording the scattering under contrast match conditions for the surfactant. This is presented as the two sets of PVP/SDS/ethanol/water SANS, 5mM*d*-SDS and 30mM *d*-SDS, presented in parts a and b of Figure 4.9, respectively. For both data sets, pronounced peaks are present in the simple aqueous solution scattering but absent in the higher ethanol concentration systems.

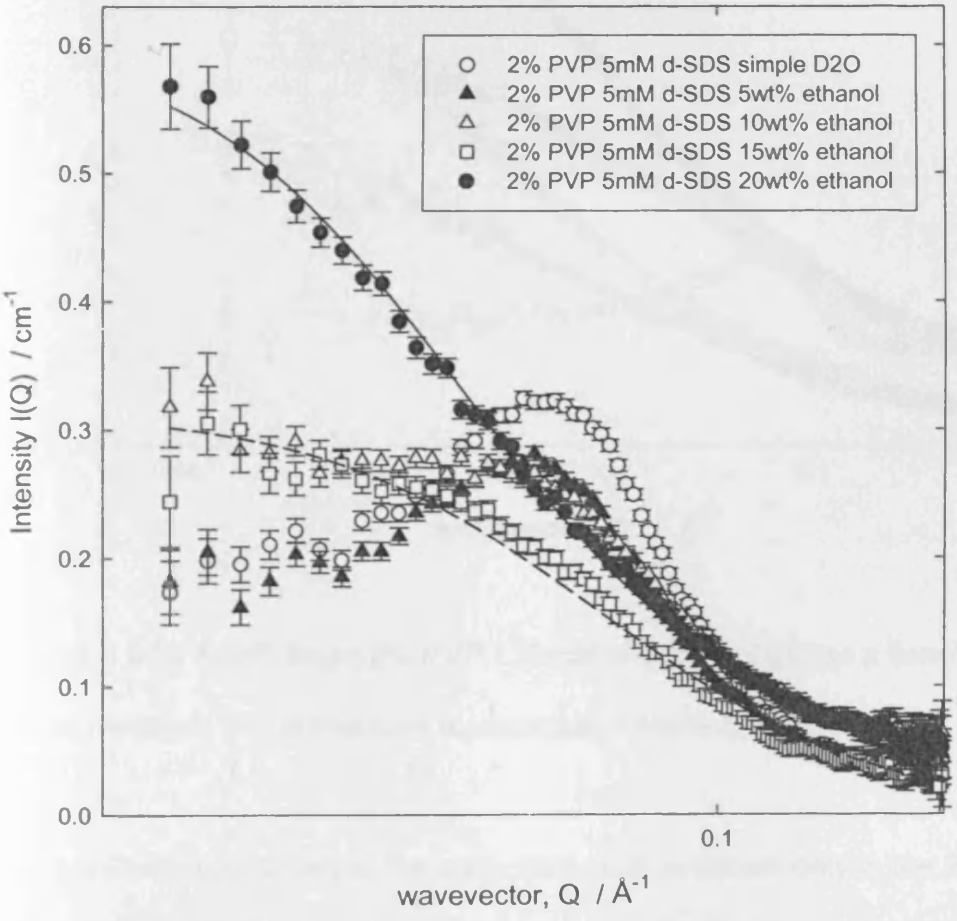

Figure 4.9(a) SANS from 2% PVP / 5mM d-SDS in D2O as a function of d-ethanol concentration; the surfactant is contrast matched.

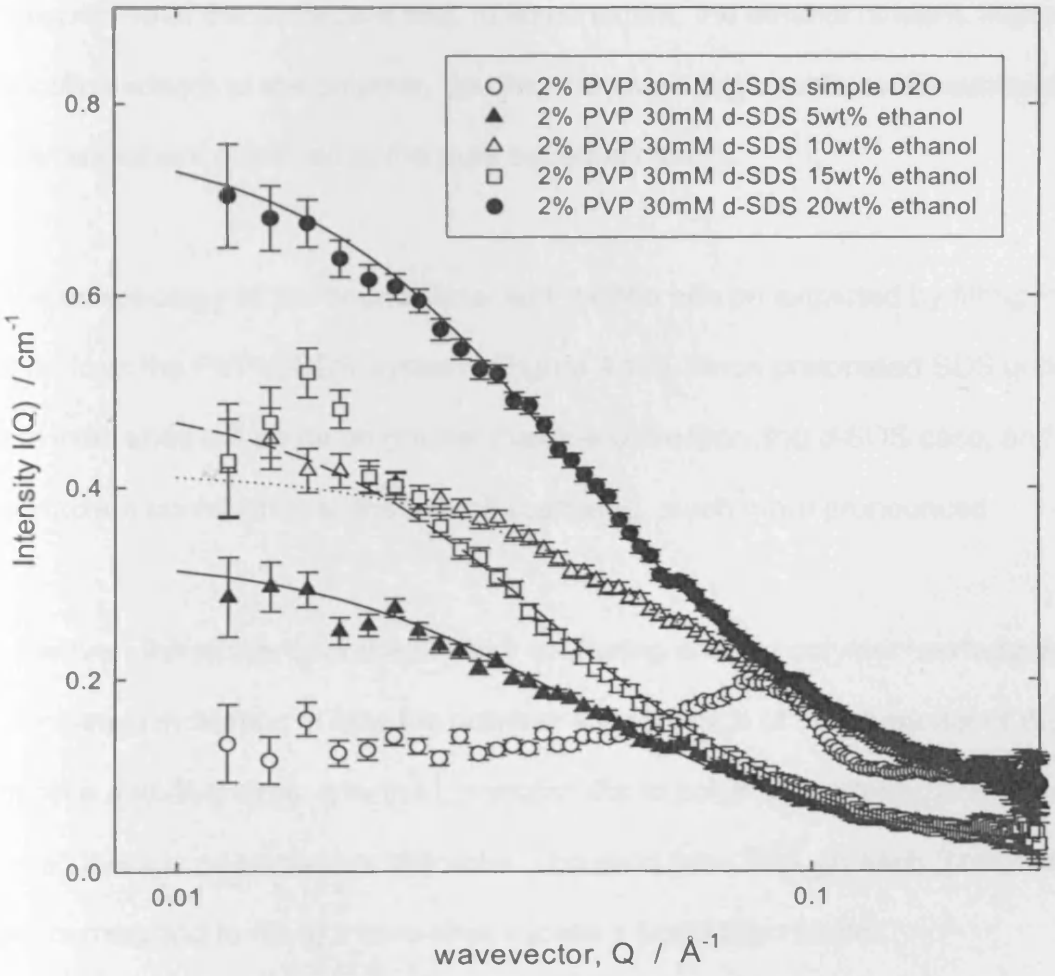

Figure 4.9(b) SANS from 2% PVP / 30mM d-SDS in D2O as a function of d-ethanol concentration; the surfactant is contrast matched.

For the 5mM *d*-SDS series, the surfactant peak is absent only in the 20 and 15% ethanol cases. For these samples, $\xi_{20wt\%}$ = 24(±2) Å and $\xi_{15wt\%}$ = 15(±4) Å.

For the 30 mM *d*-SDS series, the surfactant peak is only clearly observed in the absence of ethanol. The Lorentzian fits correspond to $\xi_{20wt\%}$ = 24(±2) Å, $\xi_{15wt\%}$ = 25(±2)

Å, $\xi_{10wt\%}$ = 15($\pm$3) Å, $\xi_{5wt\%}$ = 25($\pm$2) Å. The similarity of these correlation lengths irrespective of the surfactant and, to some extent, the ethanol content, implies that the micelles adsorb to the polymer, causing the same large scale conformational rearrangement observed in the pure aqueous case.

The morphology of the bound surfactant micelle can be extracted by fitting the SANS data from the PVP/*h*-SDS systems (Figure 4.10). Since protonated SDS is now used, the intensities will be much greater than the corresponding *d*-SDS case, and the surfactant contribution to the overall scattering, much more pronounced.

However, the similarity of the polymer scattering and the polymer+surfactant scattering is a simple indication of how the polymer adopts much of the character of the bound micelle and, therefore, why the Lorentzian fits to polymer scattering are only meaningful when there is no surfactant character. The solid lines through each (protonated) data set correspond to fits to a core-shell micelle + Lorentzian model.

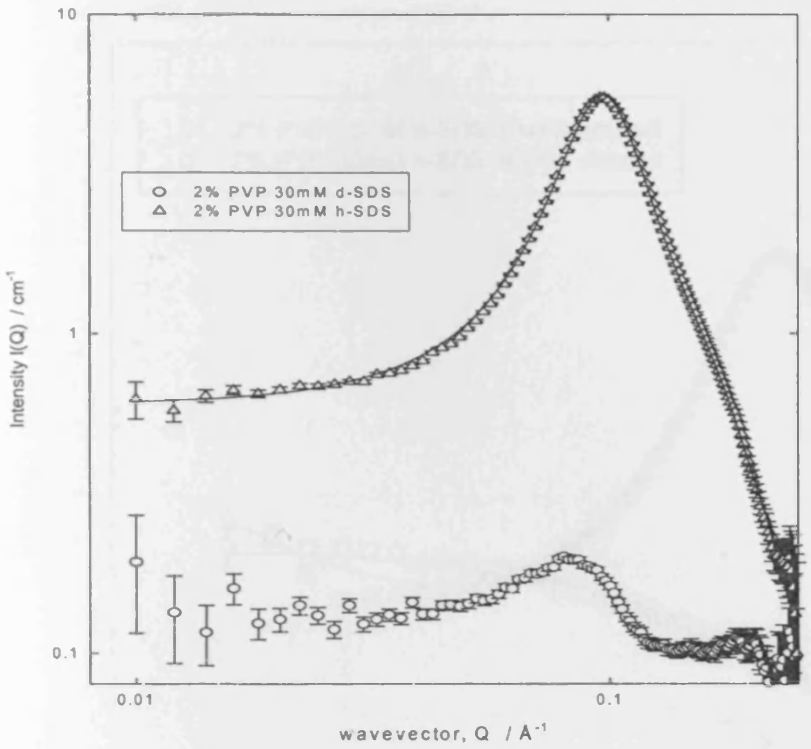

Figure 4.10(a) SANS from 2% PVP and 30mM SDS in D_2O. The fit to the polymer/h-SDS dataset is based on a radius of the bound micelle R_{core}= 16.7 Å with an ellipticity of 1.3, corresponding to aggregation number of 72 (± 5). The shell thickness is slightly larger , ~5 Å, than the no-PVP case. The d-SDS dataset has been used as a "background" when fitting the h-SDS dataset to empirically account for the polymer scattering.

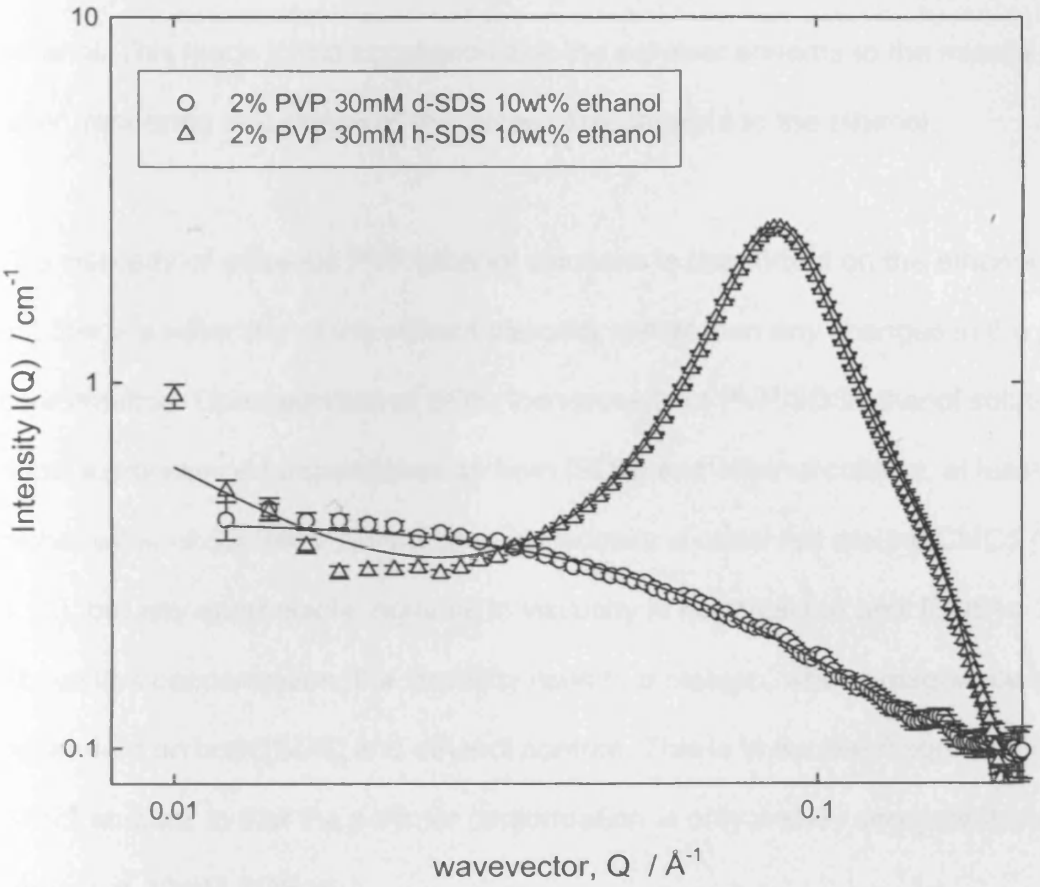

Figure 4.10(b); SANS from 2% PVP and 30mM SDS in 10% ethanol. The fit to the polymer/ h-surfactant dataset is based on a radius of the bound micelle R_{core}= 16.6 Å with an ellipticity of 1.2, corresponding to aggregation number of 65 (±6). The shell thickness is slightly larger than the no-PVP case, 4 Å. The correlation length ξ = 19 Å extracted from the d-SDS dataset was adopted in the polymer-surfactant curve.

The parameters describing these fits are presented in the figure legends. As seen by comparison with table 4.3, the effect of ethanol on the bound micelle morphology is

minimal. The bound micelle is very similar to the micelle formed in the absence of ethanol. This leads to the conclusion that the polymer adsorbs to the micelle palisade layer, rendering that region of the micelle inaccessible to the ethanol.

The viscosity of aqueous PVP/ethanol solutions is dependent on the ethanol content, but this is a reflection of the solvent viscosity rather than any changes in the polymer conformation. Upon addition of SDS, the viscosity of PVP/SDS/ethanol solutions do show a pronounced dependence on both [SDS] and ethanol content, at least at the higher ethanol contents. An increase in viscosity is observed around CMC1 (Figure 4.11), but any appreciable increase in viscosity is not detected until [SDS] > 20 mM. Above this concentration, the viscosity rises to a plateau, whose magnitude is dependent on both [SDS] and ethanol content. This is in excellent agreement with the SANS studies, in that the polymer conformation is only weakly dependent on ethanol content at 30mM SDS.

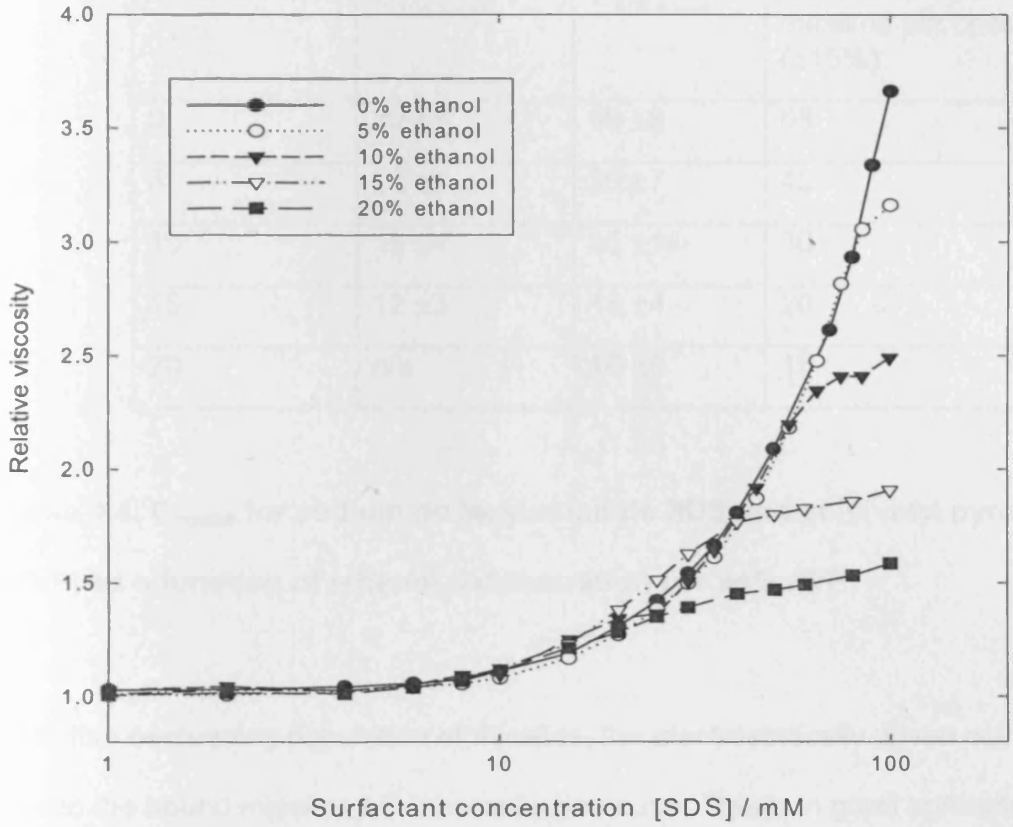

Figure 4.10 Relative viscosity of 2% w/w PVP as a function of SDS concentration for a range of ethanol contents

From table 4.4, it is possible to calculate the saturation point at the polymer concentration and, given the aggregation number extracted from the SANS analysis, the number of bound micelles.

The number of micelles per chain decreases from n = 55 in the absence of ethanol to n =15 as the ethanol concentration approaches the minimum in the CMC data of 15-20 wt% ethanol.

Ethanol / wt%	$C^{surfacetension}_{SDS\ bound}$	$C^{ANS}_{SDS\ bound}$	Number of bound micelles per chain (±15%)
0	30 ±8	40 ±8	55
5	22 ±7	30 ±7	40
10	15 ±4	25 ±14	30
15	12 ±3	15 ±4	20
20	n/a	10 ±6	15

Table 4.4. C_{bound} for sodium dodecylsulphate SDS and poly(vinyl pyrollidone) (PVP) as a function of ethanol concentration per wt% PVP

With this decreasing population of micelles, the electrostatically driven coil expansion due to the bound micelles will inherently decrease. This is in good agreement with the qualitative analysis of the scattering data, in terms of under what conditions (SDS, ethanol, concentration etc.) the Lorentzian fit is no longer valid.

Finally, the amount of polymer at the micelle interface was also examined by EPR, based on the morphology of the micelle extracted from the SANS experiments. It is assumed that the spin-probe executes rapid motion within the head group region of the micelle and its spectrum reflects the structure of that region. The separation of the two high field lines is a measure of the polarity of the head group region, specifically, the volume fraction of-OH dipoles present. The polarity sensed by the spin-probe in the SDS/ethanol system decreases (Figure 4.11) with increasing ethanol content.

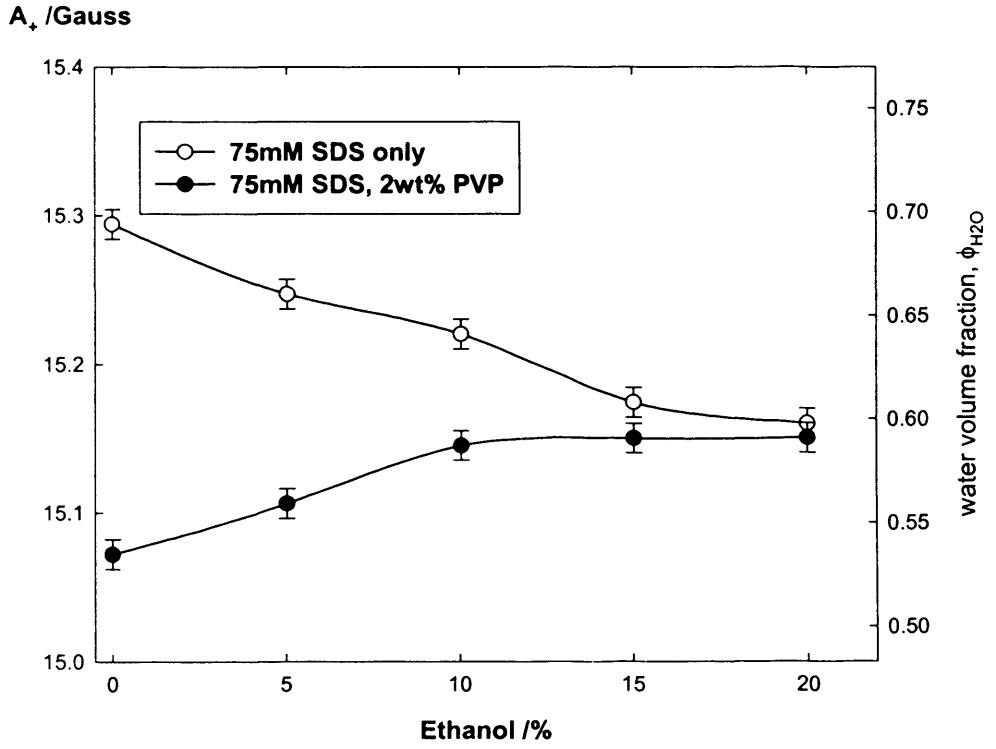

Figure 4.11 Hyperfine coupling constants of 16-DSE solubilised in 75mM SDS micelles in the presence and absence of PVP as a function of ethanol concentrations

From the SANS analysis, it may be seen that this principally corresponds to a decreasing aggregation number. The EPR results are counterintuitive since it would be expected that the volume fraction of water present in the head group region to increase as the curvature of the micelle increased, due to the larger available volume per surfactant head group within the head group region. Therefore, the decrease in polarity is reflective of the amount of ethanol present in the head group region. Since the volume of an ethanol molecule is significantly greater than that of a water molecule, a small amount of ethanol will displace a considerable amount of water.

When PVP is present, the volume fraction of –OH groups in the head group region increases with increasing ethanol content. However, the SANS results suggest that there is no change in the micelle aggregation number for bound micelles and, therefore, no change in the polar shell volume per surfactant head group. Thus, the increase in -OH volume fraction is more reflective of an increasing fraction of the available volume per surfactant head group being accessible to the solvent; that is, the polymer is being displaced from the micelle surface. As the polymer "lifts off" the micelle surface, the effects of the bound micelle are reduced, as exhibited in the SANS and viscosity data.

4.3 Discussion

The thermodynamics of surfactant micellisation and polymer/surfactant complexation have been discussed in detail by Nagarajan[16] and by Blankschtein et al[17]. Adopting the notation of Nagarajan, the free energy of formation for polymer-bound micelles has a number of contributing terms - the transfer of the surfactant tail from water into the micellar core, a contribution that is dependent on the solubility of the surfactant; the deformation of the surfactant tail as it conforms to packing requirements within the micellar core; the energy of forming the aggregate core/water interface which is dependent on the aggregation number, as this defines how much of the core is shielded from the solvent; and, finally, two terms that account for the head group interactions over the micellar surface, one steric and for ionic surfactants, an electrostatic interaction between the surfactant head groups. These last two terms are

particularly dependent on the size, shape, and orientation of the (charged) head groups and factors such as the dielectric constant of the solvent. There are also three contributions due the fact that there is polymer at the micelle surface which embody the enhanced shielding of the core, a further steric repulsion term introduced by the presence of the polymer, and a term to deal with the change in free energy of the polymer molecule itself.

The contributions that are directly affected by the solvent composition are principally the transfer of the surfactant tail from water, as this depends on the solubility of the surfactant in the solvent; with increasing ethanol content, the surfactant is more soluble. The formation of the interface between the hydrophobic core and the surrounding solvent is dependent on the surface area of the hydrophobic core that is in contact with the solvent and the macroscopic interfacial tension of the solution.

Making the assumption that the interfacial tension of the aggregate core/continuous phase follows the same trend as the surface tension of the bulk solution, that is, a decreasing interfacial term with increasing ethanol content, the energy required to produce the interface decreases (favours micelle formation). The term which considers the ionic head group interactions is a complex one, which cannot be estimated simply. A number of factors come into play in determining the energies of the head group interactions, including the dielectric constant, Debye length, and radius of the micelle. For instance, the dielectric constant of the solution decreases as the ethanol content

increases, which in turn influences the various charge effects such as counterion dissociation and hence the size and shape of the micelle.
Introducing the polymer further complicates the situation.

The shielding of the core from the solvent determines whether the interaction occurs. The greater the shielding of the core, the more favourable will be the interaction between micelles and polymers. Accordingly, non-ionic polymers/anionic surfactants show much stronger interactions than non-ionic polymers/cationic surfactants, (as the head groups of cationic surfactants are generally much bigger than those of anionic surfactants) hence, the amount of hydrophobic core exposed to the continuous phase is significantly smaller for non-ionic polymer with anionic surfactant.

The steric terms describing the polymer and its interaction with the surfactant head groups will always be unfavourable due to constraints of packing and the "wrapping" of the polymer strand around the micelles; this is therefore sensitive to the polymer conformation at the micelle surface.

The behaviour of the PVP/SDS/ethanol/water system may be rationalized by considering the electrostatic interactions between the sulphate head groups. The critical micelle concentration of the surfactant and the aggregation number of the micelle the surfactant forms are determined largely by the volume of the hydrophobic tail and the charge on the head group. As ethanol is added to the continuous phase, the dielectric constant decreases, which permits a closer separation of the head groups. The area of

the hydrocarbon core in contact with the aqueous phase decreases. The closer proximity of the head groups means that the steric terms increase, but this is a much smaller effect. In the presence of PVP, CMC1 is lower than the CMC, but this quantity and the aggregation number are both invariant with ethanol content.

However, with increasing ethanol content, the polymer increasingly attains a conformation more reminiscent of the no-SDS and no-ethanol cases, which would suggest that the area of the surfactant core "occluded" by the polymer decreases. This is compensated by the adsorption of ethanol into the palisade layer but with no significant change in the aggregation number or counterion binding.

4.4 Conclusions

Surface tension and fluorescence are shown to give complimentary estimates of the various critical micelle concentrations present in the SDS/PVP/ethanol/water system, distinguishing free and bound micelles. SANS and viscosity measurements show that the bound micelle affects the polymer conformation, a perturbing effect that is weakened once ethanol is present. EPR and SANS give a useful insight into how the polymer lifts off the micelle surface as the ethanol solubilisation increases.

Upon addition of ethanol to aqueous SDS solutions, the CMC decreases to a minimum around 15% ethanol content before subsequently increasing; that is, it follows both the co-solvent and co-surfactant effects. There is a decrease in the aggregation number as the effective dielectric constant permits a closer proximity of the surfactant head groups.

When PVP is added, the micellisation concentration CMC1 is lower than that in the no-PVP case but is invariant with increasing ethanol. Above 15% ethanol, the micellisation concentration increases once more and is numerically identical to the micellisation concentration measured in the absence of the polymer.

4.5 Future Work

A robust investigation of the SDS-PVP system in the presence of ethanol has allowed for a comprehensive overview of the physical properties of these systems to be developed. Future work could go in a number of directions. The same set of techniques can be used to probe SDS in the presence of other types of polymer, or other surfactants in the presence of PVP. The second part of this thesis embarks on that journey by replacing PVP with the pluronic P104.

The SDS-PVP system could also be investigated at the full range of ethanol concentrations, up to 100%, to determine the point at which micellisation no longer occurs and the impact that ethanol rich environments have on the micellisation process and interactions between surfactant and polymer. This system would also benefit from study across a wider range of temperatures.

References

[1] Griffiths, P.C., Hirst, N., Paul, A., King, S.M., Heenan, R.K., and Farley, R., *Langmuir,* **2004,** *20,* 6904-6913

[2] Griffiths, P.C., Paul, A., and Hirst, N., *Chem. Soc. Rev.* **2006**

[3] Turro, N.J., Baretz, B.H., Kou.P-L. *Macromolecules*, **1984**, *17,* 1321-1324

[4] Safarpour, M.A., Rafati, A.A., Gharibi, H., *J. Chin. Chem.Soc.* **1999,** *46* (6), 983-991

[5] Gharibi, H., Razavizadeh, B.M., Rafiti, A.A., *Colloids Surf., A*, **1988**, *136,* 123-132

[6] Fukual, H., Satake, I., Hayakawa, K., *Langmuir*, **2002**, *18,* 4465-4470

[7] Staples. E., Tucker. I., Penfold, J., et al. *Langmuir*, **2002**, 18, 5147-5153

[8] Griffiths, P.C., Roe. J.A., Bales. B.L., et al, *Langmuir*, **2000**, *16,* 8248-8254

[9] Griffiths, P.C., Roe, J.A., Abbott, R.J., Howe, A.M., *Imaging Sci. J.* **1997**, *45*, 224-228

[10] Zana, R., *Adv. Colloid Interface Sci.,* **1995**, *57*, 1-64

[11] Dhara, D., Shar. D.O., *J. Phys. Chem. B.* **2001**, *105*, 7133-7138

[12] Gharibi, H., Rafati, A.A., *Langmuir,* **1998**, *14,* 2191-2196

[13] Caponetti, E., Chillura Martino, D., Floriano, M.A., Triolo, R. *Langmuir*, **1997**, *13*, 3277

[14] Almgren, M., Swarup, S., *J. Colloid Interface Sci.* **1983**, *91,* 256

[15] Rafati, A.A., Gharibi, H., Rezaie-Sameti, M., *J. of Molecular Liquids,* 111, **2004**, 109-116

[16] Esumi, K., Ueno, M., *Structure-performance relationships in surfactants:* Marcel Dekker: New York, 1997, Vol.70 Chapters 1 and 12

[17] Blanckschtein, D., *Langmuir*, **1994**, *10*, 3512

Chapter 5
Context

With a comprehensive set of results obtained for SDS with PVP in water/ethanol mixtures, the study then moved on to investigate SDS with a pluronic, P104, in water/ethanol mixtures. Poly(ethylene oxide) – poly(propylene oxide) – poly(ethylene oxide) (PEO-PPO-PEO) triblock copolymers in D_2O and D_2O/d-ethanol solvent mixtures were analysed using pyrene fluorescence, ^1H NMR and SANS. The PEO-PPO-PEO polymer used in this experiment was a commercial Pluronic, P104 as described in the chapter 3. Pluronic P104 was selected since it offered a CMC and CMT across concentration and temperature ranges that were convenient to measure and work with. It is also a widely used polymer with a vast number of chemical, pharmaceutical and industrial applications.

Fluorescence was used to track changes to the CMC, ^1H NMR to investigate the most probable origin of the interaction and therefore indirectly, the CMC plus SANS to investigate the size and shape of micelles. The study investigated whether a competitive micellisation process exists for SDS and P104, and how the presence of ethanol and SDS and change in temperature affects the properties of P104 in solution.

This was a more challenging system to study than PVP with SDS, because the polydispersity of the pluronic results in broad data curves, unlike the sharp breaks obtained with the SDS-PVP system. When ethanol is present in solution this causes further broadening of features, as was noted with the SDS-PVP system. Ultimately, this led to a less clear understanding of the nature of the interaction. However, some clear trends were established and these will be described in this chapter.

5.1 Fluorescence

Poly(ethylene oxide) – poly(propylene oxide) – poly(ethylene oxide) (PEO-PPO-PEO) triblock copolymer used in this experiment was a commercial Pluronic, P104. This was studied in H_2O and H_2O/ethanol solvent mixtures using pyrene probe fluorescence recorded on a Perkin-Elmer LB 50 Luminescence spectrophotometer, on samples equilibrated at 25°C and 35°C ± 1°C. The CMC of P104 in a range of ethanol/water ratios was determined at 25°C and 35°C, and at 25°C in the presence of SDS.

Using a pyrene probe which preferentially solubilises in hydrophobic environments, it can be seen that a break in fluorescence intensity ratio occurs upon increasing P104 concentration, indicating the formation of micelles. Figure 5.1 shows the effect of increasing the concentration of P104, producing a sigmoidal curve with two breaks as is consistent with the literature[1,2,3]. The breaks in the data are broad due to of the nature of such polymer aggregation but estimates of the CMC ranges can be obtained. Due to the amphiphilic nature of the P104 block copolymer, it will demonstrate features such as CMC, and a preference for adsorbing on interfaces to reduce unfavourable interactions of the hydrophobic domains in water[4], as described in chapter 1.

Alexandridis et al[5] used surface tension to determine that P104 adsorbs on the air/water interface until the point of complete coverage, at which point the molecules rearrange, leading to a break in the surface tension curve. At a higher concentration of P104, a second break is seen, corresponding to the formation of micelles in the bulk solution.

Surface tension was not used for this investigation of P104 in water/ethanol mixtures since the addition of ethanol rendered the surface tension curves too featureless to determine breaks in data from. Alexandridis reported good correlation between the CMCs obtained through surface tension and dye solubilisation. It has also been noted that different techniques produce a wide variation in the values obtained due to their sensitivity to the quantity of unimers present in solution, or lack of sufficient temperature control. Block copolymers also are not well defined but can have a broad molecular weight distribution which may also lead to ambiguous interpretation of results.

In figure 5.1, a sigmoidal curve is seen as the concentration of pluronic P104 is increased, with the first inflection indicating micellisation, second inflection indicating full solubilisation of the probe[6]. There has been discussion in the literature of which point in the curve should be used for determining the CMC. Alexandridis et al used the first point of inflection which produced values of an order of 1 magnitude difference than those produced by Schmolka and Raymond[7], who had apparently misinterpreted the curve and based the CMC on the second inflection. The transition region over which the CMC appears to occur could be due to the molecular weight distribution of the polymer or the presence of by-product impurities from the manufacturing process.

5.1.1 Effect of Ethanol on the CMC of P104

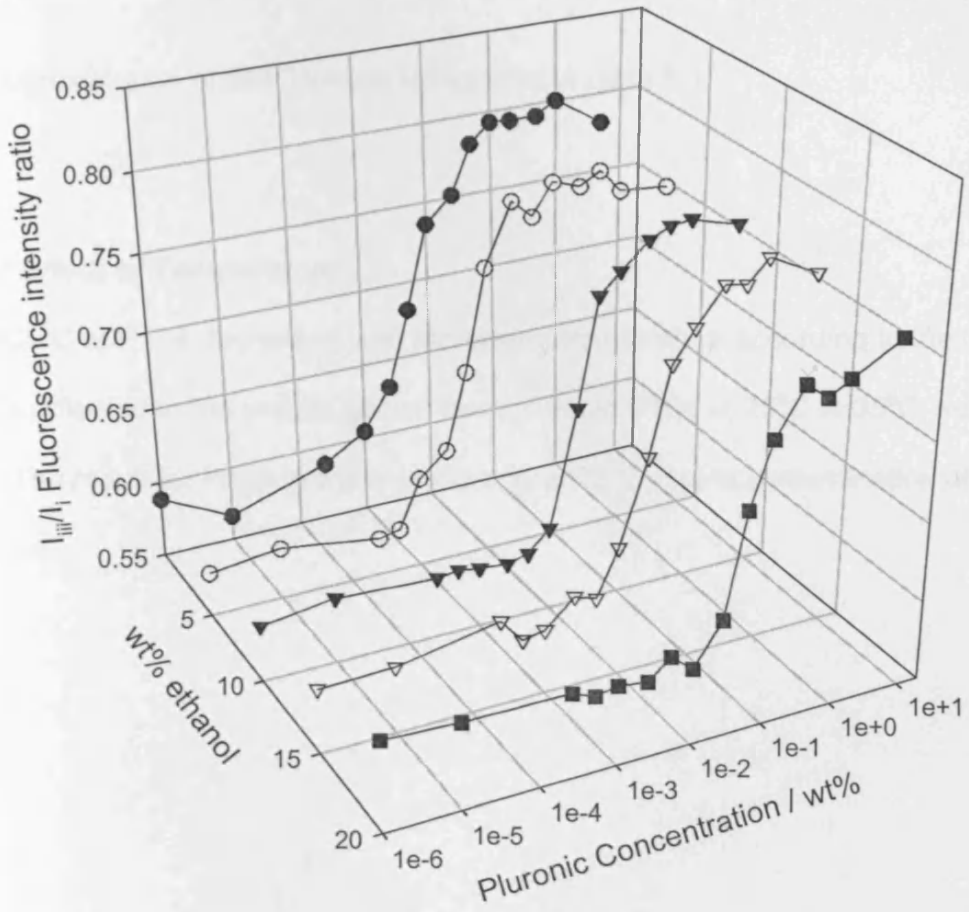

Figure 5.1 Pyrene fluorescence intensity ratio for P104 as a function of concentration at 25°C in 0% to 20% ethanol concentration

It can be seen that increasing the ethanol content of solution results in only a weak increase in the CMC. The increasing hydrophobicity of the solution with increasing ethanol content disfavours micellisation by providing a better solvent for the hydrophobic block of P104. Unlike the co-surfactant/co-solvent effects on SDS-only leading to a decrease and then increase in the CMC, P104 appears to experience a

steady co-solvent effect resulting in an increase in CMC as ethanol content is increased. It is worth noting that 0% to 5% ethanol shows little change, jumping to 10% ethanol which changes little to 15%. A larger increase in CMC is seen at 20% ethanol.

An approximation of CMC values is included in table 5.1.

5.1.2 Effect of Temperature

The CMC of P104 decreases with increasing temperature according to the literature and this is reflected in the results gained from pluronic P104 at 25°C to 35°C, seen in figure 5.2. The result for P104 in water is missing at 35°C due to contamination of the original sample.

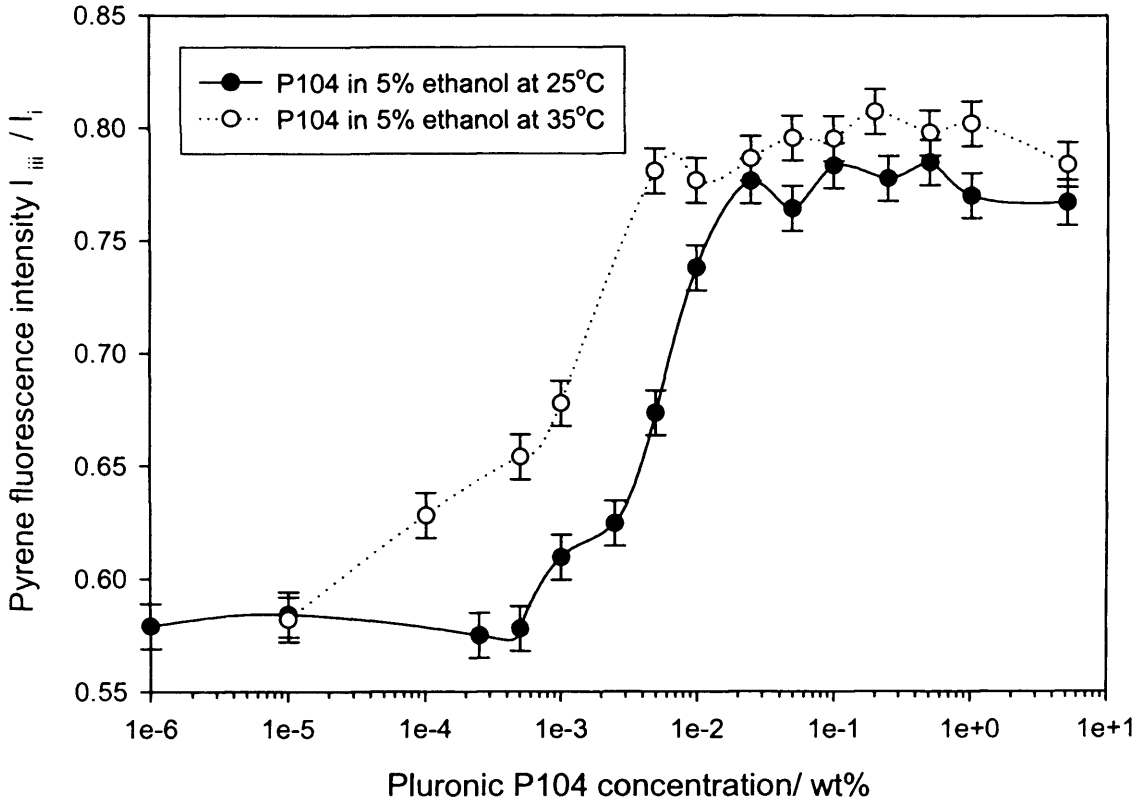

Figure 5.2 Pyrene fluorescence intensity ratio for P104 in 5% ethanol as a function of concentration at 25°C (closed circles) and 35°C (open circles)

Using 5% ethanol content as an example, it is clear that the CMC has decreased with increasing temperature for P104. This was the case for all ethanol concentrations investigated. As ethanol content is increased, the curves become more unstable and features harder to determine at 35°C. The inflection in the curves become broader and greater experimental error due to difficulty in avoiding temperature fluctuations leads to larger error in determining CMC values. CMC ranges are provided in table 5.1.

The next stage was to investigate the effect of adding SDS to a solution of P104 micelles.

5.1.3 Fluorescence of P104 with SDS in water/ethanol mixtures

The CMC of SDS in the presence of P104 was investigated, at concentrations of P104 above and below its own CMC. Figure 5.3 shows the curve obtained for increasing the concentration of SDS in the presence of P104 below its CMC, across the range of ethanol concentrations.

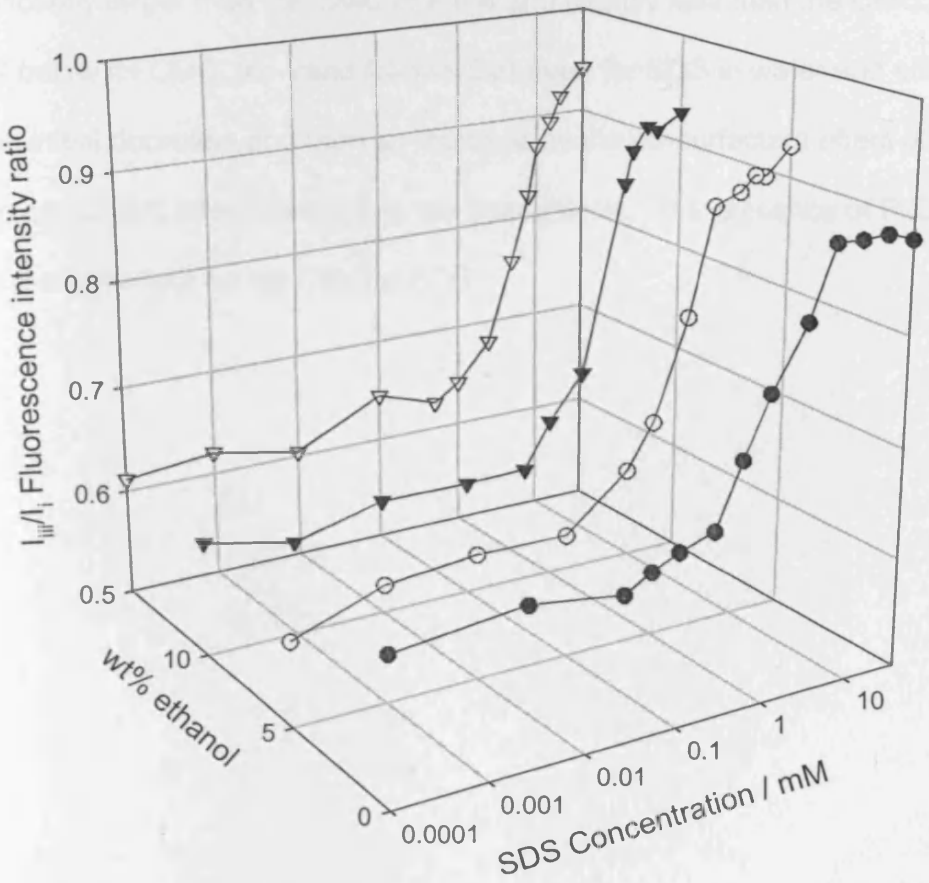

Figure 5.3 Pyrene fluorescence intensity ratio for 0.0005% P104 as a function of SDS concentration in water/ethanol at 25°C

Only one break in the curve is observed, as expected. Unlike the example of PVP, SDS does not form micelles along the P104 polymer, therefore only one CMC is observed as

SDS forms micelles in solution, regardless of the presence of polymer. As observed with other systems in this study, increasing ethanol content creates a broadening of the curves. The trend for SDS in water/ethanol mixtures with P104 is similar to that observed for SDS-only in water/ethanol mixtures, and outlined in chapter 4.

Although CMC values are presented as broad ranges (table 5.1), it can be seen that the CMC increases as the concentration of ethanol is increased. The CMC values are significantly larger than the CMC of P104 and slightly less than the CMC of SDS. With P104 below its CMC, the trend follows that seen for SDS in water and ethanol mixtures i.e. an initial decrease and then an increase as the co-surfactant effect of ethanol shifts to the co-solvent effect dominating the interactions. The presence of P104 appears to have a small effect on the CMC of SDS.

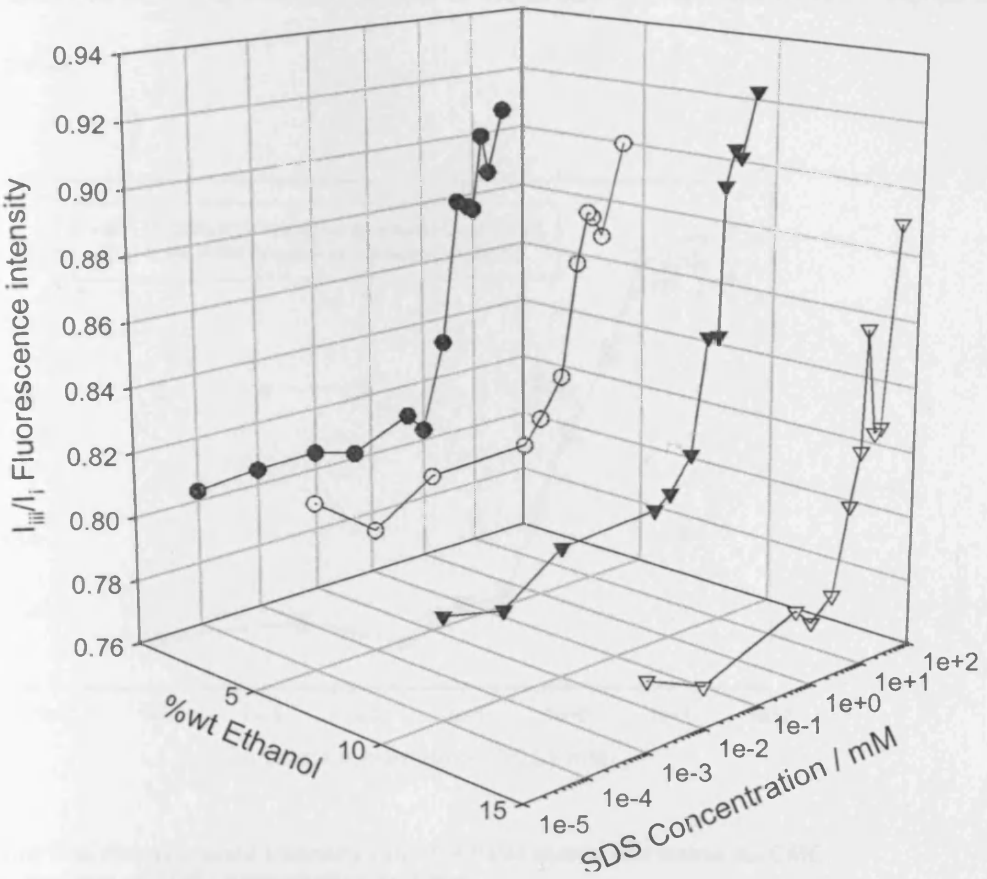

Figure 5.4 Pyrene fluorescence intensity ratio for 0.5% P104 as a function of SDS concentration in water/ethanol at 25°C

Figure 5.4 shows the curve obtained for SDS in the presence of P104 above its own CMC, at 25°C. It is notable that when P104 is present above its own CMC, the curve is shallower and breaks in the data are less sharp making it harder to determine what is happening to the CMC of SDS in this example. Curves are shallower because probe is already solubilised in P104 micelles. As SDS micelles form, a break in the data is observed as more probe solubilises and/or preferentially moves over to the SDS micelles. Since P104 micelles are already present in solution, the pyrene probe will be

partitioning between P104 micelles and SDS micelles. SDS micelles are clearly more hydrophobic than the P104 micelles, or no break in the CMC of SDS would be observed.

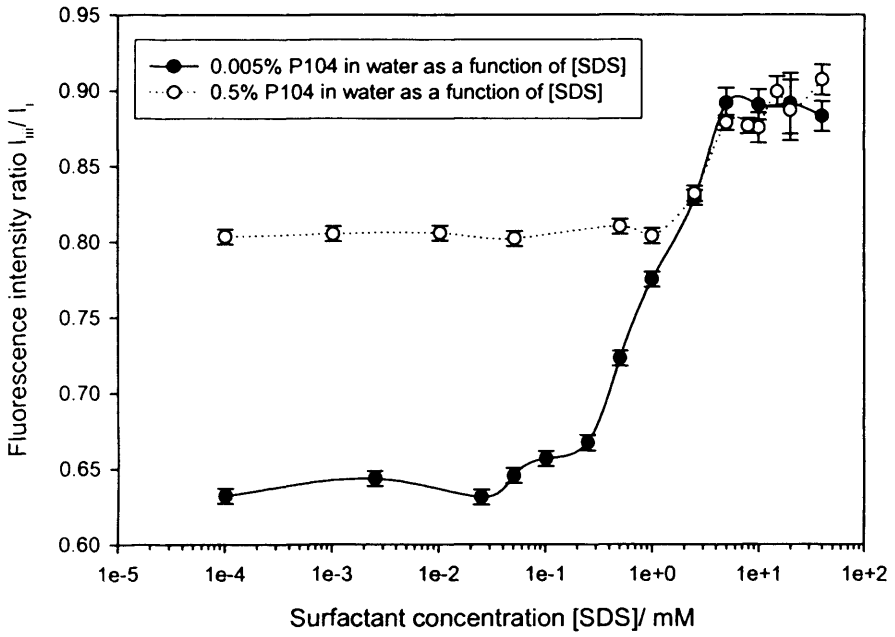

Figure 5.5a Fluorescence intensity ratio for P104 above and below its CMC, as a function of SDS concentration in water

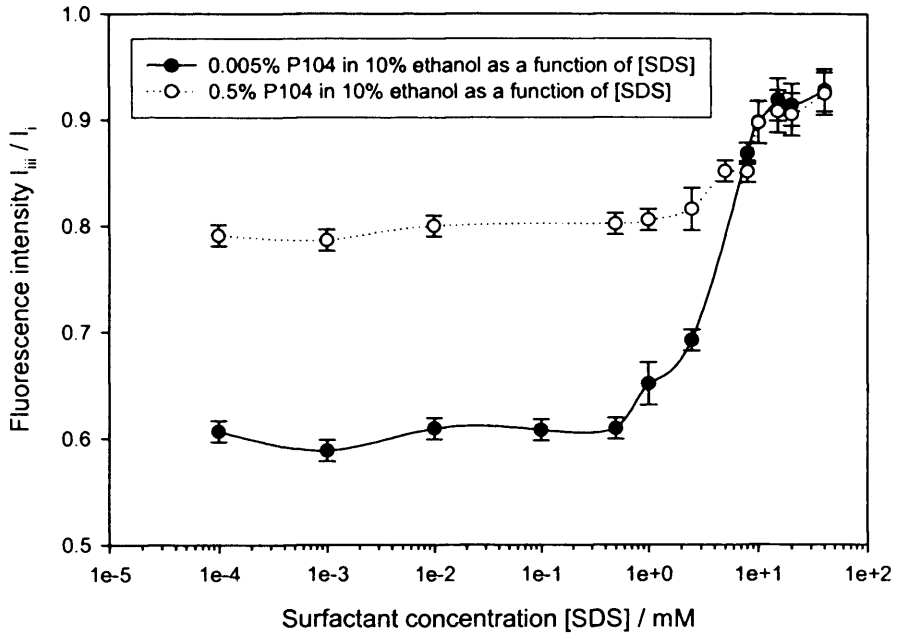

Figure 5.5b Pyrene fluorescence intensity of P104 above and below its CMC, as a function of SDS concentration, in 10% ethanol

Both above and below the CMC of P104, the data appears to be charting the micellisation of SDS and there is only a small change to the CMC of SDS in the presence of P104 as demonstrated by figure 5.5 (a and b). This is the case both in water and in the presence of ethanol. The CMC of SDS in the presence of 0.5 wt% P104 (i.e. P104 above it's CMC) appears to be slightly higher in water but not significantly so.

The conclusion drawn is that P104 is present in such low concentration as to have only a very small impact on the SDS micelles. If mixed micelles are present, the evidence suggests that they are largely SDS micelles, both in the absence and presence of ethanol.

	P104 CMC/mM		P104 with SDS CMC/mM	
% Ethanol	25°C	35°C	0.0005% P104	0.5%P104
0	0.004 – 0.04	-	4 – 6	2 – 8
5	0.009 – 0.04	0.003 – 0.01	3 – 5	4 – 10
10	0.03 – 0.3	0.01 – 0.05	8 – 10	8 – 10
15	0.03 – 0.3	0.01 – 0.06	8 – 11	8 – 12
20	0.1 – 0.3	0.06 – 0.2	-	-

Table 5.1 CMC values for pluronic P104 in water/ethanol mixtures at 25 °C and 35°C; and with SDS above and below the CMC of P104, given as ranges, obtained through pyrene fluorescence spectroscopy.

5.2 NMR

In this stage of the investigation, P104 was examined in D_2O, 5% d-ethanol/ D_2O and 10% d-ethanol/ D_2O. Carbon-13 NMR gave inconclusive and noisy results, so the following analysis considers proton NMR using a Bruker 400MHz Spectrometer as described in previous chapters.

Ma et al[8] have previously assigned the hyperfine structure of the propylene oxide group in D_2O solutions of (PEO-PPO-PEO) with a variety of ratios of PPO to PEO, identifying the Critical Micelle Temperature (CMT) and giving information on the conformation and extent of hydrogen bonding in the polymer.

A concentration range of 0.001% to 5% P104 was examined in this study. Below 0.001%, the background noise began to obscure the proton peaks and above 5%, the lines broadened to the point that features were no longer providing useful information. Information obtained from the chemical shift, and line shapes appear to give an indication of the CMC of P104 and the effect of ethanol on the CMC and the coiling of the polymer.

5.2.1 Line shapes

The sharpness of the peaks corresponding to the EO segment protons remained unaffected upon addition of ethanol or on reaching the CMC of P104. This leads to the conclusion that the polar EO segments remain largely in contact with the solution and are able to move freely. This suggests that the EO segments are hydrated in the corona of the micelle and still have significant freedom of movement, which complements the literature findings. It is possible that the ethanol molecules largely align with the more hydrophobic PO segments, protecting the PO moiety from water and not drastically changing the environment of the EO moiety. This is supported by reduced impact on the chemical shift of increased ethanol concentration beyond 5%, suggesting that the partitioning of ethanol between bulk solution and the micellar corona reaches an optimum.

The resonance peaks of the CH_2 protons of the PO segment broaden upon micellisation, suggesting that the PO block is in a more viscous environment.

The broadening of lines (figure 5.9) was used to determine the CMC as the concentration of P104 was increased, since the point of broadening gives the clearest visual indication of micellisation. This was then compared to changes in the chemical shift, although this gives slightly ambiguous results. This could be due to the presence of ethanol in solution altering the shape of the unimer in solution as well as altering the conformation of unimers within the micelles.

There appears to be slight broadening of the PO peaks as ethanol concentration is increased which could be due to a change in conformation of the unimers as ethanol is

added to the solution. This reduces the mobility of the PPO moiety as ethanol aligns with the hydrophobic PO groups. Addition of ethanol thus alters the conformation of the PO moiety of the unimer in solution, as well as altering the make up of the micelles and the conformation of unimers within the micellar environment. As such, comparison of the chemical shift plots with the CMCs determined from the line broadening is not well correlated for 5% and 10% ethanol, since the addition of ethanol hides features in the curve that would normally indicate the CMC. The CMC of P104 in D_2O as estimated through chemical shift of the PO peaks, is 0.5-2% [P104] which roughly corresponds to the CMC value of 0.5%-1% that is determined by looking at the point of line broadening.

	Line width CMC / wt% P104	
% Ethanol	EO	PO
0	0.5 – 1	0.5 – 1
5	0.3 – 0.5	0.3 – 0.5
10	0.3 – 0.5	0.3 – 0.5

Table 5.2 CMC ranges obtained by proton NMR line width observations

5.2.2 Peak assignment

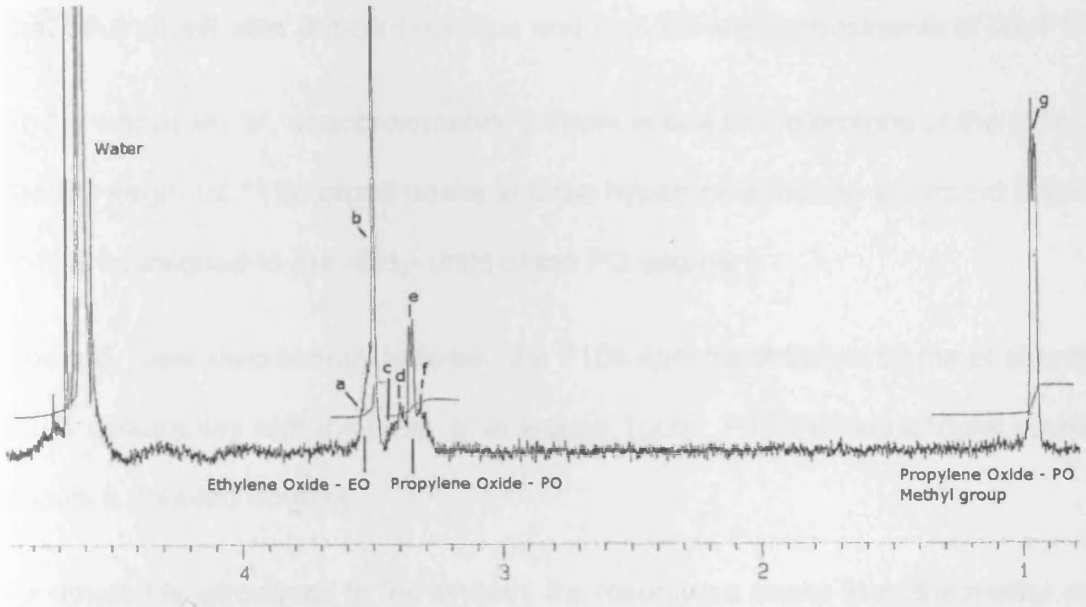

Figure 5.6 Assignment of hyperfine structure for 0.1 wt% P104 in D_2O

The hyperfine structure was assigned by 'Ma et al' for P105 by comparing the P105 structure with that of PPO2700 and PEG2000 to isolate the hyperfine structure for the PO and EO segments.

Close similarities between P105 and P104 structure and spectra allow the P105 interpretation from Ha et al to be applied to P104.

P104: MW= 5900; no. PO Units= 61; No. EO units= 2x27:

P105: MW= 6500; no. PO units= 56; no. EO units = 2x37

The signal at approximately 1ppm ('g') belongs to the protons of the PO -CH_3 groups. *Although a triplet is expected, a doubled doublet is present in the P104 spectra.* This may be due to steric constraints altering the splitting pattern. The shape of the PO –

CH_3 peak changes slightly as ethanol is added to the system which supports the view that ethanol will alter the configuration and thus the steric constraints of the PO moiety.

The sharp peak, 'b', at approximately 3.7ppm is due to the protons of the $(CH_2)_2$ units of the EO segment. The broad peaks and the hyperfine structure at around 3.45-3.65ppm, 'c-f', are assigned to the $-CH_2-$ units of the PO segment.

The only clear discrepancy between the P105 spectra obtained by Ha et al and the P104 spectra lies with the peak 'g' at around 1ppm. P105 shows a triplet whereas P104 shows a doubled doublet.

As ethanol is introduced to the system, the resonance peaks from the methyl and methylene of the ethanol could be expected from any residual protons in the solvent. At lower P104 concentration, additional singlets appear at approximately 3.5ppm and around 1ppm, in 5 and 10% d-ethanol, marked as 'h' and 'i', figure 5.7.

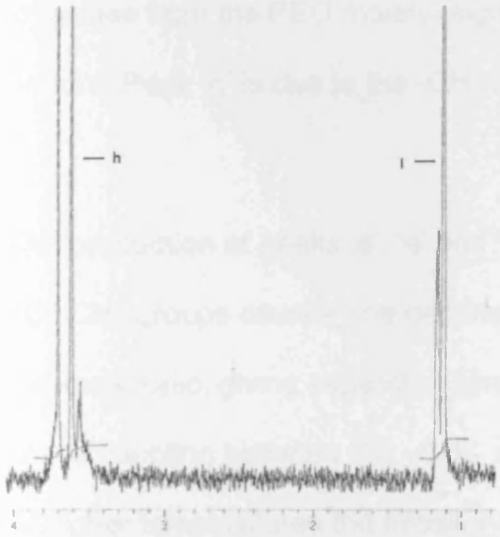

Figure 5.7 Assignment of ethanol peaks in the hyperfine structure of P104 in D_2O

'h' and 'i' are attributed to the ethanol protons, with the disappearance of these peaks as the P104 concentration is increased due to the relative proton ratios of the solvent vs the polymer becoming much lower.

The peaks arise at the expected chemical shift for the methylene and methyl shifts of ethanol and appear as singlets due to rotational motion in the solvent.

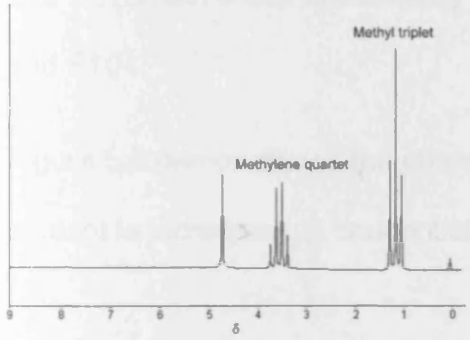

Figure 5.8 'Textbook' H^1 NMR spectrum of ethanol

Referring again to figure 5.6, peaks 'd', 'e' and 'f' belong to the PO -CH_2- protons, triplet 'c' comes from the PEO moiety, signal 'a' from the EO -CH_2- and 'b' due to the PO –CH- proton. Peak 'g' is due to the -CH_3 on the PO units.

The production of peaks 'd', 'e' and 'f', may be due to the chiral centre of the PO –$CHCH_3$ groups causing the geminal hydrogen atoms of the PO –CH_2- to become diastereotopic, giving separate signals. The peaks could also arise from direct through space coupling between PO –CH_2- and –CH_3 protons.

At higher temperatures the micellar core contains some water as some methyl groups become hydrated. The NMR experiments were run only at 20°C across a range of P104 wt% at 0, 5 and 10% ethanol concentration. Trends that occur with increasing

temperature, as demonstrated by other studies, can also be seen at constant temperature and increasing P104 concentration.

The polarity of the EO group allows it to be soluble in water and ethanol, and it would not be likely to be affected by the increase in ethanol concentration or through the increase in P104 concentration to the same extent as the PO units. The EO peaks, 'a' and 'c', remain sharp and broadly unaffected by increases in concentration of ethanol and P104.

Figure 5.9 demonstrates the changes to the hyperfine structure of P104 as ethanol content is increased, at concentrations of P104 above and below its CMC.

Figure 5.9 Trends across [P104] and [Ethanol]

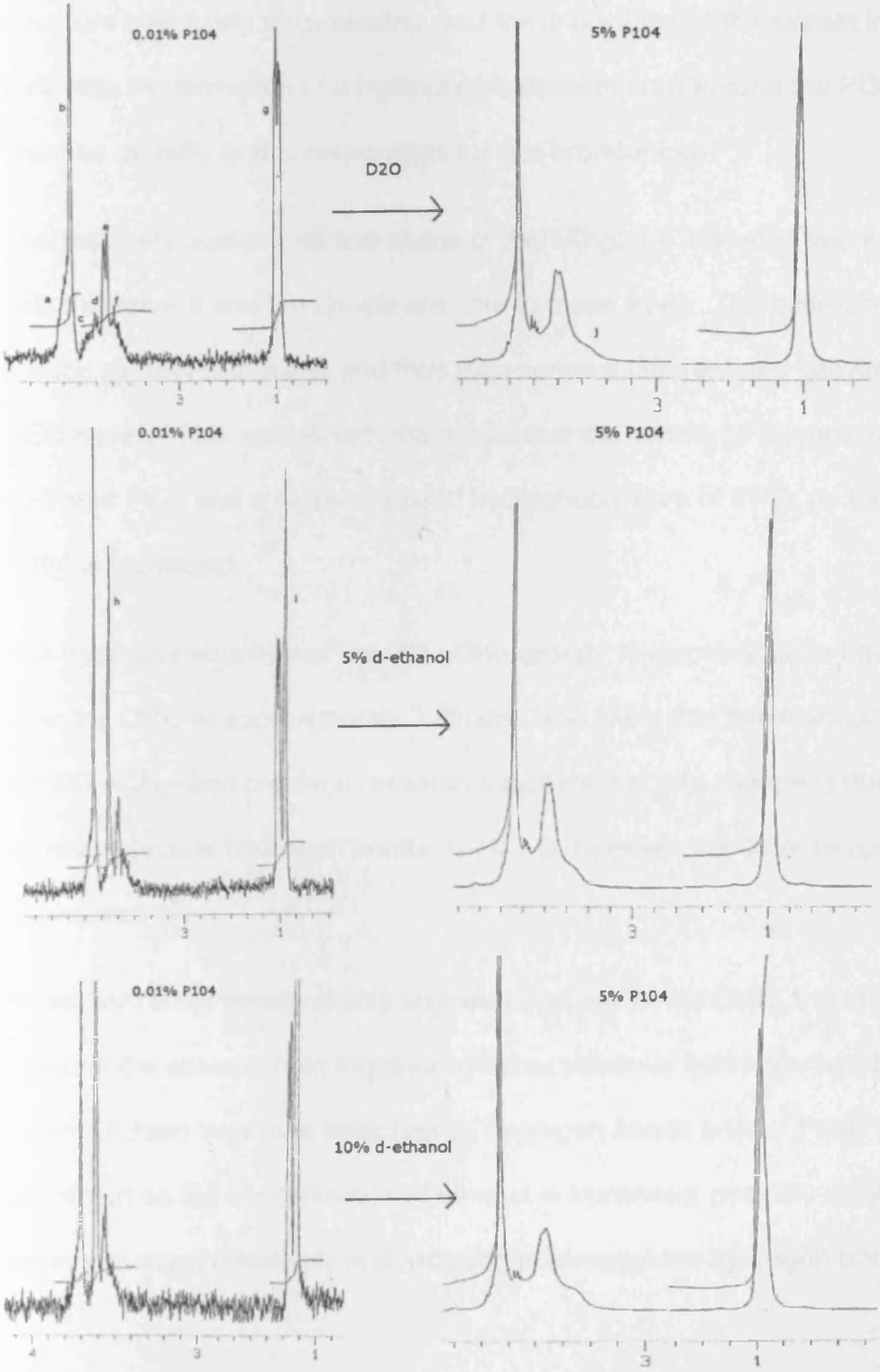

As the CMC is reached, the peaks of the PO groups begin to change, with the hyperfine structure eventually disappearing, and the line widths of the signals increasing. This indicates the formation of a hydrophobic micellar core around the PO groups which reduces mobility and is responsible for line broadening.

The relatively unchanged line shape of the EO group indicates that it is still in contact with the solvent and the chains are able to move freely. The hydrophobic PPO blocks reduce contact with water and thus experience a different microenvironment from the PEO moiety. This agrees with the model that the corona of Pluronic micelles consists of hydrated PEO and a more compact, hydrophobic core of PPO, as the concentration of P104 is increased.

The hyperfine structure of the PO $-CH_2-$ groups disappears but a new peak 'j', appears after the CMC at approximately 3.25ppm. It is likely that this resonance is also due to the PO $-CH_2-$ and previous research suggests that this change is due to the breakdown of intramolecular hydrogen bonds (C-H)...O, between the ester oxygens and the PO $-CH_2-$ protons[8].

In line with other research, this suggests that below the CMC, the unimer chains are coiled in the solvent, held together by intra-molecular hydrogen bonds. Above the CMC, the PPO chain becomes stretched as hydrogen bonds break. Peak 'j' becomes more prominent as the concentration of ethanol is increased, possibly solubilising the PO segments more effectively and reducing intramolecular hydrogen bonding.

5.2.3 CMC determined by NMR spectral line shape change

Analysis of the line shapes suggests that the CMC occurs between 0.5-1wt% P104 in D_2O, and between 0.3-0.5wt% for P104 in 5% and 10% d-ethanol, as demonstrated by the swift broadening of the lines.

Figure 5.10 shows the progression of line shapes from 0.001wt% to 5wt% P104 in D_2O. There is a distinct shape change and loss of hyperfine structure as the lines broaden upon reaching the CMC. However, the point of line broadening decreases as the ethanol content is increased. If the broadening purely signifies the CMC, then this would not be consistent with the literature that shows that ethanol content increases the CMC of P104 by acting as a better solvent.

It has been noted that an increase in ethanol content can reduce the mobility of the PO segments, and thus will lead to broadening of the PO peaks in the NMR spectra. It is possible that the presence of ethanol falsely reduces the value at which the CMC is observed by the effect of reduced mobility of the PO segments caused by the solvent, compounding the effect of increasing concentration of P104, especially as the CMC is neared and aggregates/micelles occur over a range of [P104].

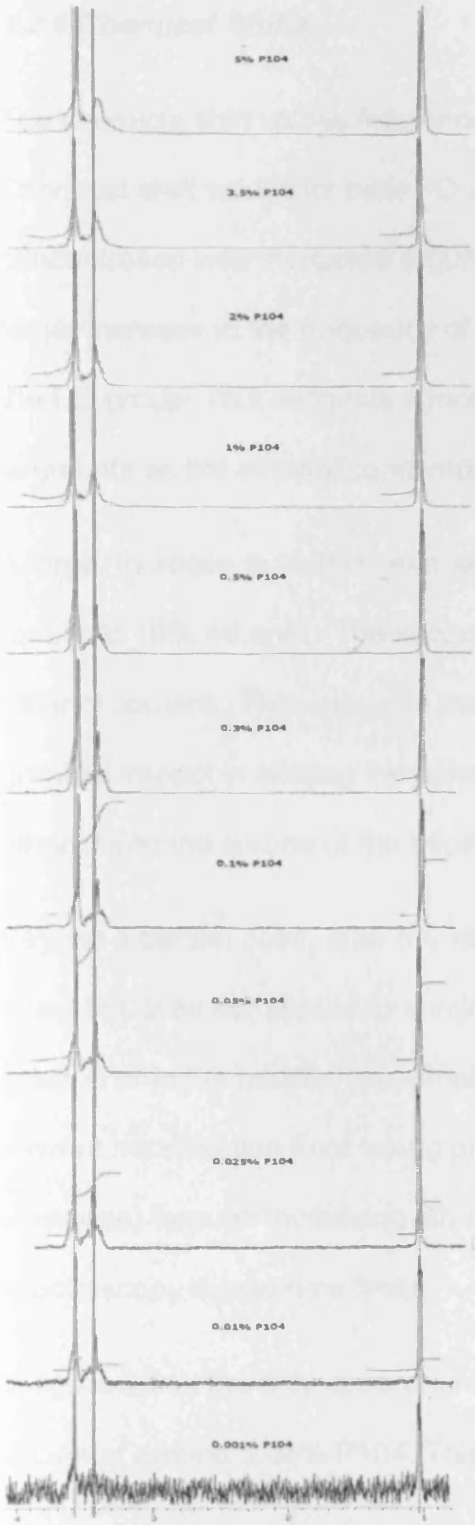

Figure 5.10 Hyperfine structure changes and chemical shift for 0.001wt% to 5wt% P104 in D_2O

5.2.4 Chemical Shifts

The chemical shift values referenced to the residual H_2O peak were obtained. Chemical shift values for both PO and EO groups increased in frequency as ethanol concentration was increased (figure 5.10 and 5.11). The PO group resonance showed a larger increase in the frequency of the H shift with increasing ethanol concentration than the EO group. This suggests a more hydrophobic microenvironment for the PO segments as the ethanol concentration is increased.

A larger increase in shift is seen when moving from 0% to 5% ethanol content, than that for 5% to 10% ethanol. The impact of adding ethanol is less noticeable the greater the ethanol content. This suggests that the initial addition of ethanol to the solution has the greatest impact in altering the solvation of the unimer and the degree of penetration of ethanol into the corona of the micelle.

Beyond a certain point, after 5% ethanol, further addition of ethanol has some further effect but does not appear to continue to drastically alter the solvation of unimers in solution or in the micelle, presumably until ethanol concentration is high enough to prevent micellisation from taking place. The point at which micellisation is prevented (or otherwise) through increasing ethanol concentration was not investigated using NMR spectroscopy due to time limits.

In figure 5.11a the only apparent feature is the break in the curve for P104 in D_2O which occurs at around 0.08% P104. This correlates with a break in the PO methylene data.

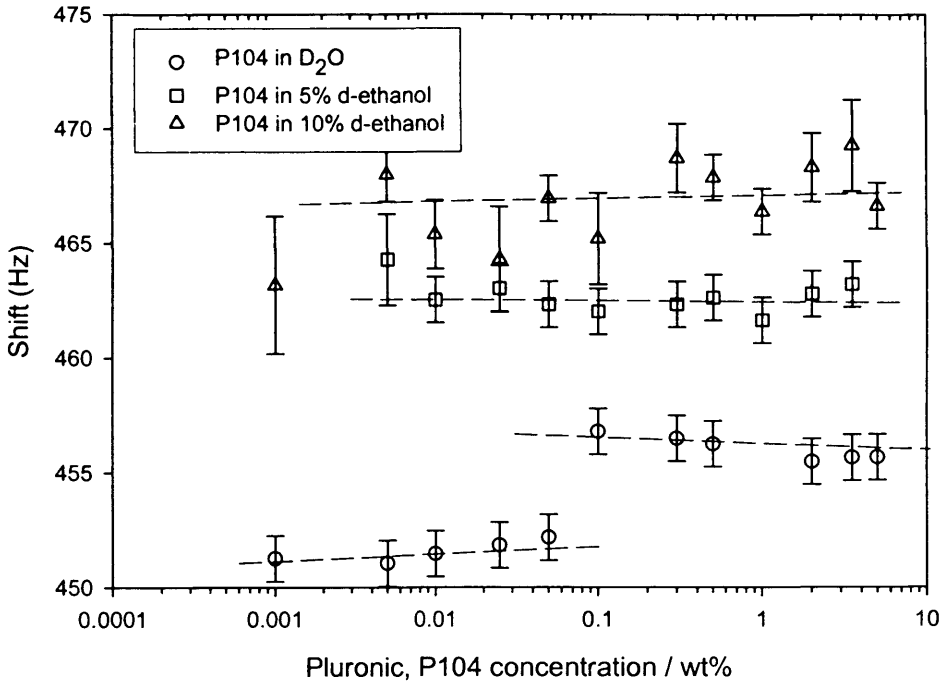

Figure 5.11a EO H^1 NMR Shift as a function of P104 concentration in D_2O/d-ethanol

The data at 5% and 10% ethanol do not give any clear features that are within reasonable error margins. The presence of ethanol appears to obscure any changes to the system for the purposes of monitoring changes using NMR. Ethanol is not expected to have any significant affect on EO segments (demonstrated by the sharpness of EO peaks upon increase of P104 concentration through it's CMC) and as such is it unsurprising to see no features in the data.

The break in the EO curve in water at around 0.04wt% to 0.2wt% does not correlate accurately with the value obtained through change to line shape (0.5-1wt%) and given the evidence that there is little change to the EO segments upon micellisation, it does not appear that the chemical shift of EO peaks provides any useful indicator of micellisation.

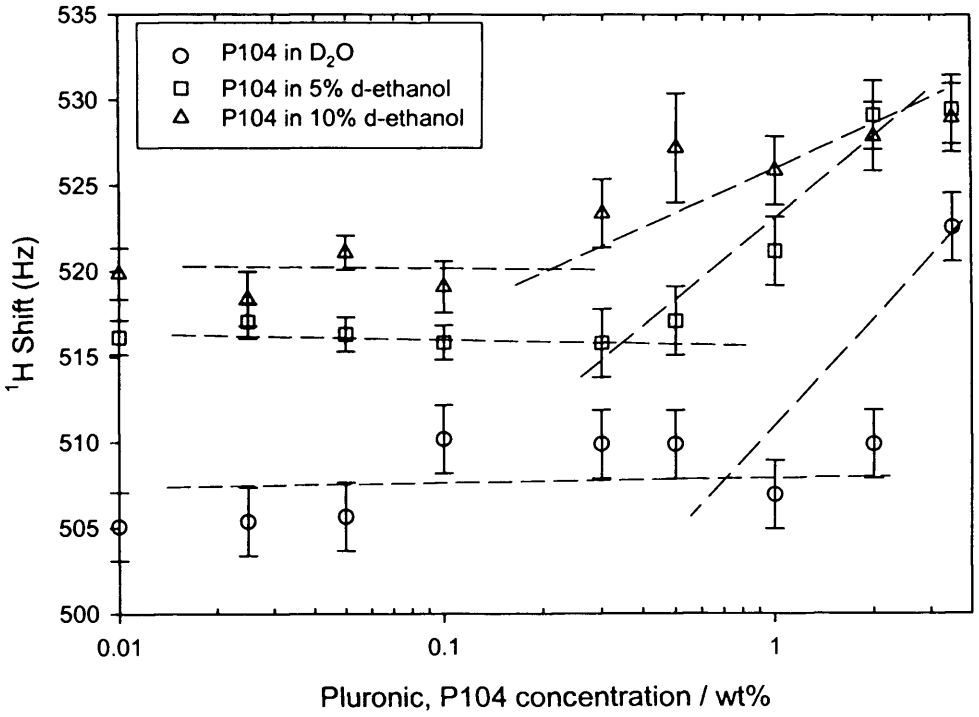

Figure 5.11b PO methylene ^{1}H NMR shift as a function of P104 in D_2O/d-ethanol

Again, upon addition of ethanol, the data becomes largely featureless as figure 5.11b shows. In the case of PO shift, there is a broad increase in shift frequency as the concentration of P104 is increased in the presence of ethanol. This could correlate with an increase in CMC but these conclusions are at the resolution of the experimental data.

The increase in frequency of the shift for PO in the presence of ethanol is more obvious than for the featureless EO shifts. Since the environment of the EO segments changes little upon micellisation (in the presence and absence of ethanol) it is perhaps unsurprising that presence of ethanol obscures any changes that occur upon micellisation.

The changes to the PO segments should be more apparent but again, these are also obscured by the presence of ethanol although an increase in shift is observed as P104 concentration is increased. Approximate CMC ranges can be obtained from the PO peak chemical shift positions and these are compared with those obtained through line width changes in table 5.2.

	Line width CMC / wt% P104		**Chemical shift CMC / wt% P104**	
% Ethanol	EO	PO	EO	PO
0	0.5 – 1	0.5 – 1	-	0.5 – 2
5	0.3 – 0.5	0.3 – 0.5	-	0.1 – 0.3
10	0.3 – 0.5	0.3 – 0.5	-	0.2 – 0.7

Table 5.2 CMCs obtained through proton NMR, considering line width and chemical shift

A small decrease in CMC of P104 is observed, and the cause of this is explained in section 5.2.3.

5.2.5 NMR comparison with fluorescence

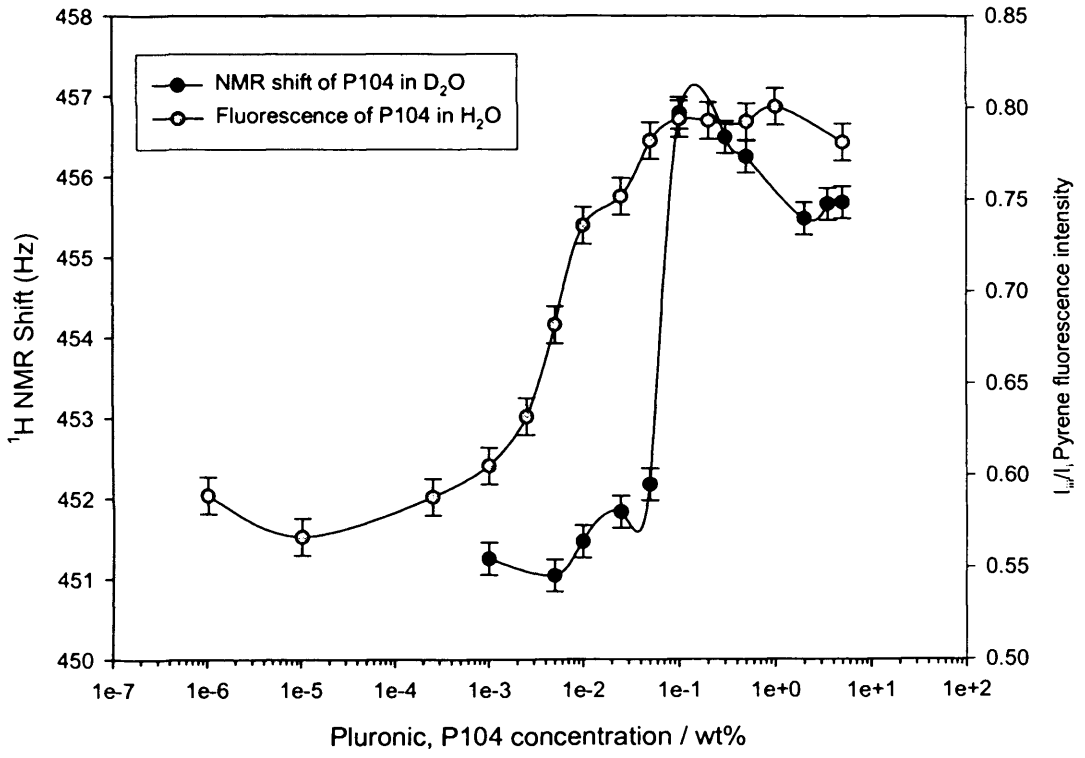

Figure 5.12 Ethylene Oxide ^{1}H NMR shifts compared to pyrene fluorescence as a function of P104 concentration in D_2O/H_2O

Displaying the ethylene oxide ^{1}H NMR chemical shifts against the pyrene fluorescence of P104 does not provide a clear correlation of results after the addition of ethanol.

In D_2O the EO shift does not correlate with fluorescence data. Due to only small changes expected to be taking placing for the EO group upon micellisation, it is perhaps not surprising that the comparison is ambiguous. All approximate CMC values obtained by NMR are higher than those obtained using fluorescence, thus indicating that the two techniques are not measuring the same properties of the system.

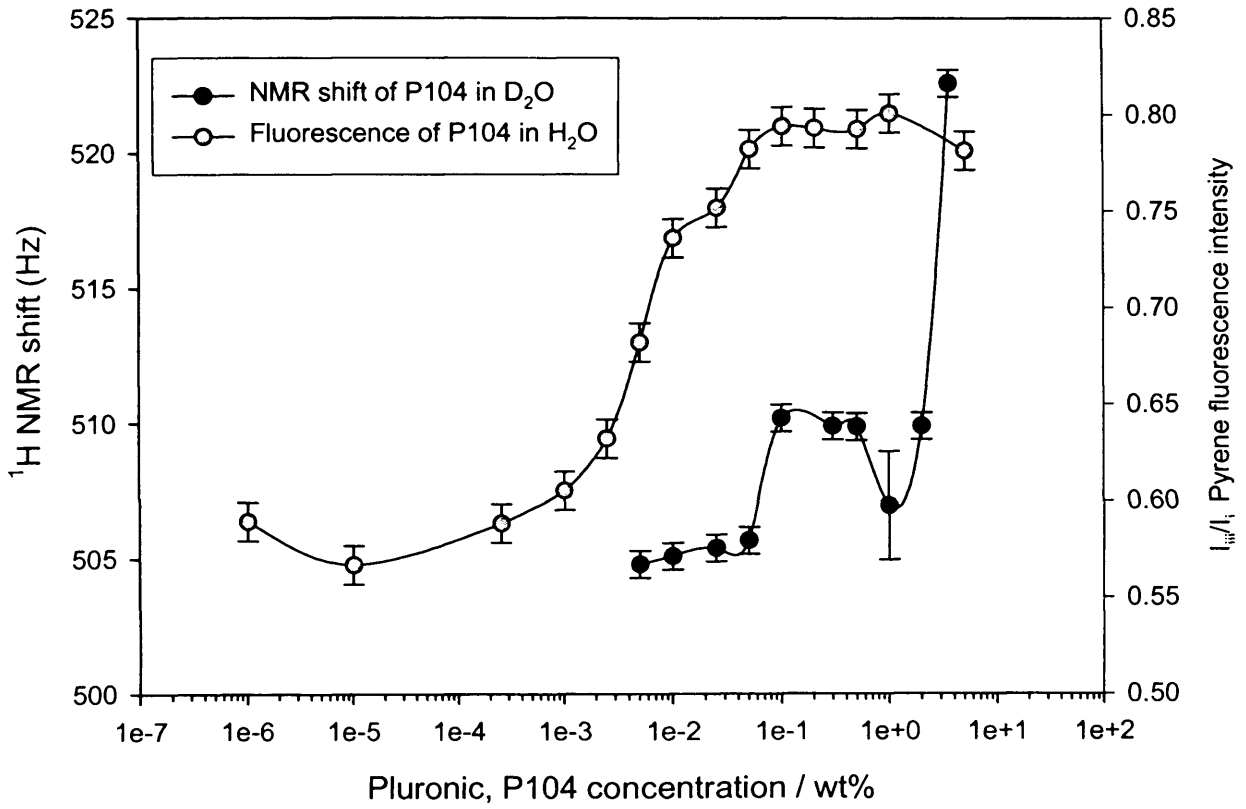

Figure 5.13 PO Methylene H1 NMR shifts compared to pyrene fluorescence of P104 in D_2O/H_2O

Comparison of PO methylene chemical shifts with the fluorescence is shown in figure 5.13. This shows the NMR shift of P104 in D_2O compared with the fluorescence curve of P104 in water with pyrene probe which appears to provide a good correlation for the first 'break' of the NMR curve. However, the CMC ranges obtained through investigating the chemical shifts are higher than the fluorescence values, measured here by the second 'break' at around 0.4wt% to 1wt% P104. This could indicate that the concentration range studied by NMR was not low enough to capture the CMC using chemical shift as the indicator. If so, the broadening of the peak lines (which appear to

correlate with CMC values obtained through the chemical shift) may be measuring another property.

As is the case with EO ^{1}H NMR shifts, the comparison is too ambiguous once ethanol is present to obtain any CMC values.

It is unfortunate that the NMR technique did not allow for lower P104 concentrations to be explored, which would have confirmed whether or not the rise in chemical shift at 0.001 % P104 for 5 and 10% d-ethanol concentration was a real effect that coincides with the break in the fluorescence curves.

5.3 Small Angle Neutron Scattering

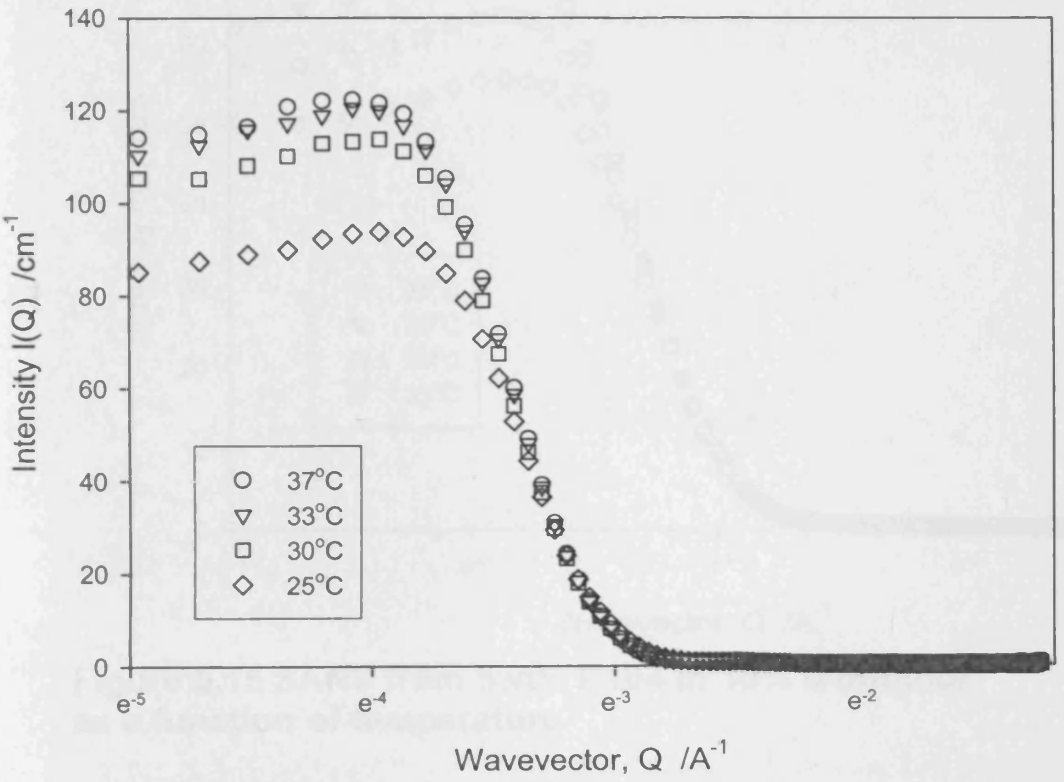

Figure 5.14 SANS from 5wt%P104 in D_2O as a function of temperature

At lower temperature there are more unimers present. As the temperature is increased, more micelles are formed and therefore the intensity of the structure factor increases. A core shell model fitting strategy would need to be employed to obtain morphology and size of the micelles. The largest increase in intensity occurs between 25°C to 35 °C which crosses through the CMT of P104[9].

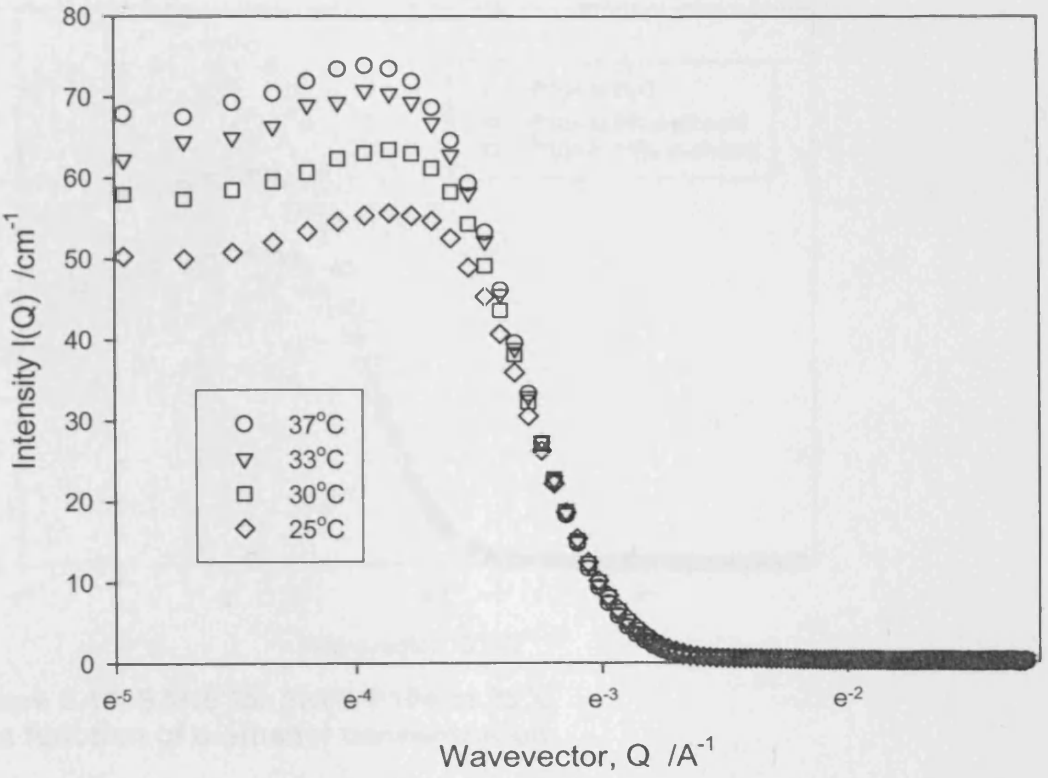

Figure 5.15 SANS from 5wt% P104 in 15% d-ethanol as a function of temperature

The intensity can be seen to rise with temperature for figure 5.15 although not to the same extent as intensity rises for figure 5.14 in D_2O. The scattering intensity is weaker but the shapes are unchanged indicating no change to the micelles.

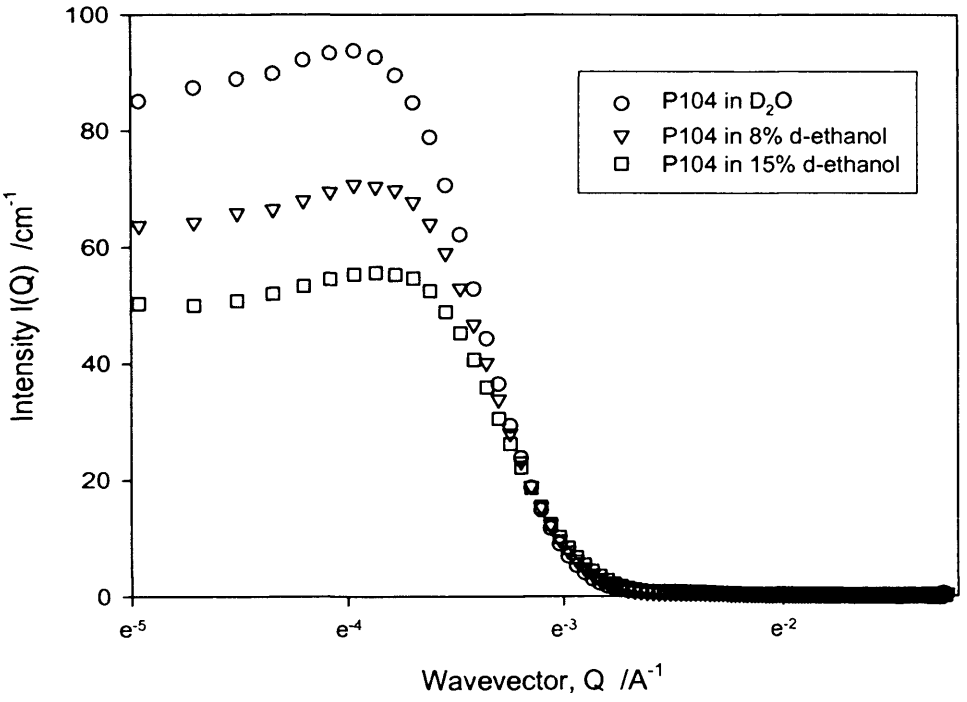

Figure 5.16. SANS for 5wt% P104 at 25°C as a function of d-ethanol concentration

In figure 5.16 it can be seen that the scattering is strong but there is no change to the shape of the curve, signalling that there is no change to the shape of the micelles.

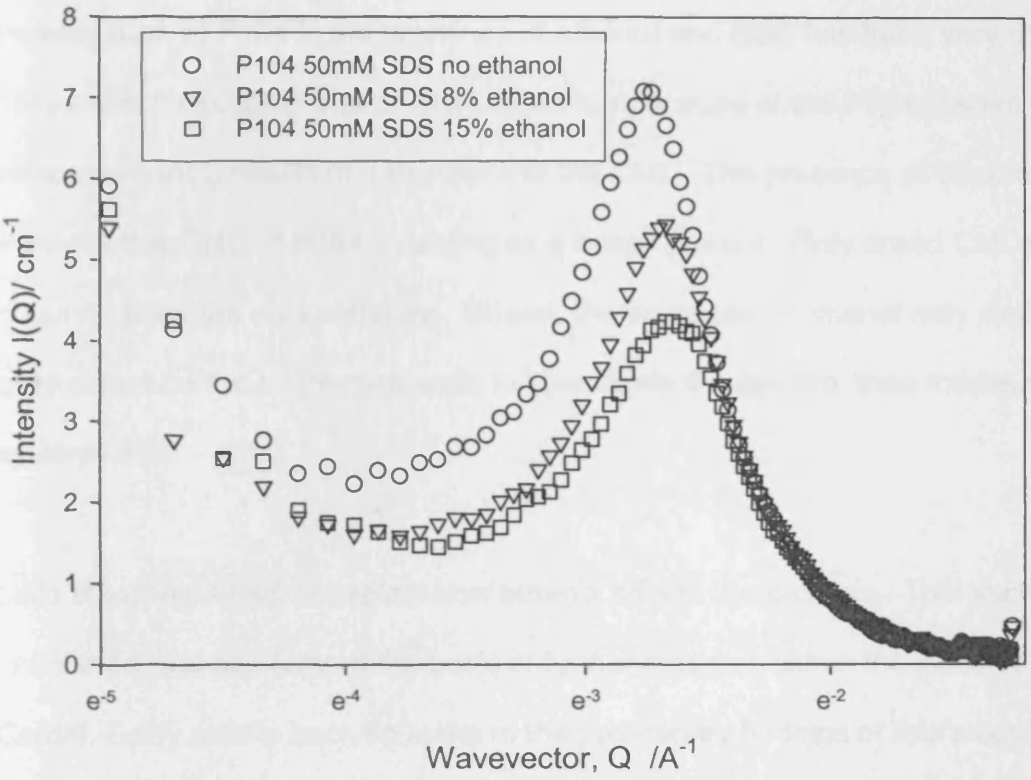

Figure 5.17 SANS from 5wt% P104 with 50mM SDS at 25°C as a function of ethanol concentration

The decrease in intensity as ethanol content is increased could be due to the change in charge on the micelle as the ethanol content alters the dielectric constant of the solvent. There is a very slight shift of the peak to a higher Q value, indicating that there is an increase in micelle separation with ethanol content suggest fewer scatterers, that is, an increase in the CMC (since there is no evidence in the other SANS data that the micelles have increased in size.)

To obtain more information on size and shape of micelles, the SANS data needs to be fitted to the core shell model.

5.4 Conclusions and future work

Investigation of P104 in the presence of ethanol and SDS has been very challenging. These results suggest that an increase in temperature of the P104 system (with and without ethanol) results in a decrease to the CMC. The presence of ethanol appears to increase the CMC of P104 by acting as a better solvent. Only broad CMCs can be obtained from the data collected. Indeed, the presence of ethanol may well have more of an effect on the techniques used to investigate the system, than it does on the system itself.

Little literature exists to explain how ethanol effects the pluronic. This section of work is unfinished and has formed the basis of further research within the Colloids team at Cardiff. Early results back up some of the preliminary findings of this study and should yield further useful information for characterizing the effect of ethanol on polymer-surfactant systems.

It is apparent that some of the methods employed have not been ideal for investigating the system and further methods need to be utilised to triangulate and clarify the results. Different techniques seem to be sensitive to different properties of the system and sensitive to the presence of ethanol, leading to variation in values obtained for the CMC and hence ambiguity in interpreting the data, especially where different techniques do not correlate.

The limits of NMR as a technique lie in the inability to work across a large pluronic concentration range. Surface tension did not produce strong features in the data and thus was not discussed in this chapter. Alternative methods of measuring dynamic surface tension (bubble method) may provide more useful results. Fluorescence appears to provide a view of the trends seen upon addition of ethanol to P104 and to SDS, yet the presence of ethanol broadens the data curves and increases the error in the value ranges obtained.

The initial pluronic SANS data would benefit from a more detailed analysis and an extension of the use of SANS across a wider range of ethanol concentrations and temperatures, both for P104 alone and in the presence of SDS.

At the concentration range of ethanol used in this study, it is apparent that the impact of ethanol on micellisation is not extremely significant, and the concentration range could be widened towards ethanol rich mixtures, to determine the point at which micellisation will no longer occur for P104.

Given that the pluronic, SDS and ethanol systems have not been investigated comprehensively, this would be a useful area of work to continue given the wide availability and use of all components within industry and pharmaceuticals. Using a wider range of techniques to study a range of pluronics with SDS, in a full range of ethanol concentrations would provide a robust overview allowing characterisation of this largely uninvestigated area.

References

[1] Jonsson, N., Lindman, B., Holmberg, K. and Kronberg, B., *Surfactants and polymers in aqueous solution,* Wiley, **1998**

[2] Zana, R., *Aqueous Surfactant-alcohol systems: A review. Advances in Colloid and Interface Science*, **1995**, *57*, 1-64

[3] Flory, P. J., *Principles of Polymer Chemistry*, Cornell Univ. Press, Ithaca NY, **1953**.

[4] *Nonionic Surfactants: Polyoxyalkylene Block Copolymers,* Ed. Nace, V.M., CRC Press, **1996**

[5] Alexandridis, P,. Athanassiou, V., Fukuda, S., Hatton, T.A., *Langmuir,* **1994**, *10* 2604-2612

[6] Alexandridis, P.; Holzwarth, J. F.; Hatton, T. A. *Macromolecules*, **1994**, *27*, 2414-2425

[7] Schmolka, I. R., and Raymond, A. J., *J. Am. Oil Chem. Soc.* **1965,** *42*, 1088

[8] Ma, J., Guo, C., Tang, Y., Wang, J., Zheng, L., Liang, X., Chen, S., Lui, H., *J. Colloid and Interface Sci.,* **2006,** 299, *15*, 953-961

[9] Alexandridis, A., Nivaggioli, T., Hatton, T.A., *Langmuir*, **1995,** *11*, 1468-1476

Effect of Ethanol on the Interaction between Poly(vinylpyrrolidone) and Sodium Dodecyl Sulfate

P. C. Griffiths,*,† N. Hirst,† A. Paul,† S. M. King,‡ R. K. Heenan,‡ and R. Farley†

School of Chemistry, Cardiff University, P.O. Box 912, Cardiff CF10 3TB, U.K., and ISIS Facility, Rutherford Appleton Laboratory, Chilton, Didcot OX11 0QX, U.K.

Received March 12, 2004. In Final Form: May 13, 2004

The effect of ethanol on the interaction between the anionic surfactant sodium dodecyl sulfate (SDS) and the nonionic polymer poly(vinylpyrrolidone) (PVP) has been investigated using a range of techniques including surface tension, fluorescence, electron paramagnetic resonance (EPR), small-angle neutron scattering (SANS), and viscosity. Surface tension and fluorescence studies show that the critical micelle concentration (cmc) of the surfactant decreases to a minimum value around 15 wt % ethanol; that is, it follows the cosurfactant effect. However, in the presence of PVP, the onset of the interaction, denoted cmc(1), between the surfactant and the polymer is considerably less dependent on ethanol concentration. The saturation point, cmc(2), however, reflects the behavior of the cmc in that it decreases upon addition of ethanol. This results in a decrease in the amount of surfactant bound to the polymer [C_{bound} = cmc(2) − cmc] at saturation. The viscosity of simple PVP solutions depends on ethanol concentration, but since SANS studies show that ethanol has no effect on the polymer conformation, the changes observed in the viscosity reflect the viscosity of the background solvent. There are significant increases in bulk viscosity when the surfactant is added, and these have been correlated with the polymer conformation extracted from an analysis of the SANS data and with the amount of polymer adsorbed at the micelle surface. Competition between ethanol and PVP to occupy the surfactant headgroup region exists; at low ethanol concentration, the PVP displaces the ethanol and the PVP/SDS complex resembles that formed in the absence of the ethanol. At higher ethanol contents, the polymer does not bind to the ethanol-rich micelle surface.

Introduction

In many applications, surfactants are formulated with a variety of additives to achieve a desired range of properties and alcohols are frequently used as a cosurfactant. With an increasing concentration of alcohol, the properties and structure of the aqueous solvent mixture[1] are modified in such a manner that the solubility of an ionic surfactant increases; that is, the solution is more hydrophobic. Concomitantly, the dielectric constant of the solvent decreases, thereby increasing the electrostatic interaction between the ionic headgroups. Both these factors have the effect of increasing the critical micelle concentration (cmc), a process known as the cosolvent effect.[1,2] However, an opposing effect can occur as the nonionic character of the alcohol leads to a diluted surface charge density in the palisade layer (that region of the micelle around the hydrocarbon/water interface between the headgroups)[3], a process that promotes a decrease in the cmc. This is known as the "cosurfactant effect".[4]

The effects of alcohol on micellar systems have been studied widely.[5] In general, short chain alcohols act as cosolvents; they are localized in the continuous phase and affect the solvent structure around the headgroup.[5] Medium chain alcohols partition between the palisade region and the aqueous solution,[6] whereas long chain alcohols are solubilized into the micellar core. For sodium dodecyl sulfate (SDS), a decrease in the cmc with increasing ethanol content is observed at low ethanol concentrations (cosurfactant effect), which subsequently gives way to the cosolvency effect at higher ethanol concentrations, that is, an increasing cmc with increasing ethanol concentrations.[7] Hence, the cmc goes through a minimum value at some ethanol concentration.[2,7] There is a decrease in the aggregation number, as shown by small-angle neutron scattering (SANS)[8] and fluorescence.[9] The SANS study of Caponetti et al.[8] recorded for a surfactant concentration of [SDS] = 200 mM shows that the aggregation number decreases from ~85 in the absence of ethanol to ~75 in the presence of 1.9% v/v ethanol in solution. Over this range of surfactant concentrations, the charge per surfactant molecule on the micelle, and hence the degree of counterion dissociation, is constant within experimental error. The fluorescence study of Almgren[9] was presented rather differently—on the basis of the measured partitioning of ethanol into the micelle, the solutions were prepared such that the concentration of ethanol within the micelle spans a wide range of ethanol concentrations, namely 0 mM < [ethanol] < 30 mM. The SDS concentration 110 mM < [SDS] < 130 mM was not too dissimilar to that used in Caponetti's SANS study. The aggregation number decreased from ~70 in the absence of ethanol to ~35 at the highest ethanol solubilization. These studies are in agreement with those of

† Cardiff University.
‡ Rutherford Appleton Laboratory.

(1) Huang, J.-B.; Mao, M.; Zhu, B.-Y. *Colloids Surf., A* **1999**, *155*, 339-348.
(2) Gharibi, H.; Razavizadeh, B. M.; Rafati, A. A. *Colloids Surf., A* **1998**, *136*, 123−132.
(3) Rosen, M. J. *Surfactants and Interfacial Phenomena*; Wiley-Interscience: New York, 1989.
(4) Cinelli, S.; Onori, G.; Santucci, A. *Colloids Surf., A* **1999**, *160*, 3−8.
(5) Zana, R. *Adv. Colloid Interface Sci.* **1995**, *57*, 1−64.
(6) Manabe, M.; Tokunaga, A.; Kawamura, H.; Shiomi, M.; Hiramatsu, K. *Colloid Polym. Sci.* **2002**, *280*, 929−935.
(7) Safarpour, M. A.; Rafati, A. A.; Gharibi, H. *J. Chin. Chem. Soc.* **1999**, *46* (6), 983−991.
(8) Caponetti, E.; Chillura Martino, D.; Floriano, M. A.; Triolo, R. *Langmuir* **1997**, *13*, 3277.
(9) Almgren, M.; Swarup, S. *J. Colloid Interface Sci.* **1983**, *91*, 256.

10.1021/la049348o CCC: $27.50
Published on Web 06/19/2004

Backlund et al.,[10] citing light scattering and gel filtration data. Backlund et al.[11] also presented electromotive force (EMF) measurements and conductivity data on SDS/pentanol and higher alcohol systems. Their results suggest only a slight increase (~10%) in the counterion dissociation, in agreement with the (more empirical) observation of Caponetti.[8]

Mixtures of water-soluble polymers and surfactants also have numerous applications in industry. Whereas nonionic polymers and nonionic surfactants show only very weak interactions, nonionic polymers and anionic surfactants,[12-21] polyelectrolytes and oppositely charged surfactants,[22-25] and hydrophobically modified polymers and anionic surfactants [18,26-33] show strong interactions. Whether a particular combination of polymer and surfactant form polymer/micelle complexes is determined by the thermodynamics driving the self-aggregation of the surfactant monomers. The point at which micelles form on the polymer strand is named the critical association concentration (CAC) or, more recently, cmc(1). The point of saturation beyond which free micelles form in the bulk phase is named cmc(2).

The driving force for polymer/surfactant complexation is due to the adsorption of polymer segments into the micelle palisade layer,[34] shielding part of the hydrophobic core of the micelle from the aqueous phase. This is a more favorable arrangement, as the polymer is inherently more hydrophobic than water, and thus, a decrease in the micellization concentration of the surfactant results. Short chain alcohols bind to the same region of the micelle which may lead to the same type of competitive effects often seen in polymer/anionic surfactant/nonionic surfactant mixtures.[35] Further, if the solvent polarity is altered, this will cause a change in the effective dielectric constant of the media which in turn will have a profound effect on the electrostatic interactions present between the bound micelles.

Since strong interactions between micelles and polymers are mostly confined to ionic surfactant micelles, it follows that polymer-adsorbed micelles are generally (negatively) charged. An electrostatic repulsion exists between the micelles bound to the same polymer molecule and thereby increases the viscosity of the solution. Hence, the viscosity of polymer/surfactant systems often exhibits a strong ionic strength dependence as the electrostatic interactions become screened. Ultimately, the saturation level is attained when the electrostatic repulsion associated with binding another micelle is such that it is thermodynamically more favorable to form a nonbound micelle in solution.[36,37]

A consequence of this is that the concentration of surfactant unimer in solution increases as the average number of micelles per polymer molecule increases.[38] Therefore, the second characteristic concentration or saturation level, cmc(2), corresponds to a unimer concentration equal to the polymer-free cmc of the surfactant (at the appropriate ionic strength and pH).

It is widely accepted that micelle/polymer interactions occur for the polymer poly(vinylpyrollidone) (PVP)/SDS system[39-42] with the micelles adsorbing to the polymer strands such as beads on a string.[43,44] However, there are very few studies concerning polymer/surfactant systems and PVP/SDS, in particular, in polar solvents other than water.[45] Notably though, in an electrode study, Shirahama et al.[46] observed that the binding affinity of dodecylpyridinium chloride to poly(styrene sulfonate) decreased with an increase in ethanol content. Against this background, the present study was undertaken, to investigate the effect of increasing ethanol concentration on the interaction between the nonionic PVP and the SDS. Of particular interest here is the onset of the interaction, its effect on polymer conformation and micelle size, and the relationship of these factors with solvent composition.

Experimental Section

Materials. SDS (Aldrich; purity, 98%) was purified by repeated recrystallizations from ethanol until the impurity "dip" in the surface tension versus log(concentration) curve could no longer be observed. PVP (Aldrich; $M_w = 1.3 \times 10^6$ g/mol) was used as received. Analytical grade ethanol (Aldrich) and doubly distilled water (and, for the SANS studies, deuterated equivalents where stated) were used to prepare all solutions.

Surface Tension. The surface tensions were determined by the Du Nöuy ring method consisting of a small (1 cm diameter) platinum ring suspended from a zero displacement balance (CI Electronics, U.K.), calibrated by reference to distilled water/ethanol mixtures. All measurements were taken at room temperature, 22 ± 2 °C.

(10) Backlund, S.; Randt, K. *J. Colloid Interface Sci.* **1981**, *79*, 578.
(11) Backlund, S.; Randt, K.; Veggeland, K.; Høiland, K. *Prog. Colloid Polym. Sci.* **1987**, *74*, 93.
(12) Chari, K.; Antalek, B.; Lin, M. Y.; Sinha, S. K. *J. Chem. Phys.* **1994**, *100*, 5294-5300.
(13) Goddard, E. D. *J. Am. Oil Chem. Soc.* **1994**, *71*, 1-16.
(14) Goddard, E. D. *Interactions of surfactants with polymers and proteins*; CRC Press: Boca Raton, FL, 1993.
(15) Lin, M. Y.; Sinha, S. K.; Chari, K. *J. Phys. IV* **1993**, *3*, 6.
(16) Cabane, B.; Duplessix, R. *J. Phys. (Paris)* **1987**, *48*, 651-662.
(17) Cabane, B. *Colloids Surf.* **1985**, *13*, 19-33.
(18) Francois, J.; Dayantis, J.; Sabbadin, J. *Eur. Polym. J.* **1985**, *21*, 165-174.
(19) Nikas, Y. J.; Blankschtein, D. *Langmuir* **1994**, *10*, 3512-3528.
(20) Schick, M. J. *Nonionic Surfactants: Physical Chemistry*; Surfactant Science Series 23; Marcel Dekker: New York, 1987.
(21) Li, Y. J.; Xia, J. L.; Dubin, P. L. *Macromolecules* **1994**, *27*, 7049-7055.
(22) Li, Y. J.; Dubin, P. L.; Havel, H. A.; Edwards, S. L.; Dautzenburg, H. *Macromolecules* **1995**, *28*, 3098-3102.
(23) Guillemet, F.; Piculell, L.; Nilsson, S.; Djabourov, M.; Lindman, B. *Prog. Colloid Polym. Sci.* **1995**, *98*, 47-50.
(24) Guillemet, F.; Piculell, L. *J. Phys. Chem.* **1995**, *99*, 9201-9209.
(25) Gelman, R. A.; Barth, H. G. *Adv. Chem. Ser.* **1986**, *213*, 101-110.
(26) Gelman, R. A.; Barth, H. G. *Polym. Mater. Sci. Eng.* **1984**, *51*, 556-560.
(27) Varelas, C. G.; Steiner, C. A. *Stud. Polym. Sci.* **1990**, *8*, 259-273.
(28) Dualeh, A. J.; Steiner, C. A. *Macromolecules* **1990**, *23*, 251-255.
(29) Loyen, K.; Iliopoulos, I.; Olsson, U.; Audebert, R. *Prog. Colloid Polym. Sci.* **1995**, *98*, 42-46.
(30) Magny, B.; Iliopoulos, I.; Audebert, R.; Piculell, L.; Lindman, B. *Prog. Colloid Polym. Sci.* **1992**, *89*, 118-121.
(31) Magny, B.; Iliopoulos, I.; Zana, R.; Audebert, R. *Langmuir* **1994**, *10*, 3180-3187.
(32) Sarrazin-Cartalas, A.; Iliopoulos, I.; Audebert, R.; Olsson, U. *Langmuir* **1994**, *10*, 1421-1426.
(33) Whitesides, T. H.; Miller, D. D. *Langmuir* **1994**, *10*, 2899-2909.
(34) Griffiths, P. C.; Stilbs, P.; Howe, A. M.; Cosgrove, T. *Langmuir* **1996**, *12*, 2884-2893
(35) Griffiths, P. C.; Roe, J. A.; Jenkins, R. L.; Reeve, J.; Cheung, A. Y. F.; Hall, D. G.; Pitt, A. R.; Howe, A. M. *Langmuir* **2000**, *16* (26), 9983-9990.
(36) Whitesides, T. G.; Miller, D. *Langmuir* **1994**, *10*, 2899.
(37) Blankschtein, D. *Langmuir* **1994**, *10*, 3512.
(38) Sesta, B.; D'Aprano, A.; Segre, A. L.; Proietti, N. *Langmuir* **1997**, *13*, 6612-6617.
(39) Li, Y.; Ghoreishi, S. M.; Warr, J.; Bloor, D. M.; Holzwarth, J. F. *Langmuir* **1999**, *15*, 6326-6332.
(40) Li, Y.; Bloor, D. M.; Penfold, J.; Holzwarth, J. F.; Wyn-Jones, E. *Langmuir* **2000**, *16*, 8677-8684.
(41) Purcell, I. P.; Lu, J. R.; Thomas, R. K.; Howe, A. M.; Penfold, J. *Langmuir* **1998**, *14*, 1637.
(42) Lu, J. R.; Thomas, R. K.; Penfold, J. *Adv. Colloid Interface Sci.* **2000**, *84*, 143-304.
(43) Cabane, B.; Duplessix, R. *J. Phys. (Paris)* **1987**, *48*, 651.
(44) Bury, R.; Desmazieres, B.; Treiner, C. *Colloids Surf., A* **1997**, *127*, 113-124.
(45) Smitter, L. M.; Torres, M. E.; Miller, A. J.; Saez, A. E. *J. Colloid Interface Sci.* **2001**, *244*, 164-172.
(46) Shirahama, K.; Liu, J.; Aoyama, I.; Takisawa, N. *Colloids Surf., A* **1999**, *147*, 133-138.

Fluorescence Studies. The fluorescence probe 8-anilino-1-naphthalene sulfonic acid (ANS) (Aldrich) was used as received. All solutions were prepared from a stock solution of distilled water with the appropriate concentration of ethanol, containing a stock ANS probe at a concentration of 2×10^{-5} M. Emission intensities were determined by integration of the fluorescence intensity over the range 490–520 nm, with excitation at 320 nm using a scan speed of 240 nm s^{-1} and slit widths of 5.0 nm. All emission spectra, recorded on a Perkin-Elmer LB 50 Luminescence spectrophotometer, were obtained on samples equilibrated at 25 ± 1 °C.

Small-Angle Neutron Scattering. The SANS measurements were performed at 25 ± 1 °C on the fixed-geometry, time-of-flight LOQ diffractometer (ISIS Spallation Neutron Source, Oxfordshire, U.K.). Experimental measuring times were between 40 and 80 min. All scattering data were normalized for the sample transmission and incident wavelength distribution and corrected for instrumental and sample backgrounds and for the linearity and efficiency of the detector response. The data were put onto an absolute scale using a well-characterized partially deuterated polystyrene-blend standard sample.

SANS Fitting. For surfactant micelles, we invoke a charged, elliptical core–shell model. For SDS micelles, which are not polydisperse, we have shown that this is preferable to invoking a charged, polydisperse spherical model.[47] Accordingly, the intensity of scattered radiation, $I(Q)$, as a function of the wave vector, Q, is given by

$$I_{\text{surfactant}}(Q) = n[\langle|F(Q)|^2\rangle S(Q) + |\langle F(Q)\rangle^2| - \langle|F(Q)|^2\rangle] + B_{\text{inc}} \quad (1)$$

where $F(Q) = V_1(\rho_1 - \rho_2)F_0(QR_1) + V_2(\rho_2 - \rho_0)F_0(QR_2)$. The first term represents the scattering from the core (subscript 1), and the second, the polar shell (subscript 2). $V_i = {}^4/_3\pi R_i^3$ and $F_0(QR_i) = 3j_i(QR_i)/QR_i$ (j_i is the first-order spherical Bessel function of the first kind). $S(Q)$ represents the spatial arrangement of the micelles in solution, and n, the micelle number density. ρ_i is the neutron scattering length density of the micellar core (subscript 1), the polar shell (subscript 2), and the solvent (subscript 0). The structure factor $S(Q)$ was calculated using the Hayter and Penfold model for spheres of a given micellar concentration, charge, and ionic strength, incorporating refinements for low volume fractions and a penetrating ionic background.

A simple Lorentzian function is invoked to describe the scattering from the localized structure of the polymer network:

$$I_{\text{polymer}}(Q) = (\rho_{\text{polymer}} - \rho_{\text{solvent}})^2 \frac{I_\xi(Q=0)}{[1 + Q^2\xi^2]} \quad (2)$$

where ξ is the network correlation length.

Electron Paramagnetic Resonance (EPR). Experimental details for the EPR measurements are identical to those described previously,[48] and only brief details are repeated here. A stock solution of the surfactant with a spin-probe/surfactant molar ratio of $^1/_{400}$ was mixed with an appropriate polymer solution to yield the desired solution composition. These nondegassed samples were sealed with a gas-oxygen torch into melting point capillaries, which were housed within a quartz EPR tube for the measurements. The temperature was controlled to 25 ± 1 °C by a Bruker Variable Temperature Unit BVT 2000 instrument. Five spectra were recorded at X-band on a Bruker ESP-300 spectrometer.

EPR Line Shape Fitting and Analysis. The line shapes were fitted to a Voigt approximation to separate the Gaussian and Lorentzian components of the spectral lines and to locate the resonance fields of the three EPR lines of a nitroxide radical to a precision of a few milligauss. Rotational correlation times are computed from the overall line width of the center line and the peak-to-peak heights of the three lines and subsequently corrected for inhomogeneous broadening using the procedure outlined by Bales.[49,50]

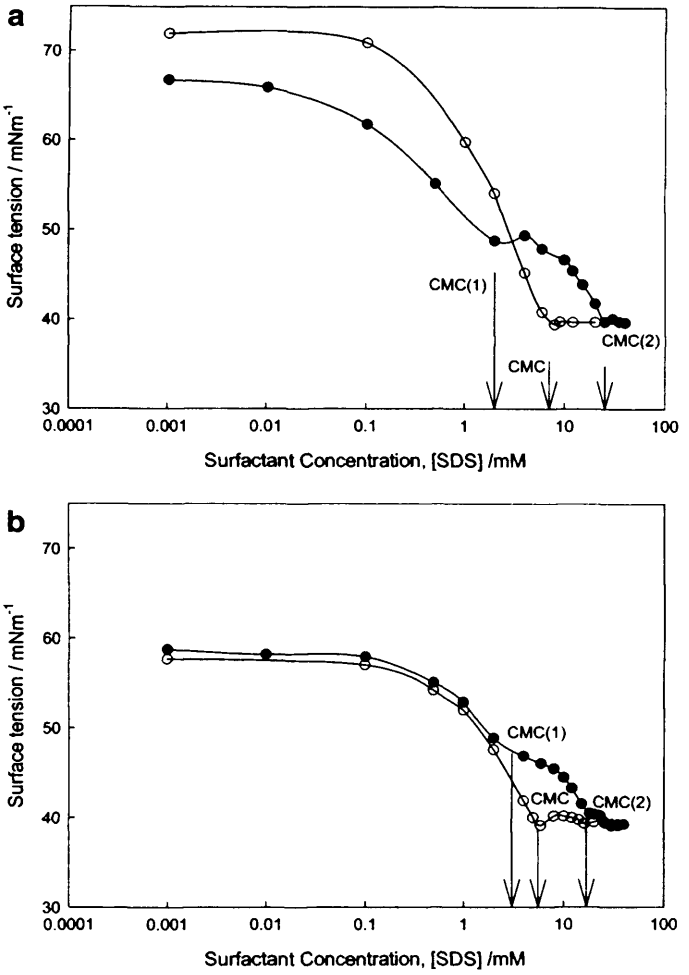

Figure 1. (a) Surface tension behavior of SDS in water (open circles) and SDS with 0.5% w/w PVP in water (filled circles). The cmc of SDS in water is clearly visible, as are cmc(1) and cmc(2) for SDS in the presence of PVP. (b) Surface tension behavior of SDS in 5 wt % ethanol/water mixtures (open circles) and SDS with 0.5% w/w PVP in 5 wt % ethanol/water mixtures (filled circles).

The separation ($A+$) of the low and center lines ($M_i = +1$ and $M_i = 0$) is directly related to the polarity index H(25 °C), defined as the molar ratio of OH groups in a given volume relative to water, ϕ_{OH}. For simple SDS solutions, H(25 °C) corresponds to the volume fraction of water in the polar shell, ϕ_{water}. The presence of ethanol in the polar shell will also contribute to the value of ϕ_{OH}, but it is not possible to decouple these two contributions.

Results

The aim of this paper is to illustrate how the addition of ethanol to a PVP/SDS solution affects the polymer/surfactant interaction. Accordingly, we first present experimental data of the onset of the interaction, we subsequently present studies on how the interaction affects the size/shape of the polymer/surfactant complex, and we ultimately present the impact of these complexes on the bulk solution viscosity.

Onset of Surfactant Micellization. Figure 1a shows the surface tension versus surfactant concentration of simple SDS in the absence and presence of 0.5 wt % PVP. For the simple SDS case, there is clearly only one break

(47) Griffiths, P. C.; Paul, A.; Heenan, R. K.; Penfold, J.; Ranganathan, R.; Bales, B. L. *J. Phys. Chem. B* **2004**, *108*, 3810–3816.
(48) Bales, B. L.; Ranganathan, R.; Griffiths, P. C. *J. Phys. Chem. B* **2001**, *105* (31), 7465–7473.
(49) Bales, B. L. In *Inhomogeneously Broadened Spin-Label Spectra*; Berliner, L. J., Reuben, J., Eds.; Biological Magnetic Resonance 8; Plenum Publishing Corporation: New York, 1989; p 77.
(50) Bales, B. L.; Stenland, C. *J. Phys. Chem.* **1993**, *97*, 3418.

Table 1. Surface Tension Derived cmc, cmc(1), and cmc(2) Values for Sodium Dodecyl Sulfate (SDS) and Poly(vinylpyrollidone) (PVP) as a Function of Ethanol Concentration[a]

ethanol/wt %	cmc/mM	cmc(1)/mM	cmc(2)/mM
0	8.0 ± 0.2	2.0 ± 1	23.0 ± 4
5	5.0 ± 0.5	2.0 ± 2	16.0 ± 3
10	3.5 ± 2	2.0 ± 2	11.0 ± 2
15	4.0 ± 3	5.0 ± 3	11.0 ± 3
20	7.0 ± 3	10.0 ± 3	25.0 ± 3

[a] [PVP] = 0.5 wt %.

in the curve yielding cmc = 8 ± 0.2 mM, in excellent agreement with the literature value. In the presence of the PVP, two "breaks" are observed on the surface tension data indicating cmc(1) and cmc(2). Our estimate of cmc(1) is in good agreement with the earlier work by Turro et al.[51] At cmc(2), the unimer concentration of SDS corresponds to that at the cmc of SDS in the absence of PVP, so cmc(2) − cmc gives a measure of the amount of polymer-bound surfactant, C_{bound}.

In the presence of 5 wt % ethanol (Figure 1b), the surface tension of SDS both with and without PVP is significantly reduced. The break in the surface tension curve for the no-PVP SDS cases occurs at lower SDS concentrations compared with the no-ethanol case, confirming that micellization is promoted (the cmc decreases) by the presence of these amounts of ethanol—the cosurfactant effect. This behavior is in good agreement with the work of Safarpour et al.[7] Similar behavior is observed for the polymer/surfactant/ethanol mixture to that observed in the simple aqueous SDS/PVP case (i.e., no ethanol), two breaks corresponding to cmc(1) and cmc(2), respectively. Interestingly, cmc(1) is largely invariant with ethanol concentration, at least to ~10% ethanol, Table 1. In contrast, cmc(2) is dependent on the ethanol content, at least at the lower ethanol concentrations; cmc(2) decreases monotonically to a minimum around 15 wt % ethanol, Table 1. Subsequent increases in ethanol content further reduce the surface tension of the solutions, causing a broadening of the curves which ultimately makes accurate determination of the cmc values somewhat difficult, a conclusion reached in other studies.[2,7,52] Nonetheless, cmc, cmc(1), and cmc(2) increase with subsequent increases in ethanol beyond 15 wt %.

It should be noted that surface tension is a measure of the surface characteristics of the solution, and thus, there are limitations on the interpretation of these data to explain bulk characteristics.[53] To supplement these data, we use (static) fluorescence to obtain a separate measurement of the critical micelle concentrations.

Fluorescence probes can be used to study the microenvironment of the probe and, hence, the structure of the polymer/surfactant complex. The fluorescence probe in this study, 8-anilino-1-naphththalene sulfonic acid (ANS) and related dyes, behaves in such a way as to provide a qualitative indication of the polarity of the probe environment.[54] Such probes find use in the determination of cmc or cmc(1) by detecting changes in polarity. The probe is not considered to perturb the structure of the micelle

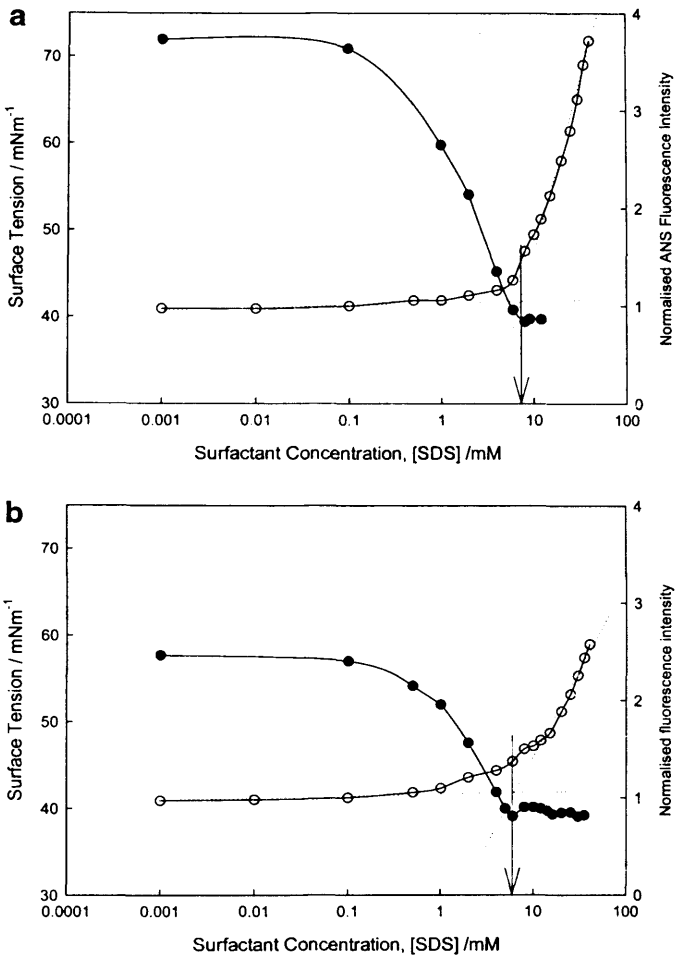

Figure 2. (a) Fluorescence intensity of ANS in SDS in water (open circles) as a function of SDS concentration. Also shown is the corresponding surface tension data showing the correlation between the two techniques (filled circles). (b) Fluorescence intensity of ANS in SDS in 5 wt % ethanol/water mixtures (open circles) as a function of SDS concentration. Also shown is the corresponding surface tension data showing the correlation between the two techniques (filled circles).

significantly,[55] since estimates of the cmc of SDS measured by ANS fluorescence compare favorably with those determined by other techniques.

We have previously shown[55] that, for alkyl chain lengths greater than the octyl, ANS associates predominantly with the micelle and executes rapid motion between the polar shell and the surrounding aqueous pseudophase. The fluorescence intensity of ANS increases with increasing hydrophobicity, and thus, the measured fluorescence is an average of the intensity within the polar shell and in the aqueous pseudophase. In our previous work where polymers were present, at concentrations below the cmc, the fluorescence intensity is low and independent of concentration of both surfactant and polymer. As the surfactant concentration passes through cmc(1), micelles form, and a sharp increase in fluorescence intensity is seen. This has been shown to be due to the preferential solubilization of the ANS into the polar shell of the micelle.

The ANS fluorescence intensity versus surfactant concentration is shown in Figure 2 for SDS solutions as a function of ethanol concentration. The same picture emerges; a low fluorescence intensity below the cmc that increases significantly as the surfactant concentration passes through the cmc. The intersection of the limiting

(51) Turro, N. J.; Baretz, B. H.; Kou, P.-L. *Macromolecules* **1984**, *17*, 1321–1324.
(52) Fukual, H.; Satake, I.; Hayakawa, K. *Langmuir* **2002**, *18*, 4465–4470.
(53) Staples, E.; Tucker, I.; Penfold, J.; et al. *Langmuir* **2002**, *18*, 5147–5153.
(54) Abuin, E. B.; Lissi, E. A.; Aspee, A.; Gonzalez, F. D.; Varas, J. M. *J. Colloid Interface Sci.* **1997**, *186*, 332.
(55) Griffiths, P. C.; Roe, J. A.; Bales, B. L.; et al. *Langmuir* **2000**, *16*, 8248–8254.

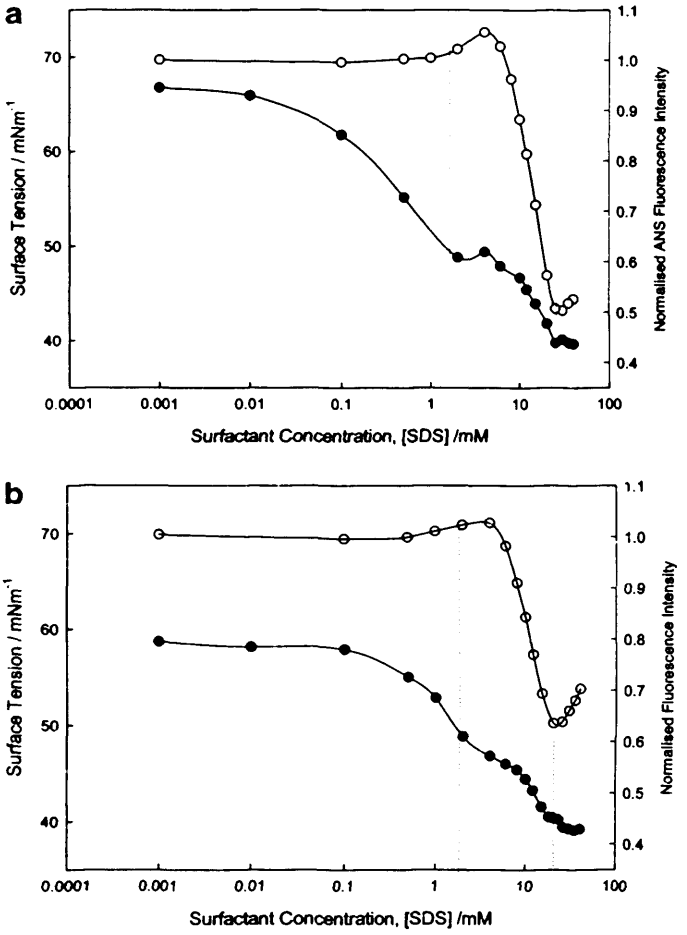

Figure 3. (a) Fluorescence intensity of ANS in 0.5% w/w PVP/SDS in water (open circles) as a function of SDS concentration. Also shown is the corresponding surface tension data showing the correlation between the two techniques (filled circles). (b) Fluorescence intensity of ANS in 0.5% w/w PVP/SDS in 5 wt % ethanol/water mixtures (open circles) as a function of SDS concentration. Also shown is the corresponding surface tension data showing the correlation between the two techniques (filled circles).

Table 2. ANS Fluorescence Derived cmc, cmc(1), and cmc(2) Values for Sodium Dodecyl Sulfate (SDS) and Poly(vinylpyrollidone) (PVP) as a Function of Ethanol Concentration[a]

ethanol/wt %	cmc/mM	cmc(1)/mM	cmc(2)/mM
0	8.0 ± 1	2.0 ± 1	29 ± 3
5	5.0 ± 1.5	1.0 ± 2	20 ± 2
10	4.0 ± 2	1.0 ± 2	17 ± 5
15	4.0 ± 2	1.8 ± 1	11 ± 4
20	6.0 ± 3	2.0 ± 1	10 ± 5

[a] [PVP] = 0.5 wt %.

slope and the initial slope gives a reasonable estimate of the cmc, although, for the higher ethanol content systems, some curvature of the data is apparent. Nonetheless, there is a clear correlation between the surface tension derived cmc's, which are also shown, and those extracted from the fluorescence study, Table 2. For the SDS/PVP systems (Figure 3), two breaks in the curve are seen, corresponding to cmc(1) and cmc(2). While not always numerically coincident due to the quite different inherent natures of the two techniques, the overall behavior is analogous; thus, ANS fluorescence studies compliment surface tension studies.

There are a number of interesting differences between the ANS data for the SDS and SDS/PVP systems. The ANS intensity data in Figure 3 have been normalized by

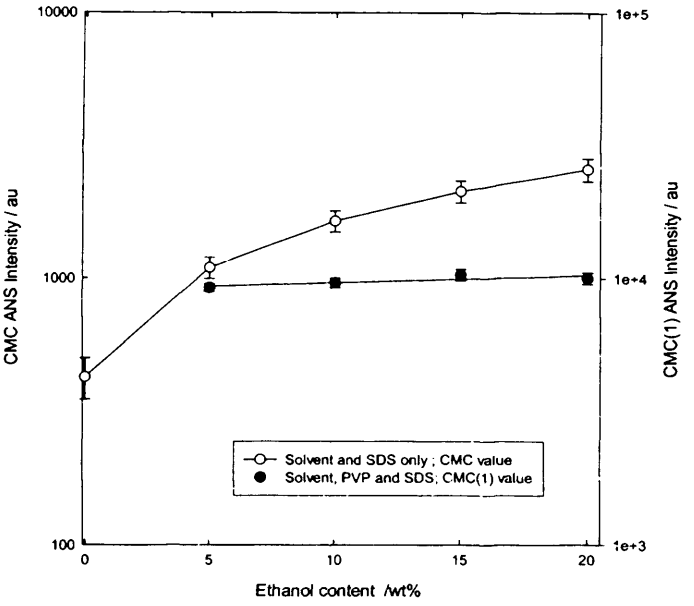

Figure 4. Fluorescence intensity of ANS at a surfactant concentration corresponding to the cmc for SDS (left-hand scale) and at cmc(1) for 0.5% w/w PVP/SDS (right-hand scale) as a function of ethanol concentration.

the measured intensity in the absence of SDS. This behavior is shown in Figure 4. In the absence of PVP, the (normalized) fluorescence intensity has a low value which increases significantly around the cmc as the probe relocates into the micelles (Figure 2). In the presence of PVP, the fluorescence intensity is substantially higher—compare the ethanol = 0 cases in Figure 4—and around cmc(1), there is a small further increase in intensity, at least at low ethanol concentrations. With increasing surfactant concentration, there is a further significant decrease until a second increase in intensity is observed, and previous work has shown this to coincide with cmc(2).

The substantial fluorescence intensity of ANS in the presence of PVP is not seen for poly(ethylene oxide) (PEO) or gelatin,[56,55] and therefore, we conclude that some ANS binds to the PVP. The substantial *de*crease in fluorescence intensity with increasing SDS concentration is attributed to polymer-bound ANS being displaced by the surfactant micelles. Hence, the ANS experiments still give a measure of the onset of the interaction, Table 2, between the polymer and the surfactant. The initial rise in intensity around cmc(1) arises due to the polymer collapsing onto the micelle surface,[5,57,58] creating a more hydrophobic environment without displacing significant quantities of the ANS. The reduction of the peak with increasing ethanol content would then suggest a less hydrophobic environment, that is, a smaller amount of polymer binding and the preferential solubilization of the ANS into the micellar phase.

With increasing ethanol concentration and in the absence of both surfactant and polymer, the fluorescence intensity of the ANS increases as a result of increased hydrophobicity for the solvent. The data presented in Figure 3 have, however, been normalized to account for this by dividing through by the appropriate intensity in the absence of SDS. It can also be seen in Figure 3 that, as the ethanol concentration increases, the fluorescence

(56) Griffiths, P. C.; Roe, J. A.; Abbott, R. J.; Howe, A. M. *Imaging Sci. J.* **1997**, *45*, 224–228.
(57) Dhara, D.; Shar, D. O. *J. Phys. Chem. B* **2001**, *105*, 7133–7138.
(58) Gharibi, H.; Rafati, A. A. *Langmuir* **1998**, *14*, 2191–2196.

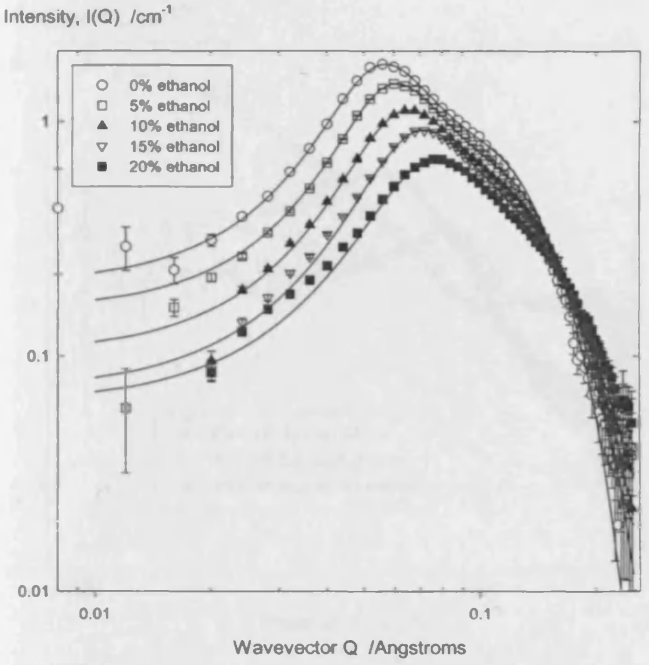

Figure 5. SANS from 75 mM *h*-SDS in D_2O solutions as a function of *d*-ethanol content. The solid lines correspond to fits to the core–shell model as described in the text.

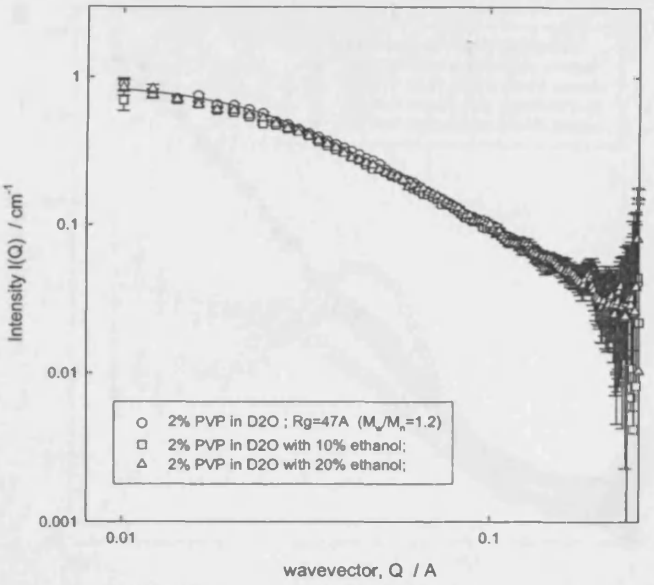

Figure 6. SANS from 2 wt % PVP in D_2O solutions as a function of *d*-ethanol content. The solid lines correspond to fits to a simple Lorentzian to account for scattering from a polymer network.

curves become shallower, and therefore, the hydrophobic character sensed by the ANS upon association with the micelle surface is becoming increasingly similar to that of the corresponding bulk solution. Accordingly, there is less polymer associated with the micelle surface and/or the probe molecule and, by inference, the micelle surface is more accessible to the solvent. The polarity (hydrophobicity) reported by the fluorescent probe at the cmc and cmc(1) is presented in Figure 4 as a function of ethanol concentration. Clearly, in the presence of the polymer, the hydrophobicity is significantly greater (Figure 4) and less dependent on ethanol content compared with the no-polymer case. This suggests that the ethanol participates to a far smaller degree in the micellization process when the polymer is present. This is in agreement with the behavior of cmc(1) which does not vary with ethanol content.

The surface tension data for systems with ethanol contents of >20% ethanol are particularly featureless, and we therefore concern ourselves primarily with the concentration region 0 wt % < ethanol < 15 wt %. Changes in the ANS fluorescence intensity (and, as we shall see, the SANS) however suggest that micellization does take place.

Structure of the PVP/SDS/Ethanol Complex. Before we discuss the effects of ethanol on the structure of the polymer/surfactant complex, we must first fully characterize the effects of ethanol on the simple SDS micelle. Figure 5 presents SANS data from 75 mM SDS solutions as a function of ethanol content. In these studies, deuterated ethanol has been used. The scattering length density of CD_3CD_2OH is sufficiently similar to that of D_2O that over the range of ethanol concentration studied here, 0 wt % < [ethanol] < 20 wt %, the scattering length density of the solvent changes by <5%. Nonetheless, these small variations are implicitly included in the fitting procedure and subsequent analysis.

At this surfactant concentration, the data exhibit a strong structure factor peak as a result of the electrostatic interaction between adjacent micelles. With increasing ethanol content, this peak becomes progressively weaker, suggesting that the ionic character of the micelle is decreasing, although the electrostatic interaction is a strong function of the dielectric constant of the medium. Further, the peak moves toward a higher Q value, associated with a closer proximity of the micelles. At a fixed surfactant concentration, this implies that the micelles are becoming smaller. The data have been fitted to the charged core–shell ellipse as described previously. Key parameters are presented in Table 3. The aggregation numbers thus calculated are in very good agreement with those presented by Caponetti[8] and Almgren et al.[9]

Table 3. SANS Fitting Parameters for SDS/Ethanol Systems

ethanol/ wt %	R_{core}/ Å	shell thickness, δ/Å	axial ratio	polar shell –OH volume fraction	aggregation number, N_{agg}
0	16.7	3.2	1.25	0.70	65
5	15.8	2.9	1.25	0.66	58
10	15.8	2.5	1.0	0.64	46
15	15.7	2.3	0.95	0.61	44
20	15.4	2.2	0.90	0.60	38

Having characterized the effects of ethanol on the surfactant micelle, it is appropriate to quantify the effects of ethanol on the polymer conformation in the absence of surfactant. SANS (Figure 6) and viscosity (not shown) have been used to this end. The SANS data clearly show that the polymer scattering is unaffected by the presence of ethanol, and the scattering may be described by a simple Lorentzian with a correlation length of $\xi = 55$ Å. The viscosity of simple PVP solutions however does change upon addition of ethanol, but since the polymer conformation is unaffected (Figure 6) by the addition of ethanol, the changes observed in the viscosity merely reflect the change in the solvent viscosity rather than a change in the polymer conformation.

It has become well-established from SANS studies that when an anionic surfactant is added to an aqueous nonionic or polyampholytic polymer solution at low ionic strengths, the polymer scattering adopts some character of the micelle scattering. This principally involves the appearance of the peak characteristic of surfactant scattering in the *polymer* scattering; in other words, the

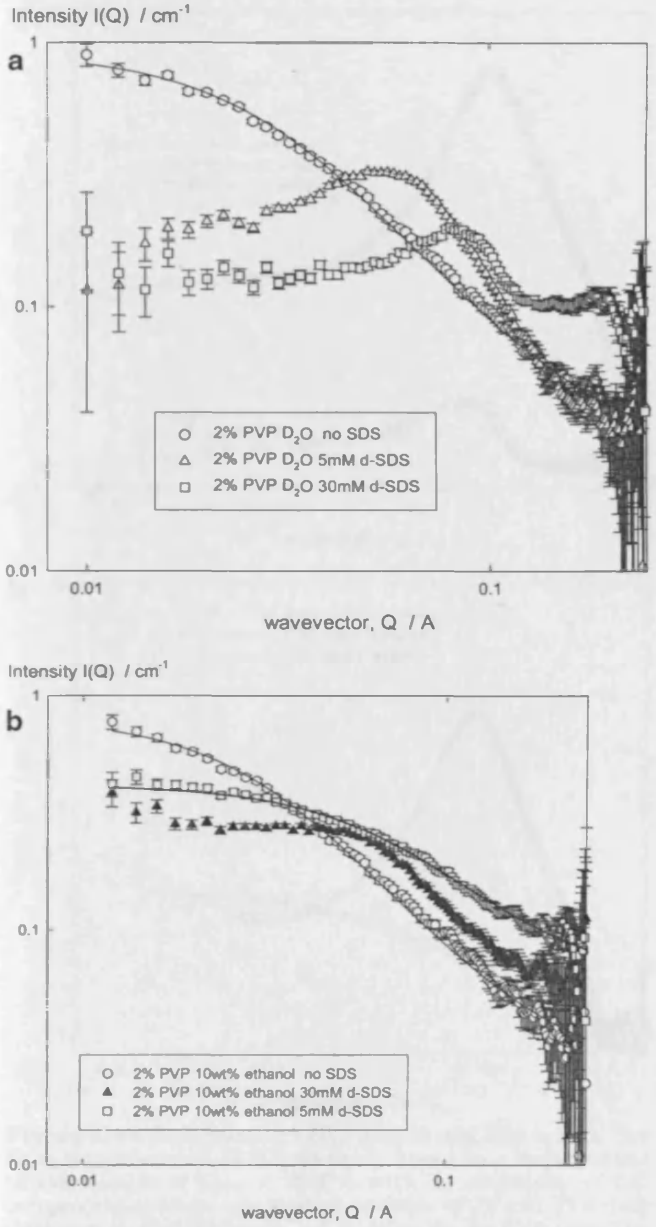

Figure 7. (a) SANS from 2% PVP in D_2O as a function of *d*-SDS concentration, i.e, conditions of contrast match for the surfactant. (b) SANS from 2% PVP in D_2O/10% *d*-ethanol solutions as a function of deuterated SDS concentration; the surfactant is contrast matched.

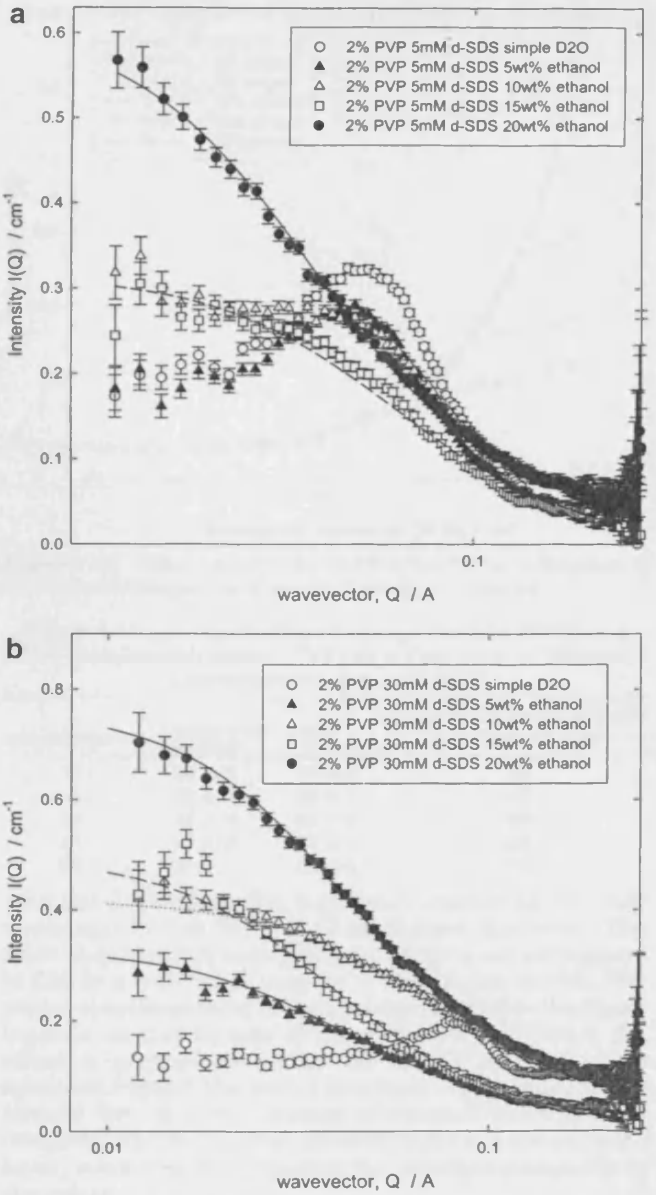

Figure 8. (a) SANS from 2% PVP/5 mM *d*-SDS in D_2O as a function of *d*-ethanol concentration; the surfactant is contrast matched. (b) SANS from 2% PVP/30 mM *d*-SDS in D_2O as a function of *d*-ethanol concentration; the surfactant is contrast matched.

polymer coil wraps around the surfactant micelle, adopting a significant character of the micelle morphology, at least over the Q range being investigated. This is very easily demonstrated using deuterated SDS (and other deuterated surfactants) in D_2O such that the surfactant is rendered invisible, the so-called "contrast match" point. The slight changes in the scattering length density of the solvent induced by adding *d*-ethanol to D_2O are again negligle but are included in the data analysis. Accordingly, just as in the surfactant scattering (e.g., Figure 5), the structure peak will move to higher Q with increasing surfactant concentration. The PVP/SDS system is no different (Figure 7a). However, in the presence of, for example, 10 wt % ethanol (Figure 7b), the situation is quite different to the simple aqueous case with only small changes observed in the scattering and no pronounced structure peak. This implies that the intermicellar repulsion is significantly reduced in the presence of ethanol, in an analogous manner to the addition of salt. Now, the surfactant micelle adsorbs to the polymer without causing the polymer to collapse onto the micelle surface, or "wrap around" the micelle to any significant extent.

The effect of bound surfactant on the size and shape of the polymer can be studied by recording the scattering under contrast match conditions for the surfactant. Consider the two sets of PVP/SDS/ethanol/water SANS, 5 mM *d*-SDS and 30 mM *d*-SDS, presented in parts a and b of Figure 8, respectively. For both data sets, pronounced peaks are present in the simple aqueous solution scattering but absent in the higher ethanol concentration systems. For the 5 mM *d*-SDS series, the surfactant peak is absent only in the 20 and 15% ethanol cases. For these samples, $\xi_{20wt\%} = 24(\pm2)$ Å and $\xi_{15wt\%} = 15(\pm4)$ Å. For the 30 mM *d*-SDS series, the surfactant peak is only clearly observed in the absence of ethanol. The Lorentzian fits correspond to $\xi_{20wt\%} = 24(\pm2)$ Å, $\xi_{15wt\%} = 25(\pm2)$ Å, $\xi_{10wt\%} = 15(\pm3)$ Å, and $\xi_{5wt\%} = 25(\pm2)$ Å. The similarity of these correlation

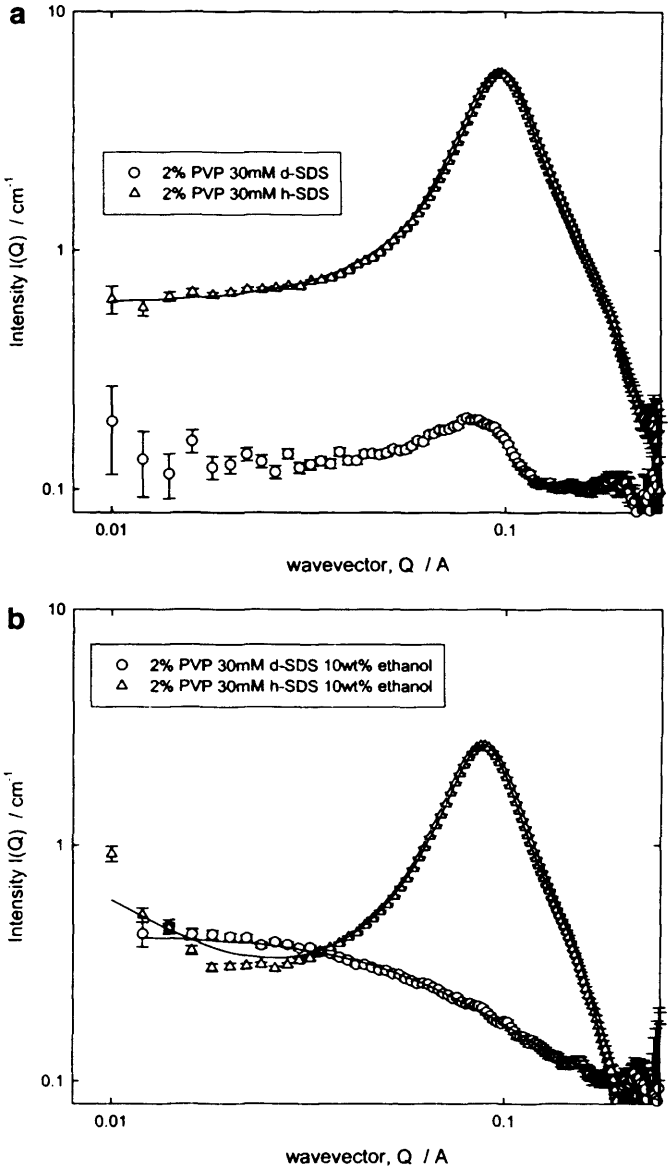

Figure 9. (a) SANS from 2% PVP and 30 mM SDS in D_2O. The fit to the polymer/*h*-SDS data set is based on a radius of the bound micelle of R_{core} = 16.7 Å with an ellipiticity of 1.3, corresponding to an aggregation number of 72(±5). The shell thickness is slightly larger, ~5 Å, than the no-PVP case. The *d*-SDS data set has been used as a "background" when fitting the *h*-SDS data set to empirically account for the polymer scattering. (b) SANS from 2% PVP and 30 mM SDS in 10% ethanol. The fit to the polymer/*h*-surfactant data set is based on a radius of the bound micelle of R_{core} = 16.6 Å with an ellipticity of 1.2, corresponding to an aggregation number of 65(±6). The shell thickness is slightly larger than the no-PVP case, 4 Å. The correlation length ξ = 19 Å extracted from the *d*-SDS data set was adopted in the polymer/surfactant curve.

lengths—irrespective of the surfactant and, to some extent, the ethanol content—is tacit confirmation that the micelles adsorb to the polymer, causing the same large scale conformational rearrangement observed in the pure aqueous case.

The morphology of the bound surfactant micelle can be extracted by fitting the SANS data from the PVP/*h*-SDS systems (Figure 9). Since protonated SDS is now used, the intensities will be much greater than the corresponding *d*-SDS case, and the surfactant contribution to the overall scattering, much more pronounced. However, the similarity of the polymer scattering and the polymer + surfactant scattering is a simple indication of how the polymer adopts much of the character of the bound micelle and, therefore,

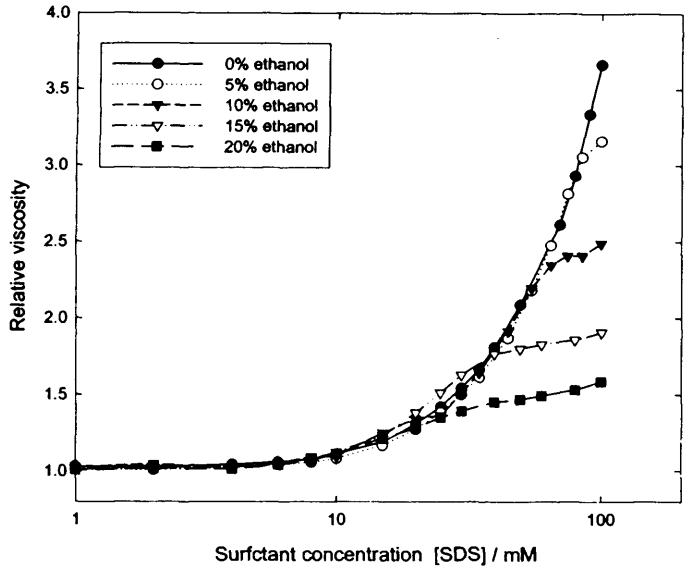

Figure 10. Relative viscosity of 2% w/w PVP as a function of SDS concentration for a range of ethanol contents.

Table 4. C_{bound} for Sodium Dodecyl Sulfate (SDS) and Poly(vinylpyrollidone) (PVP) as a Function of Ethanol Concentration per wt % PVP

ethanol/wt %	$C_{SDSbound}^{surfacetension}$	$C_{SDSbound}^{ANS}$	number of bound micelles per chain (±15%)
0	30 ± 8	40 ± 8	55
5	22 ± 7	30 ± 7	40
10	15 ± 4	25 ± 7	30
15	12 ± 3	15 ± 4	20
20	n/a	10 ± 6	15

why the Lorenztian fits to polymer scattering are only meaningful when there is no surfactant character. The solid lines through each (protonated) data set correspond to fits to a core–shell micelle + Lorentzian model. The parameters describing these fits are presented in the figure legends; as may be seen by comparison with Table 3, the effect of ethanol on the bound micelle morphology is minimal; indeed, the bound micelle is very similar to the micelle formed in the absence of ethanol. Therefore, we conclude that the polymer adsorbs to the micelle palisade layer, rendering that region of the micelle inaccessible to the ethanol.

The viscosity of aqueous PVP/ethanol solutions is dependent on the ethanol content, but this is a reflection of the solvent viscosity rather than any changes in the polymer conformation. Upon addition of SDS, the viscosity of PVP/SDS/ethanol solutions do show a pronounced dependence on both [SDS] and ethanol content, at least at the higher ethanol contents. An increase in viscosity is observed around cmc(1) (Figure 10), but any appreciable increase in viscosity is not detected until [SDS] > 20 mM. Above this concentration, the viscosity rises to a plateau, whose magnitude is dependent on both [SDS] and ethanol content. This is in excellent agreement with the SANS studies, in that the polymer conformation is only weakly dependent on ethanol content at 30 mM SDS. From Table 4, it is possible to calculate the saturation point at the polymer concentration and, given the aggregation number extracted from the SANS analysis, the number of bound micelles. This decreases from n = 55 in the absence of ethanol to n = 15 as the ethanol concentration approaches the minimum in the cmc data, that is, 15–20 wt % ethanol. With this decreasing population of micelles, the electrostatically driven coil expansion due to the bound micelles will inherently decrease. This is in good agreement with the qualitative analysis of the scattering data, in terms

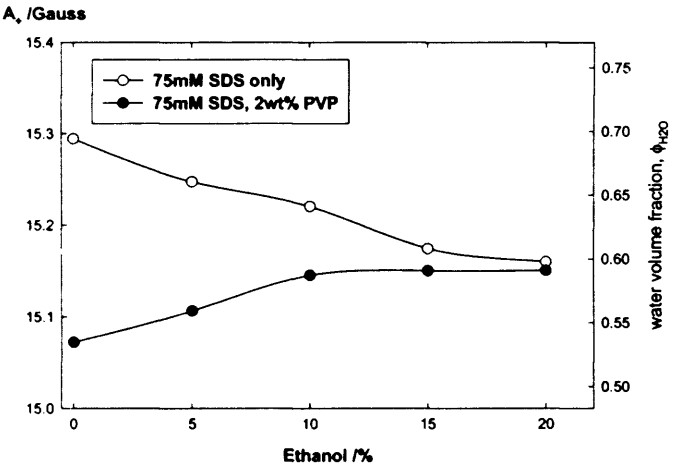

Figure 11. Hyperfine coupling constants of 16-DSE (doxyl stearic acid methyl ester) solubilized in 75 mM SDS micelles in the presence and absence of PVP as a function of ethanol concentration.

of under what conditions (SDS, ethanol, concentration, etc.) the Lorentzian fit is no longer valid.

Finally, the amount of polymer at the micelle interface may be examined by EPR, based on the morphology of the micelle extracted from the SANS experiments. It is assumed that the spin-probe executes rapid motion within the headgroup region of the micelle and its spectrum reflects the structure of that region. The separation of the two high field lines is a measure of the polarity of the headgroup region, specifically, the volume fraction of −OH dipoles present. The polarity sensed by the spin-probe in the SDS/ethanol system decreases (Figure 11) with increasing ethanol content. From the SANS analysis, it may be seen that this principally corresponds to a decreasing aggregation number. The EPR results are therefore counterintuitive—one would expect the volume fraction of water present in the headgroup region to increase as the curvature of the micelle increased, due to the larger available volume per surfactant headgroup within the headgroup region. Thus, the decrease in polarity is reflective of the amount of ethanol present in the headgroup region; since the volume of an ethanol molecule is significantly greater than that of a water molecule, a small amount of ethanol will displace a considerable amount of water.

When PVP is present, the volume fraction of −OH groups in the headgroup region increases with increasing ethanol content. However, the SANS results suggest that there is no change in the micelle aggregation number and, therefore, no change in the polar shell volume per surfactant headgroup. Thus, the increase in −OH volume fraction is more reflective of an increasing fraction of the available volume per surfactant headgroup being accessible to the solvent; that is, the polymer is being displaced from the micelle surface. As the polymer "lifts off" the micelle surface, the effects of the bound micelle are reduced, as exhibited in the SANS and viscosity data.

Discussion

The thermodynamics of surfactant micellization and polymer/surfactant complexation have been discussed in detail by Nagarajan[59] and by Blankschtein et al.[37] Adopting the notation of Nagarajan, the free energy of formation for polymer-bound micelles has a number of contributing terms—the transfer of the surfactant tail from water into the micellar core, a contribution that is dependent on the solubility of the surfactant; the deformation of the surfactant tail as it conforms to packing requirements within the micellar core; the energy of forming the aggregate core/water interface which is dependent on the aggregation number, as this defines how much of the core is shielded from the solvent; and, finally, two terms that account for the headgroup interactions over the micellar surface, one steric and for ionic surfactants, an electrostatic interaction between the surfactant headgroups. These last two terms are particularly dependent on the size, shape, and orientation of the (charged) headgroups and factors such as the dielectric constant of the solvent. There are also three contributions due the fact that there is polymer at the micelle surface which embody the enhanced shielding of the core, a further steric repulsion term introduced by the presence of the polymer, and a term to deal with the change in free energy of the polymer molecule itself.

The contributions that are directly affected by the solvent composition are principally the transfer of the surfactant tail from water, as this depends on the solubility of the surfactant in the solvent; with increasing ethanol content, the surfactant is more soluble. The formation of the interface between the hydrophobic core and the surrounding solvent is dependent on the surface area of the hydrophobic core that is in contact with the solvent and the macroscopic interfacial tension of the solution. Making the assumption that the interfacial tension of the aggregate core/continuous phase follows the same trend as the surface tension of the bulk solution, that is, a decreasing interfacial term with increasing ethanol content, the energy required to produce the interface decreases (favors micelle formation). The term which considers the ionic headgroup interactions is a complex one, which cannot be estimated simply. A number of factors come into play in determining the energies of the headgroup interactions, including the dielectric constant, Debye length, and radius of the micelle. For instance, the dielectric constant of the solution decreases as the ethanol content increases, which in turn influences the various charge effects such as counterion dissociation and hence the size and shape of the micelle.

Introducing the polymer further complicates the situation. The shielding of the core from the solvent determines whether the interaction occurs. The greater the shielding of the core, the more favorable will be the interaction between micelles and polymers. Accordingly, nonionic polymers/anionic surfactants show much stronger interactions than nonionic polymers/cationic surfactants, as the headgroups of cationic surfactants are generally much bigger than those of anionic surfactants; hence, the amount of hydrophobic core exposed to the continuous phase is significantly smaller.

The steric terms describing the polymer and its interaction with the surfactant headgroups will always be unfavorable due to constraints of packing and the "wrapping" of the polymer strand around the micelles; this is therefore sensitive to the polymer conformation at the micelle surface.

The behavior of the PVP/SDS/ethanol/water system may be rationalized by considering the electrostatic interactions between the sulfate headgroups. The critical micelle concentration of the surfactant and the aggregation number of the micelle the surfactant forms are determined largely by the volume of the hydrophobic tail and the charge on the headgroup. As ethanol is added to the continuous phase, the dielectric constant decreases, which permits a closer separation of the headgroups over the

(59) Esumi, K.; Ueno, M. *Structure-Performance Relationships in Surfactants*; Marcel Dekker: New York, 1997; Vol. 70, Chapters 1 and 12.

micelle surface; the aggregation number and the hydrocarbon core in contact with the aqueous phase both decrease. The closer proximity of the headgroups means that the steric terms increase, but this is a much smaller effect. In the presence of PVP, cmc(1) is lower than the cmc, but this quantity and the aggregation number are both invariant with ethanol content. However, with increasing ethanol content, the polymer conformation increasingly attains a conformation more reminiscent of the no-SDS and no-ethanol cases, which would suggest that the area of the surfactant core "occluded" by the polymer decreases. This is compensated by the adsorption of ethanol into the palisade layer but with no significant change in the aggregation number or counterion binding.

Conclusions

Surface tension and fluorescence are shown to give complimentary estimates of the various critical micelle concentrations present in the SDS/PVP/ethanol/water system, distinguishing free and bound micelles. SANS and viscosity measurements show that the bound micelle affects the polymer conformation, a perturbing effect that is weakened once ethanol is present. EPR and SANS give a useful insight into how the polymer lifts off the micelle surface as the ethanol solubilization increases.

Upon addition of ethanol to aqueous SDS solutions, the cmc decreases to a minimum around 15% ethanol content before subsequently increasing; that is, it follows both the cosolvent and cosurfactant effects. There is a decrease in the aggregation number as the effective dielectric constant permits a closer proximity of the surfactant headgroups.

When PVP is added, the micellization concentration cmc(1) is lower than that in the no-PVP case but is invariant with increasing ethanol. Above 15% ethanol, the micellization concentration increases once more and is numerically identical to the micellization concentration measured in the absence of the polymer.

Acknowledgment. The authors would like to acknowledge financial support from the Leverhulme Trust and the EPSRC for provision of neutron beamtime.

LA049348O